DOI 10.1007/s10778-017-0789-3
International Applied Mechanics, Vol. 53, No. 1, January, 2017

THERMOMECHANICS OF INELASTIC THIN-WALLED STRUCTURAL MEMBERS WITH PIEZOELECTRIC SENSORS AND ACTUATORS UNDER HARMONIC LOADING (REVIEW)

V. G. Karnaukhov, I. F. Kirichok, and V. I. Kozlov

Models, combined numerical–analytical methods, and results related to study of the forced resonance vibrations and self-heating of thin-walled inelastic structural members with piezoelectric sensors and actuators under monoharmonic mechanical and electric loading are presented. The thermomechanical behavior of passive and piezoactive materials is described using the concept of complex characteristics that are assumed to depend on temperature and invariants of the strain tensor. The classical and refined thermomechanical theories are used to model the vibrations and self-heating of thin-walled structural members with sensors and actuators. Nonlinear coupled thermoelastic problems for thin-walled structural members are solved by iteration and numerical methods. The thermal failure of structural members is considered. Methods for determining the critical electrical and mechanical monoharmonic loads and methods of postcritical analysis are described. The effect of various factors on the effectiveness of active damping of the resonance vibrations of inelastic thin-walled structural members by piezoelectric sensors and actuators is studied

Keywords: thin-walled structural members, resonance vibrations, inelastic material, self-heating, piezoelectric sensors and actuators

Introduction. Thin bars, plates, and shells are widely used as structural members in many fields such as aircraft engineering, mechanical engineering, rocket-and-space technology, construction, hydroacoustics, medicine, electronics, etc. One of the basic and most frequent operating modes of such elements are forced harmonic vibrations, including resonance. During vibrations, all materials sustain hysteresis losses, and mechanical or electromechanical energy dissipates as heat. Hysteresis losses are much greater in inelastic (viscoelastic, elastoplastic, and viscoelastoplastic) materials. This effect is widely used for passive damping of forced resonant vibrations of thin-walled elements. To this end, elements with high hysteresis losses are incorporated into the structure of an element with low hysteresis losses. The passive damping of vibrations is widely discussed in the literature (encyclopedias, monographs, and journal articles) [10, 17, 19, 57, 62–65, 70, 76, 95, 138, 139].

However, high hysteresis losses may be accompanied by substantial increase in temperature. This phenomenon is called self-heating and the respective temperature is self-heating temperature (SHT). It may affect either the mechanical and thermal states of a structure (stress–strains distribution, amplitude– and temperature–frequency characteristics, frequency dependence of damping factor) or the dynamic and static, mechanical and thermal stability, and creep behavior of thin-walled elements [8, 9, 28, 66]. Moreover, all materials no longer perform their function above a certain temperature (degradation point).

At the degradation point, the phase state of the material usually changes. The degradation point is the melting point for passive materials and the Curie point (at which the piezoelectric effect is lost) for piezoelectric materials. Therefore, it is believed that the SHT should be taken into account in studying the forced vibrations of inelastic structural members because neglecting

S. P. Timoshenko Institute of Mechanics, National Academy of Sciences of Ukraine, 3 Nesterova St., Kyiv, Ukraine 03057, e-mail: karn@inmech.kiev.ua. Translated from Prikladnaya Mekhanika, Vol. 53, No. 1, pp. 9–74, January–February, 2017. Original article submitted November 11, 2015.

this phenomenon can lead to unreliable results. Despite this obvious fact, the overwhelming majority of studies on the forced resonant vibrations of inelastic thin-walled elements disregard self-heating.

Recent trends are toward the use of active damping methods that incorporate piezoelectric elements into passive thin-walled metallic, polymeric, or composite structures. Foreign studies on the active control of stationary and nonstationary vibrations of structural members are reviewed in [89, 90, 150, 153, 154]. Some of the piezoelectric elements (sensors) provide information on the mechanical state of the body, while the other elements (actuators) are used to balance the mechanical load by applying an electric load to them. Passive structures with piezoactive sensors and actuators are called smart structures, and the corresponding active materials are called smart materials. Smart materials also include magnetoactive materials, shape-memory materials, etc. Smart or intelligent materials are capable of responding to internal or external loads (change in the environment). One of the most demonstrative examples of effective application of such materials is the active damping of stationary and nonstationary vibrations of thin-walled elements with piezoelectric sensors and actuators.

The effectiveness of active damping is strongly dependent on the performance of the sensors and actuators, which, in turn, depends on many factors such as their geometrical and electromechanical characteristics, geometrical and mechanical characteristics of the passive element, mechanical and electric boundary conditions, and temperature. Depending on the mechanical boundary conditions, the operation of a sensor and an actuator will be the most effective when the thin-walled element is fully or partially (spot-like) is coated with a piezoelectric material. Such spots can be made by cutting a continuous electrode coating the passive element.

Temperature has an especially noticeable effect on the performance of sensors and actuators. Usually, only the temperature resulting from the heat transfer to the environment is considered [140]. However, harmonic (including resonance) vibrations of thin-walled elements made of piezoactive and passive inelastic materials can be accompanied by a substantial increase in the SHT because of their considerable hysteresis losses, low heat conductivity, and strong temperature dependence of their properties caused by mechanical and electric loads. This phenomenon can adversely affect the performance of thin-walled elements with sensors and actuators for several reasons: (i) the temperature dependence of the electromechanical characteristics of a material can exert a strong effect on the performance of piezoelectric inclusions and, hence, the effectiveness of the active damping of the vibrations of thin-walled elements; (ii) as the self-heating temperature reaches the Curie point, the piezoelectric element keeps its integrity, but no longer performs its functions, which is a specific type of thermal failure; (iii) if the supply of heat to an inelastic element because of hysteresis losses is balanced by the transfer of heat to the environment, so-called thermal explosion (catastrophic increase in SHT) can occur. This phenomenon in passive dielectrics has been studied well and is considered classical in the physics of dielectrics [15, 72, 74, 75].

The importance of self-heating in solid mechanics was noticed after experiments on heating of solid-propellant charges where it was discovered that fuel becomes liquid during forced resonant vibrations [152]. After these experiments, the self-heating of elementary viscoelastic mechanical systems under quasistatic mechanical loading began to be studied [12, 80, 81, 88, 151, 155], which are reviewed in [88]. These theoretical results are, in fact, similar to those in the physics of dielectrics where the dissipation function generated by dielectric rather than mechanical losses plays the role of a heat source. The importance of the effect of the SHT on the vibrations of piezoactive elements was also pointed out after early experiments on the vibrations of piezoelectric transducers [4]. It was stated that the SHT is the major factor limiting their capacity. Studies on the effect of the SHT on the mechanical behavior of structural members made of inelastic passive materials were reviewed in the monographs [8, 9, 23, 28, 66] and the articles [96, 104–106, 145–147]. The results on the vibrations and self-heating of structural members made of piezoelectric materials are reviewed in [24, 28, 29, 39, 83, 100, 106]. However, these reviews disregard the effect of the SHT on the performance of sensors and actuators and on the effectiveness of the active damping of the forced harmonic vibrations of passive thin-walled elements. When vibrations are resonant and mechanical loads are high, it is necessary to allow for the effect of physical nonlinearity, the dissipative properties of materials, and the SHT on the performance of sensors and actuators and on the effectiveness of the active damping of the vibrations of thin-walled elements. There are three types of physical nonlinearity: (i) dependence of the mechanical characteristics of a passive material on temperature and dependence of the dissipation function on strains and temperature; (ii) dependence of the mechanical characteristics of a passive material and the dissipation function on invariants of the strain tensor; (iii) combination of the previous two types of nonlinearity. If the amplitude of vibrations of flexible thin-walled elements is comparable to their thickness, it is also necessary to allow for geometrical nonlinearity in studying the forced harmonic vibrations and self-heating of flexible thin-walled elements based on nonlinear kinematic equations [11].

1. Basic Equations in the Thermomechanics of Viscoelastic Materials. The theoretical basis for modeling the harmonic vibrations and self-heating of inelastic structural members are viscoelastic, plastic, and viscoelastoplastic models. The general theory of thermoviscoelasticity for passive and piezoactive materials in which mechanical, thermal, and electromagnetic fields interact is described in [8, 9, 23, 29, 66]. The constitutive equations for passive materials with fading memory are presented below.

The constitutive equations for the Piola–Kirchhoff stress tensor σ, entropy η, and internal dissipation $\hat{\sigma}$ for such materials have the form

$$\partial_{g_R} \overset{\infty}{\underset{s=0}{\psi}}[;] = 0, \tag{1.1}$$

$$\sigma = \overset{\infty}{\underset{s=0}{T_*}}[;] = \partial_E \overset{\infty}{\underset{s=0}{\psi}}[;], \tag{1.2}$$

$$\eta = \overset{\infty}{\underset{s=0}{\eta}}[;] = -\partial_\theta \overset{\infty}{\underset{s=0}{\psi}}[;], \tag{1.3}$$

$$\hat{\sigma} - \frac{1}{\rho_R \theta^2} \overset{\infty}{\underset{s=0}{h}}[;] \cdot g_R \geq 0, \tag{1.4}$$

$$\hat{\sigma} = -\frac{1}{\theta}\left\{ \delta_E \overset{\infty}{\underset{s=0}{\psi}}\left[;|\dot{E}_r^t\right] + \delta_\theta \overset{\infty}{\underset{s=0}{\psi}}\left[;|\dot{\theta}_r^t\right]\right\}, \tag{1.5}$$

where $[;] = [E_t^r, \theta_t^r, E, \theta, g_R]$, ∂_E, …, and δ_E, … are partial and Frechet derivatives; ψ is the free energy, which is, generally, a functional of the history of high strains E_t^r and temperature θ_t^r and a function of instantaneous strains E, temperature θ, and temperature gradient g_R.

The fundamental thermomechanical properties of materials with fading memory follow from Eqs. (1.1)–(1.5):

(i) according to (1.1), the functional of the free energy $\overset{\infty}{\underset{s=0}{\psi}}[;]$ does not depend on the temperature gradient g_R;

(ii) according to (1.2) and (1.3), the Piola–Kirchhoff stress tensor σ and entropy η depend on the functional of the free energy and do not depend on the temperature gradient g_R;

(iii) according to (1.5), the internal dissipation $\hat{\sigma}$ depends on the functional of the free energy $\overset{\infty}{\underset{s=0}{\psi}}[;]$ and satisfies the inequality $\hat{\sigma} \geq 0$;

(iv) the functional of the heat flow $\overset{\infty}{\underset{s=0}{h_R}}[;]$ satisfies the generalized dissipative inequality (1.4).

With (1.1)–(1.5), the energy-conservation equation becomes

$$\theta\dot{\eta} + \frac{1}{\rho_R}\operatorname{Div} h_R - \theta\hat{\sigma} - r = 0. \tag{1.6}$$

The quantity $\hat{\sigma}$ in (1.6) is called internal dissipation (or uncompensated heat). For homogeneous temperature fields, we have $g_R = 0$; then $\hat{\sigma} \geq 0$ follows from inequality (1.4). It can be seen that the material with fading memory is described by two functionals: the functional of free energy $\overset{\infty}{\underset{s=0}{\psi}}[E_r, \theta_r^t; E, \theta]$ and the functional of heat flow $\overset{\infty}{\underset{s=0}{h_R}}[E_r, \theta_r^t; E, \theta, g_R]$.

Specific constitutive equations can be derived by choosing specific expressions for these functionals. Various alternatives of free-energy expressions are given in [8, 9, 23, 29, 66]. Applying nonlinear mechanics methods for harmonic deformation processes to the above constitutive equations, we obtain the simplified constitutive equations to be detailed below.

The above results on piezoactive materials are generalized in [23, 39], where the general theory of materials with internal variables and integro-differential materials is outlined as well.

2. Constitutive Equations for Passive and Piezoactive Inelastic Materials under Monoharmonic Loading. In solid mechanics, constitutive equations play a fundamental role in modeling the vibrations and self-heating of inelastic structural members made of passive and piezoactive materials. To describe the thermomechanical behavior of passive inelastic materials, thermoviscoelastic, thermoplastic, and thermoviscoplastic models of various complexity were developed [8, 9, 21, 22, 68, 79, 85, 86]. However, to solve problems of the harmonic vibrations and self-heating of inelastic structural members, it is necessary to develop simplified models describing the behavior of their material.

For example, in the linear theory of viscoelasticity, general differential models, integral models, and model of materials with internal variables were developed, which, in the harmonic case, take the universal form of complex algebraic equations (concept of complex characteristics) [5, 8, 9, 21, 62, 66, 68, 70]. If the load is harmonic, the problem is reduced to experimental determination of the coefficients of these equations. There are experimental methods for determining the imaginary and real components of the complex material characteristics [56, 87, 138, 139]. The need arises to generalize this concept to the nonlinear case where the tensor-linear constitutive equations for inelastic materials under harmonic loading have the same form as that of the complex equations of the linear theory of viscoelasticity, but the complex characteristics of a passive material depend on the temperature and invariants of the strain tensor.

To determine the strain-dependent complex characteristics, it is necessary to develop a combined experimental/theoretical program similar to that developed in the theory of small elastoplastic deformations using elementary one-dimensional problems and a program for validation of results by solving problems that are beyond the limits of the mentioned elementary one-dimensional problems and by comparing them to experimental data. If there are no such experimental and theoretical results, the following approach is used: (i) some full thermomechanical model of an inelastic material, i.e., constitutive equations of one of the above-mentioned theories of inelasticity is proposed; (ii) an experimental/theoretical program for determining the functions and parameters of the constitutive equations of this full model is developed using the solutions of elementary one-dimensional problems; (iii) mathematical methods of nonlinear mechanics and the full model are used to derive simplified constitutive equations for monoharmonic loading based on the concept of complex characteristics; (iv) experimental/theoretical methods for determining the parameters and functions of the simplified models are developed; (v) the full and simplified models are used to solve complex problems that are beyond the limits of one-dimensional problems used to determine the characteristics of the full and simplified models; (vi) the solutions of these complex problems are compared to conclude on the accuracy of the results obtained using the concept of complex characteristics.

In studying the nonlinear vibrations of mechanical distributed-parameter systems, use is usually made of the variable separation method whereby a candidate solution of a system of differential or integro-partial differential equations is represented as a series of some full system of functions of coordinates and the original problem is reduced to a system of ordinary differential or integro-differential equations with respect to time, which are solved analytically or numerically. Such an approach allows analyzing the limits of applicability of the monoharmonic approximation. It is this approach that was used in most studies on the nonlinear vibrations of mechanical distributed-parameter systems [59], including studies on the nonlinear vibrations of thin-walled structural members with nonlinear hysteresis [57, 63–65], which is described based on the Davidenkov model [18].

If the conditions for monoharmonic approximation established in mathematical studies on the nonlinear vibrations of inelastic elements are satisfied, it is possible to apply such an approach (to be called the first) to studying the nonlinear vibrations of mechanical distributed-parameter systems, i.e., to represent the candidate solution of the original nonlinear system of partial differential equations as a series of monoharmonic functions of time with unknown coefficients and apply the variable separation method. Doing so gives a nonlinear complex system of partial differential equations with respect to the coordinates to which combined numerical/analytical methods developed in solid mechanics can be applied. It is assumed that the constitutive equations of the full model are known. For viscoelastic materials, these may be nonlinear differential or Volterra equations. The theory of small elastoplastic deformations, various models of flow theory, etc. can be applied to elastoplastic and viscoelastoplastic materials. It is also possible to use the second approach: the mechanical process is assumed monoharmonic when the loading is monoharmonic and corresponding constitutive equations for inelastic materials are derived. This theory is much simpler than the above-mentioned full theories describing the behavior of an inelastic material for more general history of deformation than monoharmonic histories. Then a program for experimental determination of the complex characteristics of an inelastic material under harmonic loading is developed. Supplementing these equations with the equations of motion, kinematic

equations, and boundary conditions, we obtain a closed-form system of equations that describes nonlinear monoharmonic processes in distributed-parameter systems.

The first approach was used in [142] for modeling the internal friction in inelastic materials and studying nonlinear oscillatory processes in mechanical systems with hysteresis. Ishlinsky's microplasticity theory [22, 142] is used as the full model. Applying the describing function method to the constitutive equations of this theory made it possible to derive nonlinear complex algebraic constitutive equations similar to the constitutive equations of the linear theory of viscoelasticity, but having complex characteristics depending on deformation amplitudes. A correspondence principle similar to the correspondence principle for linear viscoelastic materials was established in [142]: in the linear equations of elasticity, it is necessary to replace the mechanical characteristics by complex characteristics. Such an approach was used in [8, 9, 23, 28, 39, 66] to construct thermomechanical models of passive (without piezoelectric effect) viscoelastic materials. In these monographs, two approaches were used. One is to use full viscoelastic models and the describing function method to derive approximate constitutive equations for monoharmonic deformation.

The other approach is to derive the constitutive equations for monoharmonic deformation of dissipative materials (which can be viscoelastic, elastoplastic, or viscoelastoplastic), irrespective of the nature of dissipation. Similarly to the constitutive equations of elastoplastic materials, we assume that the real and imaginary components of the stress tensor are functions of the real and imaginary components of the strain tensor. There are conditions under which such constitutive equations can be written in complex form and potentiality conditions under which the constitutive equations can be expressed in terms of derivatives of some two scalar functions, which can be called potentials. With such an approach, the quasilinear constitutive equations take an algebraic form with some functions and parameters, which, as in the nonlinear theory of elasticity and in the theory of small elastoplastic deformations, are determined experimentally.

An experimental program was developed to determine the complex characteristics of an inelastic nonlinear material. The complex constitutive equations thus obtained are used to solve, analytically and numerically, problems that are beyond the limits of the elementary one-dimensional problems mentioned above. These theoretical results are compared to experimental data to validate the constitutive equations. Such an approach was outlined in [39] where the concept of complex characteristics was generalized to piezoelectric materials. In connection with the constitutive equations for monoharmonic or electric loading, we point out the following: when controlling the vibrations of thin-walled inelastic passive elements with piezoelectric inclusions, the active layers applied to these elements are much thinner than the passive element. Therefore, the effect of active layers on the dynamic characteristics and SHT of the controlled passive inelastic structure is insignificant. In this connection, the inelastic and nonlinear properties of piezoelectric sensors and actuators can be neglected in most cases. Therefore, the main task in formulating problems of the forced harmonic vibrations and self-heating of inelastic bodies is to derive the constitutive equations for passive inelastic materials under this type of loading.

2.1. Statement of Three-Dimensional Problems of the Vibrations and Self-heating of Bodies Made of Passive and Piezoactive Materials. To model the harmonic vibrations and self-heating of thin-walled elements consisting of piezoelectric and passive layers, it is necessary to formula the corresponding three-dimensional problems. It includes the universal equations of motion [16, 23, 28, 29, 39]

$$\sigma_{kl,l} + F_k = -\rho\omega^2 u_k, \tag{2.1}$$

the kinematic equations

$$\varepsilon_{kl} = \frac{1}{2}(u_{k,l} + u_{l,k}), \tag{2.2}$$

the electrostatic equations

$$D_{k,k} = 0, \tag{2.3}$$

the energy equations

$$(\lambda_{kl}\theta_{,k})_{,l} + W = \frac{\partial\theta}{\partial t}. \tag{2.4}$$

Equations (2.1)–(2.4) should be supplemented with the standard initial and boundary conditions, as in [29, 52, 153, 154]. In (2.1)–(2.3), all the quantities (except for temperature) are complex: $\sigma_{kl} = \sigma'_{kl} + i\sigma''_{kl}$, …, and, for example, $\widetilde{\sigma}_{kl}(t) = \mathrm{Re}\,\sigma_{kl} e^{i\omega t} = \sigma'_{kl}\cos\omega t - \sigma''_{kl}\sin\omega t$. The other physical and mechanical quantities are defined by similar formulas. The universal equations should be supplemented with constitutive equations, which become quasilinear algebraic complex equations in the harmonic case. For a passive material, they have the following form [8, 9, 23, 39, 66]:

$$\sigma_{kl} = E_{klmn}\varepsilon_{mn}. \tag{2.5}$$

For a piezoactive material, they are the following [23, 28, 39]:

$$\sigma_{kl} = c^E_{klmn}\varepsilon_{mn} - e_{klm}E_m, \quad D_k = \varepsilon^S_{kl}E_l + e_{klm}\varepsilon_{lm}. \tag{2.6}$$

The dissipation function has the form

$$W = \frac{\omega}{2}(\sigma''_{kl}\varepsilon'_{kl} - \sigma'_{kl}\varepsilon''_{kl}) \tag{2.7}$$

for a passive material and

$$W = \frac{\omega}{2}(\sigma''_{kl}\varepsilon'_{kl} - \sigma'_{kl}\varepsilon''_{kl} + D''_k E'_k - D'_k E''_k) \tag{2.8}$$

for a piezoactive material.

In (2.5) and (2.6), all the electromechanical quantities generally depend on field quantities such as the real and imaginary components of the strain tensor, ε'_{kl}, ε''_{kl}, and electric-field vector, E'_k, E''_k. This issue is addressed in [39]. They can also depend on temperature. As can be seen from (2.7) and (2.8), the dissipation function for active and passive materials can be found from the constitutive equations (2.5) and (2.6). Problems of the vibrations and self-heating of inelastic bodies may include three types of physical nonlinearity mentioned above. Problems of the vibrations of flexible thin-walled elements may include the fourth type of nonlinearity (geometrical nonlinearity) in which case nonlinear relations between strains and displacements should be used instead of Eqs. (2.2) [11].

The above formulation of three-dimensional problems provides a basis for modeling inelastic thin-walled elements with sensors and actuators under harmonic loading by accepting some hypotheses on the distribution of field quantities throughout the thickness of the element.

2.2. Justification of the Concept of Complex Characteristics for Physically Nonlinear Materials of the First Type. Nonlinearity of the first type is due to the dependence of complex characteristics on temperature and the nonlinear dependence of the dissipation function on temperature and strain (or stress) amplitude. Since the temperature changes a little over a period of vibration, the constitutive equations for this type of nonlinearity have the same form as the constitutive equations of linear viscoelasticity for harmonic processes, i.e., they have the same form as the constitutive equations of linear elasticity, but are complex, and the coefficients of these equations depend on temperature.

The constitutive equation for the dissipation function coincides with the period-average power so that the dissipation function can be found from the constitutive equations. The experimental results for passive materials presented in [9, 16, 30, 66] suggest the high accuracy of the simplified model for calculating the self-heating temperature. In [9, 12, 39, 66, 133], the results obtained with the full viscoelastic model or polyharmonic approximation are compared with the results obtained with the simplified model. This comparison also indicates the high accuracy of the simplified model based on the concept of complex characteristics. Experimental results on complex characteristics are presented in [9, 66, 80, 81] for passive materials and in [82, 89, 143, 144] for piezoactive materials.

2.3. Justification of the Concept of Complex Characteristics for Physically Nonlinear Materials of the Second Type. Nonlinearity of the second type is due to the dependence of complex characteristics and dissipation function on of strain (or stress) amplitude and the nonlinear dependence of the dissipation function on the strain amplitude. Coupled problems of thermoviscoelasticity with such nonlinearity were formulated in [23, 39, 66]. Nonlinearities of both types are characteristic of polymeric and metallic materials. However, nonlinearity of the first type is stronger in polymeric materials, many of which are very sensitive to temperature changes. Nonlinearity of the second type is typical for metallic materials whose behavior is

stronger affected by the dependence of the complex characteristics on the strain amplitude than by their dependence on temperature. As mentioned above, the monoharmonic approximation applies to mechanical systems that are in a sense similar to elastic. Then methods of nonlinear mechanics can be used to solve the corresponding nonlinear differential or integro-differential equations [59–61]. To justify the concept of complex characteristics for physically nonlinear materials of the second type, the inelastic model presented in [85, 86] was used in [148, 149, 157]. It helped to plot the real and imaginary components of the shear modulus versus the second invariant e_i of the deviatoric strain tensor, i.e., $G' = G'(e_i)$, $G'' = G''(e_i)$. The bulk modulus is assumed constant. The dissipation function is defined by the formula presented above. The system of equations thus derived is the same as the system of equations obtained in formulating problems of thermomechanics in monoharmonic approximation using nonlinear models of viscoelasticity [23, 26, 39]. It is also similar to the mechanical constitutive equations obtained in [142] using the describing function method.

Note that the interaction of the mechanical and thermal fields was neglected in [142]. To specify the dependence of complex characteristics on the strain intensity, a one-dimensional shear (torsion) problem is formulated, as in the deformation theory of plasticity [79]. To determine the complex characteristics of inelastic materials, the following approach is recommended in [141]: (i) determine the dynamic modulus $E^* = \sqrt{(E')^2 + (E'')^2}$ (E' and E'' are the real and imaginary components of the complex modulus $\widetilde{E} = E' + iE''$) from the so-called cyclic diagram, which is the plot of the stress amplitude σ_a versus the strain amplitude ε_a, so that $E^* = \sigma_a / \varepsilon_a$; (ii) find E'' from the area of the hysteresis loop; (iii) calculate the real component of the complex modulus by the formula $E' = \sqrt{E^{*2} - E''^2}$.

In [141], the stress or strain amplitudes calculated with the full viscoplastic model and the approximate model based on a cyclic diagram were compared and appeared to be in good agreement. In [148, 149, 157], a similar approach was proposed to determine the complex amplitudes: the dynamic modulus is determined from stress and strain ranges (amplitudes); the imaginary component of the complex modulus is calculated from the area of the hysteresis loop, while the real component from the formula given above. This approach is called a modified method for determining the components of the complex modulus. The results obtained with the full model, the describing function method, and the modified method were compared. The full model was the inelastic model [85, 86]. The parameters of the full model were obtained by processing experimental data for AMg-6 aluminum alloy and steel by the procedure described in [148]. Then the cyclic characteristics for the history $e = e_0 \sin \omega t$ were determined using the full model. The comparison shows that the modified model is in better agreement with the full model than with the standard model. The full and simplified statements of problems of the vibrations and self-heating of passive inelastic bodies with taking physical nonlinearity of the second type were used to solve many specific problems, and it was shown that the concept of complex characteristics gives quite accurate results. Aspects of justifying the concept of complex characteristics by comparing the results obtained using the full and simplified models were detailed in [147].

It should be noted that the constitutive equations for monoharmonic deformation have the same form for viscoelastic, elastoplastic, and viscoelastoplastic materials, i.e., for all types of inelastic materials. Many experimental studies on the dependence of the complex characteristics on the strain amplitude for passive materials are discussed in [84]. Experimental results on the dependence of the damping ratio on strains for a wide class of materials deforming in the microplastic region are presented in [65]. These experiments indicate that the imaginary component of complex moduli is strongly dependent on the strains and that the strains have a weak effect on the real component of the complex modulus. The solutions of the problem of the flexural vibrations of an inelastic beam with piezoactive layers (actuators) found using the full inelastic model [85, 86] and the concept of complex characteristics were compared and found to be in good agreement in [92, 93, 157, 158].

3. Mathematical Models and Combined Numerical/Analytical Methods for Solving Problems of the Thermomechanics of Inelastic Thin-Walled Elements with Piezoelectric Sensors and Actuators under Harmonic Loading. Here we will describe mathematical models and iterative methods reducing the original nonlinear problem to a sequence of linear problems of viscoelasticity and heat conduction with a known heat source. In modeling the vibrations and self-heating of thin-walled elements with sensors and actuators two approaches can be used: (i) application of some hypotheses to these linear problems; (ii) application of these hypotheses directly to the nonlinear problems of electromecanics and heat conduction formulated in the previous section. The former approach should be used when solving the problems numerically, and the latter approach should be used when solving the nonlinear coupled problems analytically.

A variational formulation of problems of the vibrations and self-heating of inelastic thin-walled elements with sensors and actuators will be given, and finite-element methods for solving the variational problems will be presented. To solve one-dimensional problems, the iterative procedures described below are used. In solving linearized heat-conduction problems

with a known heat source, the discrete-orthogonalization method in combination with finite-difference method is applied at each iteration.

3.1. Linearization Methods for Solving Nonlinear Coupled Problems of Thermoelectroviscoelasticity. In solving the nonlinear coupled problem of thermoelectroviscoelasticity, various methods can be applied to solve the associated nonlinear differential equations. For example, it is possible to use Newton's method and its various modifications, analogs of methods of variable parameters and elastic solutions, asymptotic methods (WKB method, Krylov–Bogolyubov–Mitropolsky method, etc.). Let us briefly outline some iterative methods used to solve specific problems.

To solve nonlinear problem of thermoelectroviscoelasticity with physical nonlinearity of the first type, step-by-step integration over time was performed in [9, 23, 39, 66]. The essence of the method is as follows: (i) use the temperature distribution specified at $t = 0$ to determine the electromechanical characteristics of the material and solve the linear problem of electroviscoelasticity; (ii) use the found electromechanical variables to determine the dissipation function W; (iii) solve the heat-conduction problem with a known heat source on the time interval $[0, t_1]$, the value of t_1 depending on the sensitivity of the electromechanical characteristics to temperature changes; (iv) use the temperature distribution at t_1 to calculate the complex characteristics of the material and repeat (i) and (ii); (v) use the found values of the dissipation function and the temperature distribution at t_1 to solve the heat-conduction equation on the next time interval $[t_1, t_2]$, and so on. The process is terminated at a predefined time point $t = t_k$. Solving the problem step by step, we can study the behavior of piezoelectric elements both in steady thermal state and in transient state in which the temperature is changing to reach its steady-state value.

When the material characteristics depend not only on temperature, but also on the strain (stress) amplitude and electric-field strength, the coupled problem was linearized in [9, 23, 39, 66] using iterative methods based on the idea of the method of variable elastic parameters. An elementary iteration involves solving the linearized dynamic problem of electroviscoelasticity and the heat-conduction problem. To linearized the problem at the nth iteration, the temperature- and amplitude-dependent material characteristics use field quantities $(\varepsilon^{n-1}, \sigma^{n-1}, E^{n-1}, T^{n-1})$ calculated at the $(n-1)$th iteration, i.e., the method of successive approximations is used. The convergence of the method of variable parameters was accelerated using the Steffensen–Aitken algorithm described in [66, 78]. Both methods reduce the original nonlinear problem to a sequence of linearized problems of electromechanics and heat conduction with a known heat source, which are solved numerically. For example, one-dimensional problems with temperature-dependent material characteristics were solved by the method of step-by-step integration over time in combination with the discrete-orthogonalization method [14, 77].

Two-dimensional linearized problems of electroviscoelasticity and heat conduction were solved by the finite-element method [3, 9, 66].

3.2. Modeling the Vibrations and Self-Heating of Shells Using the Kirchhoff–Love Hypotheses. When modeling the forced vibrations of thin-walled elements with sensors and actuators, the following should be taken into account. As in the three-dimensional case, the main task of the thermomechanics of thin-walled elements with sensors and actuators is to derive the constitutive equations relating mechanical and kinematic factors because the universal equations (kinematic equations, equations of motion, initial and boundary conditions) are known from the mechanics of thin-walled elements. The vibrations and self-heating of thin-walled elements with sensors and actuators modeled in [23, 28, 29, 100] taking into account physical nonlinearity of the first type. Similar models for physically nonlinear materials of the second type were developed in [28, 30, 31]. The energy equations can be derived by reducing three-dimensional problems to two-dimensional accepting certain hypotheses on the distribution of temperature throughout the thickness of the element [52].

Let us consider a thin sandwich shell of revolution of thickness $H = h_1 + h_2 + h_3$. The layers are transversely isotropic and polarized across the thickness. The shell is described in a curvilinear orthogonal coordinate system (s, θ, z). Let the mid-surface of the core layer of the shell be the datum. The shell is so thin that its mechanical behavior can be modeled using the Kirchhoff-Love hypotheses: $\sigma_{zz} = 0, \sigma_{zs} = 0, \sigma_{z\theta} = 0$. Moreover, we assume that the normal to the shell does not change its length and remains perpendicular to the mid-surface after deformation. The meridian of the datum surface is described by the equation $r = r(x)$. The surfaces $z = a_0, a_1, a_2, a_3$ (a_0 and a_1 are the faces of the first outside layer; a_1 and a_2 are the faces of the middle layer, and a_2 and a_3 are the faces of the second outside layer) are covered with continuous or cut electrodes to which potentials are applied. The Kirchhoff–Love hypotheses are supplemented with respective hypotheses for electric field quantities and it is assumed that only the normal components of the electric-field vector and electric-flux density ($E_z \neq 0, D_z \neq 0$) are nonzero. Based on these hypotheses, we obtain simplified equations of state for the kth (k = 1, 2) active layer of the shell presented in [28, 29, 100]. The simplified equations for the passive layer can be found in [1, 14, 28].

According to the kinematic Kirchhoff-Love hypotheses, the components of the displacement vector and the components of the strain tensor of the shell are defined by

$$u(s,\theta,z)=u_0(s,\theta)-\frac{\partial w(s,\theta)}{\partial s}z,$$

$$v(s,\theta,z)=v_0(s,\theta)-\frac{\partial w(s,\theta)}{r\partial\theta}z,$$

$$w(s,\theta,z)=w(s,\theta),$$

$$\varepsilon_{ss}=\varepsilon_{ss}^0+\kappa_{ss}z,\qquad \varepsilon_{\theta\theta}=\varepsilon_{\theta\theta}^0+\kappa_{\theta\theta}z,\qquad \varepsilon_{s\theta}=\varepsilon_{s\theta}^0+\kappa_{s\theta}z, \tag{3.1}$$

where $\varepsilon_{ss}^0,\dots,\kappa_{ss},\dots$ are strains determined in terms of displacements (3.1) by formulas known from the theory of shells [1, 14, 28].

Accepting the above hypotheses on electric field quantities, we obtain simplified constitutive equations for active and passive layers [1, 14, 28]. Integrating them over the thickness of the shell, we obtain complex nonlinear constitutive equations for the moments and forces for both types of nonlinearity:

$$N_{ss}=C_{11}\varepsilon_{ss}^0+C_{12}\varepsilon_{\theta\theta}^0+K_{11}\kappa_{ss}+K_{12}\kappa_{\theta\theta}-\frac{H_2^k}{H_1^k}(V_k-V_{k-1}),\ \dots,$$

$$M_{ss}=K_{11}\varepsilon_{ss}^0+K_{12}\varepsilon_{\theta\theta}^0+D_{11}\kappa_{ss}+D_{12}\kappa_{\theta\theta}-\frac{H_3^k}{H_1^k}(V_k-V_{k-1}),\ \dots, \tag{3.2}$$

where the summation is over the repeated index k; the stiffness characteristics and H_i^k are determined by the formulas presented in [29, 37].

It can be seen from (3.2) that the constitutive equations look like the equations of thermoelasticity for thin-walled shells where the thermal expansion is replaced by a quantity depending on the potential difference.

The variational statement of the problem is equivalent to the differential statement. Accepting the Kirchhoff–Love hypotheses, assuming the constancy of the normal component of the electric-flux density in each layer, integrating over the thickness, and summing the results over all layers, we reduce the three-dimensional variational equation presented in [16, 29, 39] to a two-dimensional form:

$$\delta\Im=\delta\Im_1+\delta\Im_2+\delta\Im_3, \tag{3.3}$$

where

$$\Im_1=\frac{1}{2}\iint_F\{C_{11}(\varepsilon_{ss}^0)^2+2C_{12}(\varepsilon_{ss}^0\varepsilon_{\theta\theta}^0)+C_{22}(\varepsilon_{\theta\theta}^0)^2+4C_{44}(\varepsilon_{s\theta}^0)^2$$

$$+2K_{11}(\varepsilon_{ss}^0k_{ss})+2K_{12}(\varepsilon_{ss}^0k_{\theta\theta})+2K_{21}(\varepsilon_{\theta\theta}^0k_{ss})+2K_{22}(\varepsilon_{\theta\theta}^0k_{\theta\theta})$$

$$+8K_{44}(\varepsilon_{s\theta}^0k_{s\theta})+D_{11}(k_{ss})^2+2D_{12}(k_{ss}k_{\theta\theta})+D_{22}(k_{\theta\theta})^2+4D_{44}(k_{s\theta})^2$$

$$-\omega^2\rho_1(u_0^2+v_0^2+w^2)+2\omega^2\rho_2\left(u_0\frac{\partial w}{\partial s}+v_0\frac{1}{r}\frac{\partial w}{\partial\theta}\right)-\omega^2\rho_3\left[\left(\frac{\partial w}{\partial s}\right)^2+\left(\frac{1}{r}\frac{\partial w}{\partial\theta}\right)^2\right]rdsd\theta, \tag{3.4}$$

$$\Im_2=-\frac{1}{2}\iint_F(P_su_0+P_\theta v_0+P_zw)rdsd\theta-\int_L\left(N_su_0+N_\theta v_0+N_zw-M_s\frac{\partial w}{\partial s}-M_\theta\right)dL, \tag{3.5}$$

$$\Im_3 = -\iint_F \frac{V_k - V_{k-1}}{H_1^k}[(\varepsilon_{ss}^0 + \varepsilon_{\theta\theta}^0)H_2^k + (\kappa_{ss} + \kappa_{\theta\theta})H_3^k]rdsd\theta, \tag{3.6}$$

where

$$M_s = \int_{a_{k-1}}^{a_k} f_s z dz, \quad M_\theta = \int_{a_{k-1}}^{a_k} f_\theta z dz, \tag{3.7}$$

$$\rho_1 = \int_{a_{k-1}}^{a_k} \rho^k dz, \quad \rho_2 = \int_{a_{k-1}}^{a_k} \rho^k z dz, \quad \rho_3 = \int_{a_{k-1}}^{a_k} \rho^k z^2 dz, \tag{3.8}$$

ρ^k are densities of the materials.

In (3.6)–(3.8), the sign of summation over k before the integrals is omitted. If the layer of the shell are arranged symmetrically, then $K_{11} = K_{22} = K_{33} = 0$. Differentiating the functional $\Im = \Im_1 + \Im_2 + \Im_3$ over the strains, we arrive at the constitutive equations for forces and moments.

In studying the effect of the temperature on the active damping of vibrations of a shell with sensors and actuators, the above equations should be supplemented with the energy equations describing self-heating.

To determine the SHT, the three-dimensional variational energy equation presented in [52] is used. To reduce the dimension of this equation by one, we assume that the normal component of the heat flow q_z varies linearly across the thickness of the shell: $q_z = q_0 + q_1 z$. The temperature in each layer is approximated by a quadratic polynomial in the thickness coordinate z.

Under mechanical loading, the following conditions are satisfied on the open-circuited electroded surfaces:

$$\iint_S D_z ds = 0, \tag{3.9}$$

whence we determine the potential difference between the electrodes:

$$V_k - V_{k-1} = \left\{ \iint_{(S)} \left[(\varepsilon_{ss}^0 + \varepsilon_{\theta\theta}^0)\frac{H_2^k}{H_1^k} + (\kappa_{ss} + \kappa_{\theta\theta})\frac{H_3^k}{H_1^k} \right] dS \right\} \Big/ \iint_{(S)} \frac{dS}{H_1^k}, \tag{3.10}$$

where S is the area of the electrodes. The electrodes can be either continuous or cut.

When both sensors and actuators are used for active damping of vibrations of shells, sensors indicate their mechanical state, while the potential difference related to the sensors' readings by the feedback equations is applied to the actuators [153, 154]:

$$V_a = G_1 V_s + G_2 \frac{\partial V_s}{\partial t} + G_2 \frac{\partial^2 V_s}{\partial t^2}. \tag{3.11}$$

In the harmonic case, the feedback equations (3.11) become

$$V_a = G_1 V_s + i\omega G_2 V_s - \omega^2 G_3 V_s, \tag{3.12}$$

where $G_i\ (i = 1-3)$ are control parameters.

To study the effect of the feedback factors on the stiffness, dissipative, and inertial characteristics of the shell, we will use the variational equations (3.3)–(3.6).

Substituting (3.12) into (3.6) yields

$$\Im_3 = \frac{(G_1 V_s + i\omega G_2 V_s - \omega^2 G_3 V_s)}{\iint\limits_{(S)} \frac{dS}{H_1^k}} \iint\limits_{(F)} \left\{ \frac{1}{H_1^k} \left[(\varepsilon_{ss}^0 + \varepsilon_{\theta\theta}^0) H_2^k + (\kappa_{ss} + \kappa_{\theta\theta}) H_3^k \right] \right.$$

$$\left. \times \iint\limits_{(S)} [(\varepsilon_{ss}^0 + \varepsilon_{\theta\theta}^0) H_2^k / H_1^k + (\kappa_{ss} + \kappa_{\theta\theta}) H_3^k / H_1^k] dS \right\} r ds d\theta.$$

Finite-Element Problem-Solving Method. At each iteration, the variational problem (3.3) is solved by the finite-element method (FEM) using 12-node isoparametric quadrangular elements and approximating the displacements and geometry of the shell by cubic polynomials within the quadrangle [3]. The deflection of the shell within an element is approximated by bicubic Hermite polynomials L_i [3, 53, 134]:

$$w = \sum_{i=1}^{4} L_i w_i + L_{i+4} \left(\frac{\partial w}{\partial s} \right)_i + L_{i+8} \left(\frac{\partial w}{r \partial \theta} \right)_i + L_{i+12} \left(\frac{\partial^2 w}{r \partial s \partial \theta} \right)_i, \tag{3.13}$$

where w_i, $(\partial w / \partial s)_i$, $(\partial w / r\partial\theta)_i$, $(\partial^2 w / r\partial s\partial\theta)_i$ are the amplitudes of the deflection and its derivatives at nodal points.

The tangential components of the displacements of the mid-surface within the element are approximated by cubic polynomials N_i [3, 53, 134]:

$$u_0 = \sum_{i=1}^{12} N_i u_0^i, \qquad v_0 = \sum_{i=1}^{12} N_i v_0^i. \tag{3.14}$$

A cylindrical coordinate system (r, θ, s) is used as a global coordinate system combining all finite elements. The meridional (s) and axial (x) coordinates are related by $ds = Adx$, $A = \sqrt{1 + (dr/dx)^2}$.

A normalized coordinate system ξ, η is used as a local coordinate system in which approximating functions are defined and is integration is performed. The coordinates s, r, θ and the coordinates ξ, η are related by

$$s = \sum_{i=1}^{12} N_i(\xi, \eta) s_i, \qquad r = \sum_{i=1}^{12} N_i(\xi, \eta) r_i, \qquad \theta = \sum_{i=1}^{12} N_i(\xi, \eta) \theta_i,$$

where s_i, r_i, θ_i are the nodal values of the coordinates.

Let us expand the components of the mechanical and electric loads operating within the element into series:

$$P = \sum_{i=1}^{12} N_i P_i, \qquad V = \sum_{i=1}^{12} N_i V_i.$$

Using the expressions for the displacements and strains and the stationarity condition $\frac{\partial \Im}{\partial w_i} = \sum_{m=1}^{M} \frac{\partial \Im_m}{\partial w_i} = 0$, … for the functional $\Im = \Im_1 + \Im_2 + \Im_3$, we obtain a complex system of linear algebraic equations for the tangential displacements, deflection and its derivatives. Differentiation is performed at the corner points with respect to $w, w^s, w^\theta, w^{s\theta}$ and at all points of the element with respect to u_0 and v_0. The derivatives for the ith node of the element coinciding with the corner point are defiend by

$$\frac{\partial \Im_m}{\partial w_i} = a_{ik}^w w_k + b_{ik}^w w_k^s + c_{ik}^w w_k^\theta + d_{ik}^w w_k^{s\theta} + g_{in}^w u_{0n} + h_{in}^w v_{0n} + f_i^w, \ldots,$$

$$\frac{\partial \Im_m}{\partial v_i} = a_{ik}^{v_0} w_k + b_{ik}^{v_0} w_k^s + c_{ik}^{v_0} w_k^\theta + d_{ik}^{v_0} w_k^{s\theta} + g_{in}^{v_0} u_{0n} + h_{in}^{v_0} v_{0n} + f_i^{v_0}, \tag{3.15}$$

where the numbering of nodes is local ($k = 1, 2, 3, 4,\ n = 1, 2, \ldots, 12$), the complex coefficients are expressed in terms of electromechanical and geometric characteristics of the shell, and the right-hand sides f_i^w, $f_i^{u_0}$, $f_i^{v_0}$ are determined by expanding the load into series of approximating functions.

The above system of algebraic equations is solved in the complex domain by Gaussian elimination. This allows us to find, with high accuracy, the solution of a high-dimensional system of equations, not disturbing its symmetry and bandedness. The displacements found are then used to determine the components of the strain tensor, the thickness component of electric-flux density, and the components of the electric-field strength at an arbitrary point of the finite element. This approach allows us to solve the linear problem for shells of revolution under either mechanical or electric loading.

In the case of active damping of vibrations, the variation $\Im_3$ contributes to the corresponding coefficients of the governing system, thus changing the stiffness, dissipative, and inertial characteristics of the shell.

The two-dimensional variational heat-conduction equation is solved using the same finite-element mesh. The derivative dT/dt is not varied and is replaced by the expression $dT/dt = [T(t+\Delta t) - T(t)]/\Delta t$. In what follows, we will use an implicit scheme to solve the heat-conduction equation. To accelerate the convergence of the iteration process, the Steffensen–Aitken algorithm [66, 78] is used at each time step Δt.

3.3. Modeling the Vibration and Self-Heating of Shells of Revolution Using Refined Theories. The vibrations and self-heating of thin-walled elements with sensors and actuators were modeled in [23, 28, 29] taking into account physical nonlinearity of the first type and in [30, 31] taking into account physical nonlinearity of the second type. Let us outline a refined theory based on the level-by-level approximation of displacements [69].

Let us consider a sandwich shell of revolution of thickness $H = h_1 + h_2 + h_3$ described in a curvilinear orthogonal coordinate system (s, θ, z). The layers are transversely isotropic, viscoelastic, piezoelectric, and polarized across the thickness. The shell is so thin that the three-dimensional equations can be made two-dimensional by equating $\sigma_{zz} = 0$ and assuming that the shear strains ε_{sz} and $\varepsilon_{\theta z}$ vary quadratically within each layer. The shear stresses σ_{zs} and $\sigma_{\theta s}$ must satisfy the interface conditions between the layers. The meridian of the datum surface is described by the equation $r = r(x)$. The piezoelectric surfaces $z = a_0, a_1, a_2, a_3$ are coated with continuous or discrete electrodes on which potentials $V_0, V_1, \ldots, V_3$ are specified. To model the electromechanical behavior of materials, we will use the concept of complex characteristics. The simplified constitutive equations relating stresses and strains are derived accepting mechanical hypotheses that allow for transverse-shear strains and hypotheses on the distribution of electric-field quantities over the thickness according to which the components of electric-field strength and the normal component of electric-flux density are nonzero ($D_z \neq 0, D_s = 0, D_\theta = 0$). As a result, we obtain simplified complex equations of state for active and passive layers which do not differ from the above equations for the Kirchhoff–Love hypotheses and are supplemented with relations for $\sigma_{sz}^k = 2G_{sz} e_{sz}^k$, $\sigma_{\theta z}^k = 2G_{\theta z} e_{\theta z}^k$ and modified expressions for $G_{sz}, G_{\theta z}$. The shear strains in each layer are approximated by quadratic functions of the thickness coordinate z:

$$e_{sz}^k = \frac{1}{2G_{sz}^k} u_1(s, \theta) q^k(z), \qquad e_{\theta z}^k = \frac{1}{2G_{sz}^k} v_1(s, \theta) q^k(z). \tag{3.16}$$

The functions $q^k(z)$ for a sandwich shell are given in [37].

Let the mid-surface of the core layer of the shell be the datum. Using the kinematic equations and integrating expressions (3.16) over the thickness coordinate z, we get expressions for the component of the displacement vector:

$$u^k = u_0 - \frac{\partial w}{\partial s} z + u_1 f^k(z), \qquad v^k = v_0 - \frac{1}{r}\frac{\partial w}{\partial \theta} z + v_1 f^k(z), \tag{3.17}$$

where u_0 and v_0 are the tangential displacements of the surface $z = 0$; w is the normal deflection of the shell; $f^k(z)$ are functions given in [37].

Using the kinematic equations [1, 14] and relations (3.16), (3.17), we represent the components of the strain tensor of the kth layer as

$$\varepsilon_{ss}^k = \varepsilon_{ss}^0 + \kappa_{ss} z + \delta_{ss} f^k(z), \qquad \varepsilon_{\theta\theta}^k = \varepsilon_{\theta\theta}^0 + \kappa_{\theta\theta} z + \delta_{\theta\theta} f^k(z),$$

$$\varepsilon_{s\theta}^{k} = \varepsilon_{s\theta}^{0} + \kappa_{s\theta} z + \delta_{s\theta} f^{k}(z), \qquad e_{sz}^{k} = \frac{1}{2} u_1 q^{k}(z), \qquad e_{\theta z}^{k} = \frac{1}{2} v_1 q^{k}(z). \tag{3.18}$$

The expressions for $\varepsilon_{ss}^{0}, \ldots, \kappa_{ss}, \ldots, \delta_{ss}, \ldots$ in terms of u_0, v_0, w, u_1, v_1 are presented in [37].

There are infinitely thin electrodes between the layers and on the faces of the shell to which voltages V_k are applied. Using the above hypotheses on electric-field quantities, we obtain simplified constitutive equations for each layer. Integration them over the thickness of the shell, we obtain constitutive equations for forces and moments [37]. The universal equations remain the same [69]. Note that the below variational problem statements based on classical and refined hypotheses are equivalent to local problem statements.

Finite-Element Problem-Solving Method. To solve the problem of the vibrations and self-heating of layered shells of revolution by the finite-element method (FEM), we start with the three-dimensional variational equations. Using the above hypotheses and relations, we reduce the three-dimensional variational equation of electromecanics for a shell of revolution to the two-dimensional equation (3.3), where

$$\begin{aligned}
\Im_1 = \frac{1}{2} \iint_F \Big[& C_{11}(\varepsilon_{ss}^{0})^2 + 2C_{12}\varepsilon_{ss}^{0}\varepsilon_{\theta\theta}^{0} + C_{11}(\varepsilon_{\theta\theta}^{0})^2 + 4C_{44}(\varepsilon_{\theta s}^{0})^2 \\
& + 2(K_{11}\varepsilon_{ss}^{0}\kappa_{ss} + K_{12}\varepsilon_{ss}^{0}\kappa_{\theta\theta} + K_{21}\varepsilon_{\theta\theta}^{0}\kappa_{ss} + K_{22}\varepsilon_{\theta\theta}^{0}\kappa_{\theta\theta} + 4D_{44}\varepsilon_{s\theta}^{0}\kappa_{s\theta}) \\
& + D_{11}\kappa_{ss}^2 + 2D_{11}\kappa_{ss}\kappa_{\theta\theta} + D_{11}\kappa_{\theta\theta}^2 + 4D_{44}\kappa_{s\theta}^2 \\
& + 2(C_{11}\varepsilon_{ss}^{0}\delta_{SS} + C_{12}\varepsilon_{ss}^{0}\delta_{\theta\theta} + C_{21}\varepsilon_{\theta\theta}^{0}\delta_{ss} + C_{22}\varepsilon_{\theta\theta}^{0}\delta_{\theta\theta} + 4C_{44}\varepsilon_{s\theta}^{0}\delta_{s\theta}) \\
& + 2(D_{11}\kappa_{ss}\delta_{ss} + D_{12}\kappa_{ss}\delta_{\theta\theta} + D_{21}\kappa_{\theta\theta}\delta_{ss} + D_{11}\kappa_{\theta\theta}\delta_{\theta\theta} + 4D_{44}\kappa_{s\theta}\chi_{s\theta}\delta_{s\theta}) \\
& + D_{11}\delta_{ss}^2 + 2D_{12}\delta_{\theta\theta}\delta_{ss} + D_{22}\delta_{\theta\theta}^2 + 4D_{44}\delta_{s\theta}^2 + C_{55}u_1^2 + C_{55}v_1^2 \Big],
\end{aligned}$$

$$\begin{aligned}
\Im_2 = -\frac{1}{2} \iint_F \omega^2 \Bigg\{ & \rho_1 \left(u_0^2 + v_0^2 + w^2 \right) + \rho_2 \left[\left(\frac{\partial w}{\partial s} \right)^2 + \left(\frac{1}{r} \frac{\partial w}{\partial \theta} \right)^2 \right] + \rho_3 (u_1^2 + v_1^2) \\
& - 2\rho_4 \left(\frac{\partial w}{\partial s} u_1 + \frac{1}{r} \frac{\partial w}{\partial \theta} v_1 \right) + 2\rho_6 \left(u_0 u_1 + v_0 v_1 \right) - 2\rho_5 \left(\frac{\partial w}{\partial s} u_0 + \frac{1}{r} \frac{\partial w}{\partial \theta} v_0 \right) \Bigg\} r ds d\theta,
\end{aligned} \tag{3.19}$$

$$\Im_3 = -\frac{1}{2} \iint_F \left\{ (\varphi_k - \varphi_{k-1}) \left[(\varepsilon_{ss}^{0} + \varepsilon_{\theta\theta}^{0}) \frac{H_2^k}{H_1^k} + (\kappa_{ss} + \kappa_{\theta\theta}) \frac{H_3^k}{H_1^k} + (\delta_{ss} + \delta_{\theta\theta}) \frac{H_4^k}{H_1^k} \right] - P_z \omega \right\} r ds d\theta.$$

The expressions for the stiffness characteristics are presented in [29].

Note that the constitutive equations for forces and moments are derived from (3.19) by differentiating $\Im = \Im_1 + \Im_2 + \Im_3$ with respect to the strains.

The variational problem (3.3) is solved using the same finite-element mesh as that for the classical Kirchhoff–Love problem. The deflection and its derivatives are approximated by bicubic Hermite polynomials, and the tangential displacements and transverse-shear strains by cubic polynomials. The finite element used has 64 degrees of freedom: 8 degrees $\left(w, \frac{\partial w}{\partial s}, \frac{\partial w}{r \partial \theta}, \frac{\partial^2 w}{r \partial s \partial \theta}, u_0, v_0, u_1, v_1 \right)$ at each corner point and four degrees (u_0, v_0, u_1, v_1) at each node located on the sides of the quadrangle.

The above system of linear algebraic equations is solved in the complex domain by Gaussian elimination. This allows us to find, with high accuracy, the solution of a high-dimensional system of equations, not disturbing its symmetry and bandedness. The displacements found are then used to determine the components of the strain tensor, the thickness component of electric-flux density, and the components of the electric-field strength at an arbitrary point of the finite element.

This approach allows us to solve, at each iteration, the linear problem for shells of revolution under either mechanical or electric loading taking into account the transverse-shear strains. In the case of mechanical loading and open-circuited electrodes, the potential difference between the electrodes can be found from (3.9):

$$V_k - V_{k-1} = \frac{1}{\iint\limits_S \frac{ds}{H_1^k}} \iint\limits_S \left[(e_{ss}^0 + e_{\theta\theta}^0) \frac{H_2^k}{H_1^k} + (\kappa_{ss} + \kappa_{\theta\theta}) \frac{H_3^k}{H_1^k} + (\delta_{ss} + \delta_{\theta\theta}) \frac{H_4^k}{H_1^k} \right] r dr d\theta,$$

where S is the area of the electrodes; k is the layer number. The electrodes can be either continuous or discrete.

To study the effect of feedback on the stiffness, dissipative, and inertial characteristics, we will use the formula

$$Э_3 = (V_k - V_{k-1}) \iint\limits_F \left[(e_{ss}^0 + e_{\theta\theta}^0) \frac{H_2^k}{H_1^k} + (\kappa_{ss} + \kappa_{\theta\theta}) \frac{H_3^k}{H_1^k} + (\delta_{ss} + \delta_{\theta\theta}) \frac{H_4^k}{H_1^k} \right] r dr d\theta,$$

which can be represented as

$$Э_3 = \left(G_1 + i\omega G_2 - \omega^2 G_3\right) \frac{1}{\iint\limits_{S_j} \frac{ds_j}{H_1^k}} \iint\limits_{S_j} \left[\left(e_{ss}^0 + e_{\theta\theta}^0\right) \frac{H_2^k}{H_1^k} + \left(\kappa_{ss} + \kappa_{\theta\theta}\right) \frac{H_3^k}{H_1^k} + \left(\delta_{ss} + \delta_{\theta\theta}\right) \frac{H_4^k}{H_1^k} \right] ds_j$$

$$\times \iint\limits_F \left[\left(e_{ss}^0 + e_{\theta\theta}^0\right) \frac{H_2^k}{H_1^k} + \left(\kappa_{ss} + \kappa_{\theta\theta}\right) \frac{H_3^k}{H_1^k} + \left(\delta_{ss} + \delta_{\theta\theta}\right) \frac{H_4^k}{H_1^k} \right] r ds d\theta,$$

where S_j is the area of the sensor electrode.

The above approach makes it possible to find a solution satisfying the perfect bonding conditions at the interface between the layers and to obtain the level-by-level approximation of the mechanical and electric quantities within each layer.

From these solutions, we obtain, as a special case, the solution of the problem of electroviscoelasticity for inhomogeneous shells of revolution based on the classical Kirchhoff–Love theory.

One of the widely used theories used to determine the stress–strain state of inhomogeneous plates and shells by the FEM is Timoshenko's theory [55]. This is because the functionals appearing in variational problem statements contain only first derivatives of the displacements. In developing the FEM in the linear theory of shells, use is usually made of the so-called five-modulus theory in which the displacement field is characterized by five independent functions: deflection w, two tangential displacements of mid-surface u_0, v_0, and two functions u_1, v_1 characterizing the independent turn of the normal [14, 55]:

$$w = w(s, \theta), \qquad u(s, \theta, z) = u_0(s, \theta) + z u_1(s, \theta), \quad v = v_0(s, \theta) + z v_1(s, \theta).$$

To implement the FEM, the variational problem statement presented in [32, 37] is used. The strains and the displacements are related in a well-known way [14, 52].

To increase the accuracy of calculations upon decrease in the thickness of the shell, i.e., to find a solution coinciding with the solution obtained based on the classical Kirchhoff–Love theory, we will approximate the deflection, its derivatives, tangential displacements and angles of rotation by polynomials (3.13) and (3.14).

As above, we derive a complex system of algebraic equations. This approach allows us to study the vibrations of viscoelastic inhomogeneous shells of revolution by developing a FEM algorithm for either the classical Kirchhoff–Love theory or theories that allow for the transverse-shear strains. The heat-conduction equation with a known heat source can be solved in a similar way as above.

4. Analytic Solutions of Nonlinear Problems of the Vibrations and Self-Heating of Thin-Walled Elements. Analytic solutions are important for studying the vibrations and self-heating of inelastic bodies. On the one hand, they can be used to validate numerical methods, and, on the other hand, they provide a simple way of analyzing the effect of the SHT on the thermomechanical state of inelastic bodies. For example, the maximum SHT can be found from the analytic expression for temperature. Equating it to the degradation point, we can find the critical load.

The analytic solutions of linear and nonlinear problems (nonlinearity of the first type) of the resonant vibrations and self-heating of hinged and clamped thin cylindrical shells, rectangular and circular plates with actuators are presented in [110, 113, 116, 117, 119–121]. Similar solutions for the same elements with sensors are given in [122–124]. The analytic solutions of problems of the active damping of elements with both sensors and actuators are presented in [125–127]. Analytic solutions for elements made of a nonlinear material of the second type were obtained in [41, 42]. Let us consider examples to illustrate how analytic solutions can be found.

4.1. Analytic Solution for a Hinged Rectangular Plate Made of a Physically Nonlinear Material of the First Type. For a sandwich plate with a passive isotropic core layer and two piezoelectric face layers with opposite polarization, the problem is reduced to a nonlinear complex system of differential equations for the deflection and self-heating temperature [120, 123, 126]. The analytic solution to the problem of the active damping of vibrations of elements with sensors and actuators is found by the Bubnov–Galerkin method, using the single-mode approximation of the deflection $\hat{w} = A\tilde{w}(x, y)$, where $\tilde{w}(x, y)$ is the shape function, A is the complex amplitude. In the case of hinged support, the shape function is represented by trigonometric functions automatically satisfying the boundary conditions. The temperature-dependent real and imaginary components of the shear modulus of the passive material (polyethylene) presented in [71] are approximated, with high accuracy, by linear relations $G = G' + G'', G' = G'_0 - G'_1 T, G'' = G''_0 - G''_1 T$. The thermal and mechanical characteristics of the material are presented in [98, 101, 104].

The following cubic equation for the dimensionless quantity $y = T / T_C$ is derived by the Bubnov–Galerkin method:

$$y^3 - e_2 y^2 + e_1 y - e_0 = 0. \tag{4.1}$$

Its coefficients can be found in [120, 123, 126].

After determining the temperature, the amplitude of vibrations can be found by the formulas presented in [120, 123, 126]. Equating y to the degradation point, we obtain an expression for the critical load [120, 123, 126].

4.2. Analytic Solution for a Hinged Plate Made of a Physically Nonlinear Material of the Second Type. We will present the analytic solution to the problem of the vibrations of a hinged rectangular plate made of a physically nonlinear material of the second type. The experimental data [91] on the shear modulus are used and approximated, with hair accuracy, by the functions

$$G' = a_1 - b_1 \Gamma^2, \quad G'' = a_2 - b_2 \Gamma^2 \tag{4.2}$$

$$(a_1 = 2.410 \cdot 10^5 \text{ Pa}, \quad a_2 = 1.810 \cdot 10^5 \text{ Pa}, \quad b_1 = 0.537 \cdot 10^7 \text{ Pa}, \quad b_2 = 0.380 \cdot 10^7 \text{ Pa}).$$

For a hinged plate undergoing resonant vibrations, all quantities can be represented as follows:

$$w = w_{mn} \sin k_m x \sin p_n y, \quad k_m = \frac{m\pi}{a}, \quad p_n = \frac{n\pi}{b} \, (m, n = 1, 2, 3, \dots). \tag{4.3}$$

Using approximations (4.2), (4.3) and the Bubnov–Galerkin method, we obtain a cubic equation of the form (4.1), with coefficients given in [42], for the squared amplitude of transverse displacement $y = |w_{mn}|^2 / h^2$.

The stationary self-heating temperature of the plate with heat-insulated ends can be found by solving the heat-conduction equation with a known heat source. The exact solution for temperature is as follows:

$$\theta = \theta_0 + \theta_1 \cos 2k_m x + \theta_2 \cos 2p_n y + \theta_{12} \cos 2k_m x \cos 2p_n y. \tag{4.4}$$

Expressions for $\theta_0, \theta_1, \theta_2, \theta_{12}$ can be found in [37]. The maximum temperature $\theta_{\max}$ can be found from (4.4). Equating it to the degradation point, we find the critical load.

5. Influence of Various Factors on the Performance of Sensors and Actuators and on the Effectiveness of Active Damping. We will discuss the results, obtained using numerical/analytical solutions, of studying the influence of various factors on the performance of piezoelectric sensors and actuators and the active damping of forced resonant vibrations.

The influence of the following factors was studied: dimensions, arrangement of piezoactive inclusions, mechanical boundary conditions, shear strains, geometrical nonlinearity, physical nonlinearity of the first and second types, combination of geometrical nonlinearity and physical nonlinearity of the second type. Only typical curves illustrating one effect or another are presented below.

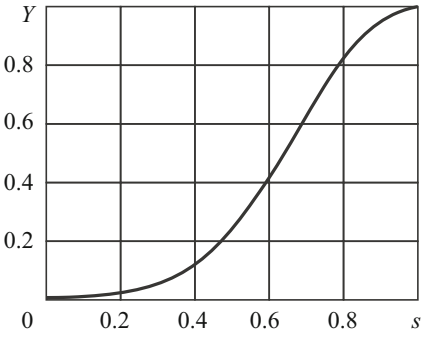

Fig. 5.1

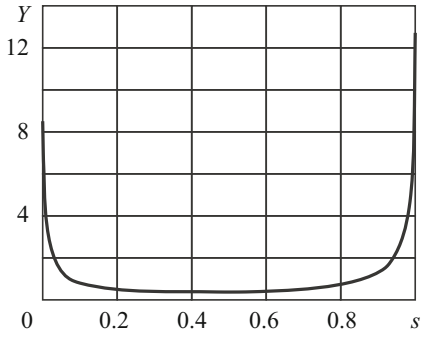

Fig. 5.2

5.1. Influence of the dimensions, arrangement of piezoactive inclusions, and mechanical boundary conditions on their performance. To study the influence of these factors on the active damping of vibrations of thin-walled elements, it is possible to use the analytic solutions of the respective problems. When using numerical methods, it is necessary to analyze various alternatives of arrangement and dimensions of piezoinclusions and to choose the optimal one.

Influence of the Dimensions of Piezoinclusions. The analytic solution to the problem of the vibrations and self-heating of a hinged rectangular plate with an actuator was found in [120] taking into account physical nonlinearity of the first type. Figure 5.1 plots the dimensionless potential difference Y that should be applied to the actuator to balance the mechanical load versus the dimensionless diagonal length $s = l / L$ of the piezoinclusion. It can be seen that this quantity tends to zero as the diagonal length decreases and tends to one as the diagonal length of the piezoinclusion tends to the diagonal length of the plate.

Thus, the performance of the sensor and actuator in a hinged plate will be maximum if its surface is fully coated with piezoinclusions.

Figure 5.2 shows a similar graph $\left(Y = \dfrac{15(a^2 + b^2)}{32a^2 b^2 p_0} V_a (h_0 + h_1)\gamma_{31} \right)$ for a clamped plate [99]. It can be seen there is the optimal dimension of the actuator at which its operation is the most effective. Such graphs for piezoelectric sensors are similar [100–102].

Influence of the Arrangement of Piezoinclusions. The potential difference that should be applied to the actuator to balance the mechanical load on a hinged plate undergoing resonant vibrations is expressed as follows [38]:

$$\overset{0}{M}_{mn} = \frac{ab}{16} \frac{\overset{0}{p}_{mn} k_m p_n}{k_m^2 + p_n^2} \frac{1}{\sin k_m \xi \sin p_n \eta \sin \dfrac{k_n c}{2} \sin \dfrac{p_n d}{2}}, \tag{5.1}$$

where $\overset{0}{M}_{mn}$ is proportional to the potential difference applied to the actuator to balance the mechanical load $\overset{0}{P}$. The center (ξ, η) of the actuator and its dimensions (c, d) are found by minimizing this difference:

$$\sin k_m \xi = 1, \quad \sin p_n \eta = 1, \quad \sin \frac{k_m c}{2} = 1, \quad \sin \frac{p_n d}{2} = 1.$$

For the mode corresponding to the resonant vibrations at the first frequency ω_{11}, the center of the actuator should be selected from $\sin k_1 \xi = 1, \sin p_n \eta = 1$. Its coordinates $\zeta = a / 2, \eta = b / 2$, i.e., the actuator center coincides with the plate center. If the actuator center is located at a different point, we have the surface

$$\overset{0}{M} / \overset{0}{m} = 1 / (\sin k_1 \xi \sin p_1 \eta), \tag{5.2}$$

where $\overset{0}{m} = (ab \overset{0}{p}_{11} k_1 p_1) \Big/ \left[16(k_1^2 + p_1^2) \sin \dfrac{k_1 c}{2} \sin \dfrac{p_1 d}{2} \right]$ is a constant.

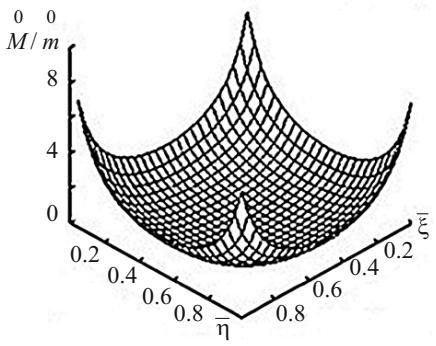

Fig. 5.3

Figure 5.3 shows a surface representing the dependence of M^0/m^0, which is proportional to the potential difference, on the dimensionless coordinates $\bar{\xi} = \xi / a$, $\bar{\eta} = \eta / b$ of the actuator center. As is seen from the figure and formula (5.2), as the coordinates of the actuator center to the edges of the plate, the potential difference applied to it tends to infinity. In the neighborhood of the point $(a/2, b/2)$, there is a large region in which the potential is nearly minimum. Therefore, the center of the actuator can also be placed in this region. The arrangement of actuators for other modes is discussed in [38].

The conclusions are similar for sensors. Let a harmonic load distributed over one of the vibration modes act on the plate. It the plate is hinged, the deflection is expressed as

$$w = w^0_{mn} \sin k_m x \sin p_n y \exp(i\omega t).$$

This vibration mode is maintained with high accuracy if the frequency of loading is close to the resonance. Then the inverse of the charge Q is defined by the following formula [38]:

$$1/Q = A \Big/ \left(\sin k_m \xi \sin p_n \eta \sin \frac{k_m c}{2} \sin \frac{p_n d}{2} \right), \tag{5.3}$$

where A is a constant that does not depend on the coordinates of the center and the dimensions of the actuator.

The main principle of operation of the sensor is that the charge must be maximum at given deflection. Then quantity (5.3) must be minimum.

Comparing formulas (5.1) and (5.3) reveals that the coordinates of the center of the sensor and its dimensions are defined by identical formulas. The above conclusions on the arrangement and dimensions of an actuator for different vibration modes also apply to sensors. If a sensor has the shape of some vibration mode, it will only respond to this mode, i.e., will act as a filter.

The above analysis is general, irrespective of the type of boundary conditions. Let an analysis of the frequencies and vibration modes of an elastic plate have revealed that under nonstationary loading, several modes, say the first four modes, make the major contribution to deformation. Then, choosing appropriately the coordinates of the centers and dimensions of four actuators, it is possible to eliminate their effect on the plate using the above formulas. These four electrodes should be separated from each other, i.e., it is necessary to use four separate square electrodes. Applying the potential differences calculated by the above formulas to these electrodes, we eliminate the four modes, thus reducing the deflection substantially.

When using the first method of damping resonant vibrations, such a potential difference is applied to the actuator that the corresponding mode does not occur under combined mechanical and electric loading. This fact is important for the damping of nonstationary vibrations because the amplitude of nonstationary vibrations is substantially decreased upon elimination of the most energy-intensive mode.

Influence of the Mechanical Boundary Conditions. We will a circular plate as an example [137] to illustrate the influence of mechanical boundary conditions on the performance of the sensors and actuators and on the effectiveness of the active damping of vibrations. Consider a circular sandwich plate of radius R. Its middle layer has thickness h_3 and is made of a passive material. Piezoceramic layers of thicknesses h_1 and h_2 and radius $r_0 \le R$ polarized throughout the thickness are on the

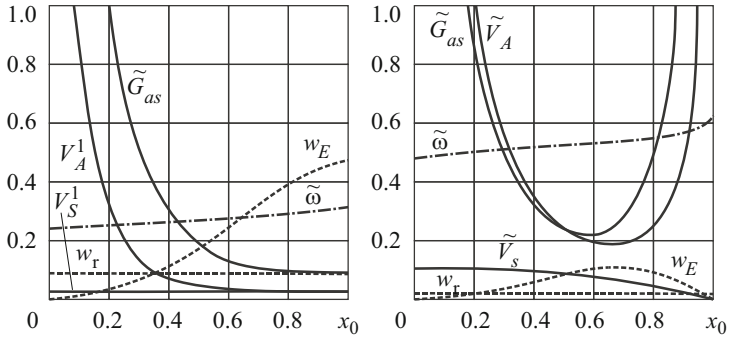

a *b*

Fig. 5.4

faces $z = \pm h_3 / 2$ of the plate. The materials of the passive and piezoactive layers are viscoelastic. The outside and inside surfaces of the piezolayers are coated with continuous infinitely thin electrodes. The inside electrodes are kept at zero potential. Let the piezolayer of thickness h_1 be an actuator, and the piezolayer of thickness h_2 be a sensor. Harmonic pressure $\widetilde{P} = P(r)\cos \omega t$ with nearly resonant frequency ω acts on the plate surface. A voltage $\varphi(-h_3 / 2) - \varphi(-h_3 / 2 - h_1) = \mathrm{Re}(V_A e^{i\omega t})$ is applied to the outside electrodes. Voltage of complex amplitude $V_S = V_S' + iV_S''$ is induced on the open-circuited electrodes of the sensor.

The problem is reduced to a system of nonlinear complex equations presented in [137]. These equations are supplemented with the hinged boundary conditions $u = 0, w = 0, M_r = 0\ (r = R)$ or the clamped boundary conditions $u = 0, w = 0, \vartheta = 0\ (r = R)$.

The boundary and initial conditions for the energy equation are

$$\frac{\partial T}{\partial r} = -\frac{\alpha_r}{\lambda}(T - T_s)\ \ (r = R),\ T = T_0\ \ (t = 0).$$

To solve the problem, we will use the iterative method of step-by-step integration over time in combination with the discrete-orthogonalization method. Numerical results were obtained for a plate made of a viscoelastic polymer with the following temperature-dependent mechanical characteristics [71]: $G' = 968 - 8.69T$ MPa, $G'' = 87.1 - 0.7T$ MPa, E', $E'' = 2(1+\nu)(G', G'')$, $\nu = 0.3636$, $\rho_3 = 929$ kg/m^3, $\lambda = 0.47$ W/(m·°C). The experimental temperature dependence of the properties of TsTStBS-2 piezomaterial is presented in [16, 137].

Figure 5.4 shows the dependence of the following quantities on the dimensionless radius $x_0 = r_0 / L$ of the piezolayers (sensor and actuator): (i) the first resonant frequency of flexural vibrations of the plate $\widetilde{\omega} = \omega \cdot 10^{-4}$ sec^{-1} (dash-and-dot curve); (ii) the maximum deflection amplitudes $w_E = |w_E^1(x = 0)| \cdot 10^5$ m (caused by the voltage $V_A' = 1$ V, $V_A'' = 0$, and $P = 0$ applied to the actuator) and $w_p = |w_p^1(x = 0)| \cdot 10^6$ m (caused by a mechanical load of amplitude $P = 1$ Pa, $V_A' = V_A'' = 0$) (dashed curves), both calculated at the first resonant frequency; (iii) the reference voltages $V_A^1, \widetilde{V}_A = V_A^1 \cdot 10$ V and $V_s^1, \widetilde{V}_s = V_s^1 \cdot 10$ V of the actuator and sensor (solid lines), respectively.

The solid curve of $\widetilde{G}_{as}$ represents the dependence of $\widetilde{G}_{as} = G_{as} \cdot 10^{-1}$ in the feedback relation on the parameter x_0. Figure 5.4*a* represents the hinged plate, while Fig. 5.4*b* represents the clamped plate.

An analysis of the curves w_p^1 (dashed lines) shows that the maximum deflection amplitude under mechanical loading weakly depends on the parameter x_0 characterizing the area of the piezoelectric pads. Except for the rather small neighborhood of the point $x_0 = 0$, the sensor voltage V_s^1 weakly changes with increase in x_0 in the hinged plate and monotonically decreases in the clamped plate. In the case of electric loading of the actuator, however, the maximum deflection amplitude w_E^1 and the reference actuator voltage V_A^1 are nonmonotonic functions of x_0. The deflection w_E^1 reaches the maximum value and the voltage V_A^1 reaches the minimum value when the pads fully cover the outside surface of the hinged plate ($x_0 = 1$) and partially cover the outside surface of the clamped plate ($x_0 = 0.67$). The actuator and the sensor are the most effective when $0.7 \le x_0 \le 1$ for the

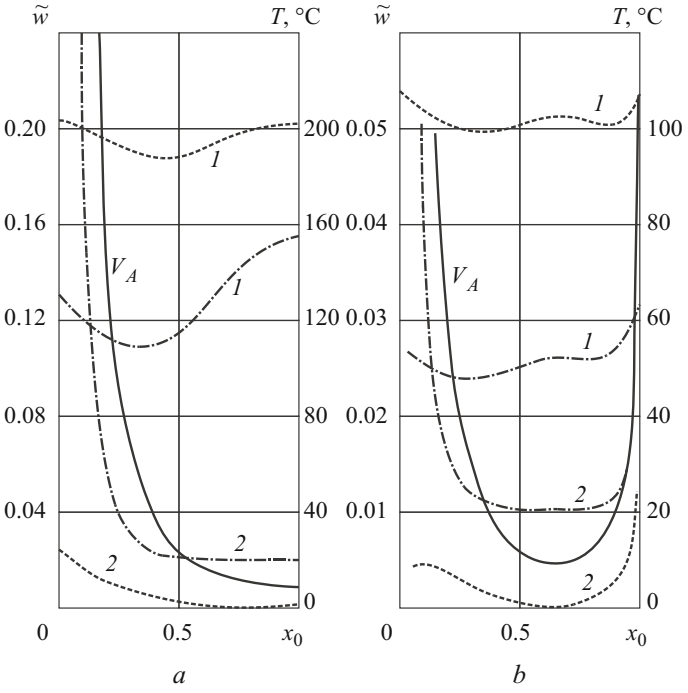

Fig. 5.5

hinged plate and $0.5 \le x_0 < 0.7$ for the clamped plate. With such dimensions of the piezoactive components, the voltage V_A applied to the actuator causes the maximum deflection w_E of the plate and minimum feedback factor (curves $\tilde{G}_{as}$). If the plate is hinged, then $G_{as} \approx 1$.

Figures 5.5*a* and 5.5*b* show the maximum deflection amplitude $\tilde{w} = |w(0)| \cdot 10^3$ m (dashed lines) and self-heating temperature $T_m = T_{\max}(0)$ °C (dash-and-dot lines) calculated at the first resonant frequency versus the parameter x_0. Curves *1* correspond to a mechanical load of amplitude $P = 0.25 \cdot 10^4$ Pa, and curves *2* to the cooperative action of this load and the actuator voltage of amplitude $V_A = |V_A| \cdot 10^{-3}$ V (solid lines) obtained from the sensor voltage taking into account the values of G_{as} in Fig. 5.4.

Comparing dashed curves *1* and *2*, we see that balancing the harmonic mechanical load by the voltage applied in antiphase to the actuator decreases the deflections considerably (curve *2*) over the whole range of the parameter x_0. The maximum self-heating temperature (dash-and-dot curve *2*) decreases to the level of the initial temperature of the plate only for $x_0 > 0.4$ of the hinged plate (Fig. 5.5*a*) and for $0.3 \le x_0 \le 0.9$ of the clamped plate (Fig. 5.5*b*). Active damping of the mechanical vibrations of the plate with nonoptimal actuators may cause a temperature considerably exceeding that of the undamped plate. This is because of the necessity of applying a high voltage V_A to the actuator.

Figure 5.6 shows the steady-state ($\tau = 0.5$) self-heating temperature as a function of the radial coordinate for the following values of x_0, ω_p, and $V_A = |V_A|$:

1) $x_0 = 0.1, \quad \omega_p = 2390 \text{sec}^{-1}, \quad V_A = 2670 \text{ V},$

2) $x_0 = 0.2, \quad \omega_p = 2430 \text{sec}^{-1}, \quad V_A = 700 \text{ V},$

3) $x_0 = 0.4, \quad \omega_p = 2580 \text{sec}^{-1}, \quad V_A = 183 \text{ V},$

4) $x_0 = 1.0, \quad \omega_p = 3030 \text{sec}^{-1}, \quad V_A = 43.1 \text{ V}$

for the hinged plate (рис. 5.6*a*) and

1) $x_0 = 0.1, \quad \omega_p = 4350 \text{ sec}^{-1}, \quad V_A = 1103 \text{ V},$

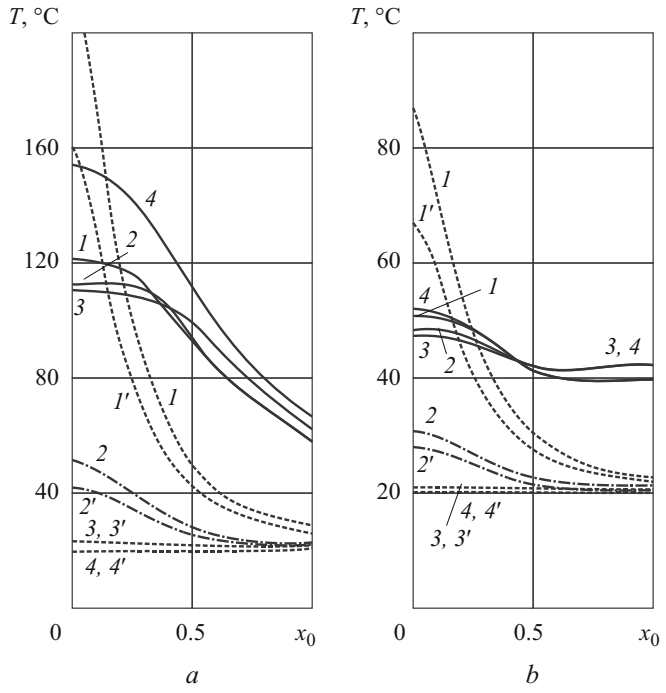

Fig. 5.6

2) $x_0 = 0.2, \quad \omega_p = 4930 \sec^{-1}, \quad V_A = 298.4\ \text{V},$

3) $x_0 = 0.4, \quad \omega_p = 5170 \sec^{-1}, \quad V_A = 82.6\ \text{V},$

4) $x_0 = 0.7, \quad \omega_p = 5370 \sec^{-1}, \quad V_A = 47.46\ \text{V}$

for the clamped plate (рис. 5.6*b*).

Solid curves *1–4* represent the case of mechanical harmonic loading with amplitude $P = 0.25 \cdot 10^4$ Pa ($V_A = 0$). Dashed curves *1–4* represent the case where the mechanical load P and the electric load V_A balancing it act both. Dashed curves *1′–4′* represent the case where the dissipation function does not include the terms responsible for the piezoelectric and dielectric losses in the piezoelectric material. Curves *1–4* in Fig. 5.7 show the radial distribution of the dissipation function.

An analysis of Fig. 5.6 reveals that the radial nonuniformity and level of the self-heating temperature are strongly dependent on the area of the sensor and actuator and the boundary conditions. For the optimal sensor and actuator, the radial distribution of self-heating temperature is uniform and close to the initial temperature in magnitude (dashed curves *3* and *4*). Nonoptimal piezopads, however, cause intensive heating where they are (dashed curves *1* and *2*). Comparing between curves *1*, *2* and *1′*, *2′* shows that the abrupt increase in the self-heating temperature in the area of the pads is due mainly to the voltage of high amplitude applied to the actuator with small area. The terms of the dissipation function that are responsible for the piezo- and dielectric losses should not be neglected (curves *1* and *2* in Fig. 5.7). This means that during active damping of inelastic plates, their vibrations should be controlled not only by the deflection amplitude, but also by the self-heating temperature, which, for certain nonoptimal dimensions of the pads and operation conditions, can reach the Curie point, at which the piezoelectric element loses its functionality because of depolarization.

Figure 5.8 demonstrates the frequency dependences of the maximum deflection amplitude $\widetilde{w} = |w(0)| \cdot 10^4$ m (solid lines) and the sensor voltage $\widetilde{V}_S = |V_S| \cdot 10^{-2}$ V (dash-and-dot lines) for a mechanically loaded ($P = 0.25 \cdot 10^4$ Pa) hinged plate with piezopads of radii $x_0 = 0.2$, 0.4, 1.0 (Fig. 5.8*a*, curves *1*, *2*, *3*) and clamped plate with piezopads of radii $x_0 = 0.2$, 0.4, 0.7 (Fig. 5.8*b*, curves *1*, *2*, *3*). The electrodes of the actuator are short-circuited ($V_A = 0$).

The frequency dependence of the maximum ($x = 0$) steady-state ($\tau = 0.5$) self-heating temperature is shown in Fig. 5.9 for the same dimensions of the pads. Dashed curves *1*, *2*, *3* represent the amplitude–frequency (Fig. 5.8) and

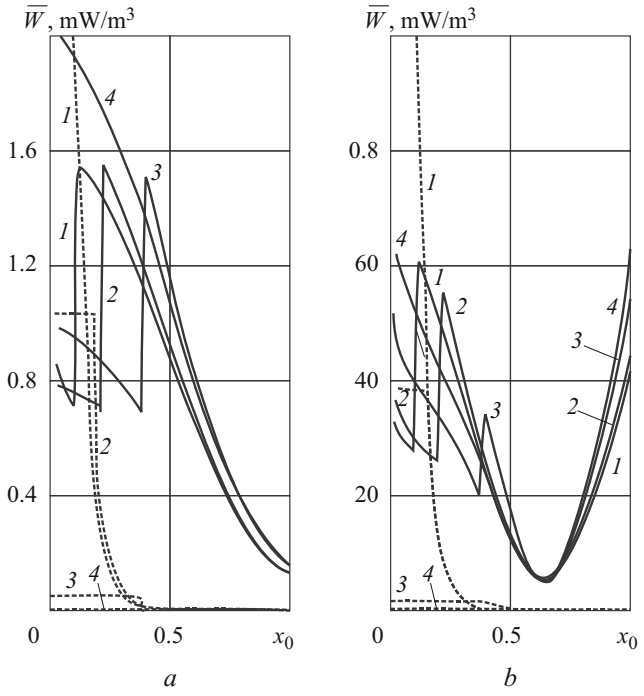

a *b*

Fig. 5.7

temperature–frequency (Fig. 5.9) dependences resulting from the joint action of mechanical load $P = 0.25 \cdot 10^4$ Pa and electric load of amplitudes $V_A = (700, 183, 43.1)$ V for the hinged plate and $V_A = (298, 82.6, 47.5)$ V for the clamped plate.

Figure 5.10 demonstrates how the temperature dependence of the moduli of the passive and piezoactive materials of the mechanically loaded ($P = 0.25 \cdot 10^4$ Pa) plate affects the frequency dependence of the maximum deflection amplitude $\widetilde{w} = |w(0)| \cdot 10^4$ m and voltage $\widetilde{V}_s = |V_s| \cdot 10^{-2}$ V (curves *1* and *2*) for $x_0 = 1.0$ and $x_0 = 0.7$ which correspond to the optimal dimensions of the sensor and the actuator in the hinged (Fig. 5.10*a*) or clamped (Fig. 5.10*b*) plate. The dash-and-dot lines represent the isothermal ($T = T_0$) viscoelastic moduli, while the solid lines the temperature-dependent moduli. Dashed lines *1′* demonstrate the amplitude–frequency dependence of the deflection $\widetilde{w}$ of the plate subject to a mechanical load and voltage V_A = 43.1 V (for hinged boundary conditions) or $V_A = 47.5$ V (for clamped boundary conditions).

An analysis of Fig. 5.10 shows that the effect of the nonlinearity of the first type is manifested as a decreased resonant frequency and soft-nonlinear amplitude–frequency characteristics of the deflection w and voltage V_S. The values of w and V_S at isothermal and thermomechanical resonances are close to each other. Therefore, in calculating the actuator voltage needed to balance the mechanical load, it is possible to use the calculated sensor voltage V_s at the resonance of the isothermal system. Comparing Fig. 5.10*a* and Fig. 5.10*b*, we conclude that the boundary conditions have a strong effect on the resonant frequency, deflection amplitude, self-heating temperature, and optimal dimensions of the sensor and the actuator.

Comparing Fig. 5.8 and Fig. 5.9, we see that the amplitude of forced mechanical vibrations at the principal resonant frequency decreases by two orders of magnitude (Fig. 5.10) and there is almost no self-heating of the plate with optimal piezopads (Fig. 5.9).

5.2. Influence of Shear Strains. To evaluate the effect of the shear strains on the performance of sensors and actuators, analytic solutions and solutions obtained by the finite-element and discrete-orthogonalization methods were used in [32, 35–37]. The refined theories outlined in Sec. 2 with quadratic approximation of shear strains and Timoshenko's theory are used. For a plate and a cylindrical panel made of a transversely isotropic material, the following simple formula for the voltage that should be applied to the actuator to balance the uniform pressure P was derived in [37]:

$$V_a = \frac{P}{(h_0 + h_1)\gamma_{31}} \frac{1}{k_m^2 + p_n^2} [1 + c(k_m^2 + p_n^2)]$$

or

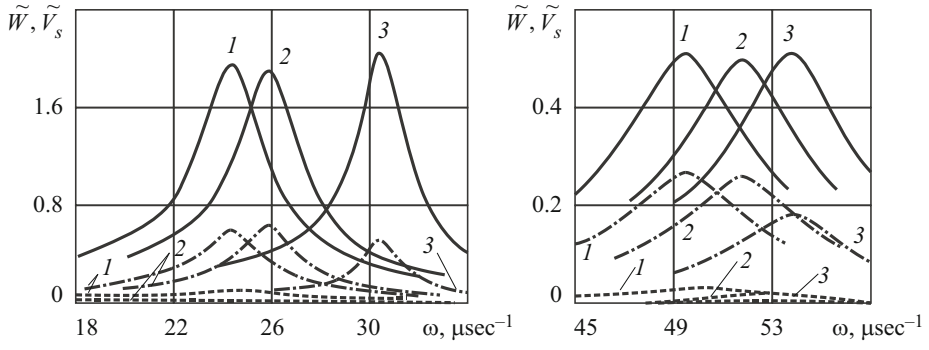

a *b*

Fig. 5.8

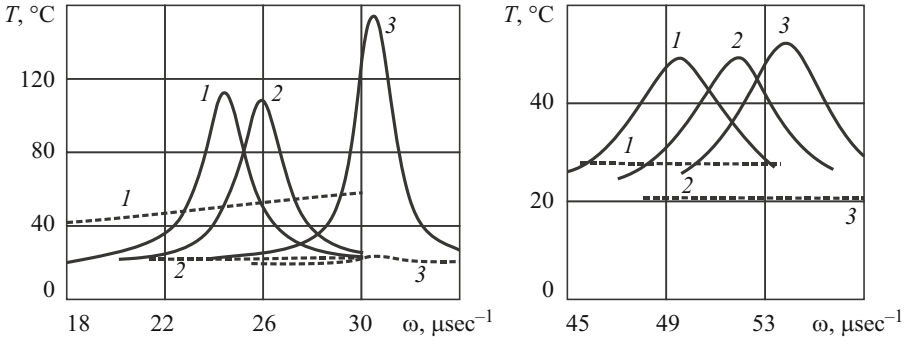

a *b*

Fig. 5.9

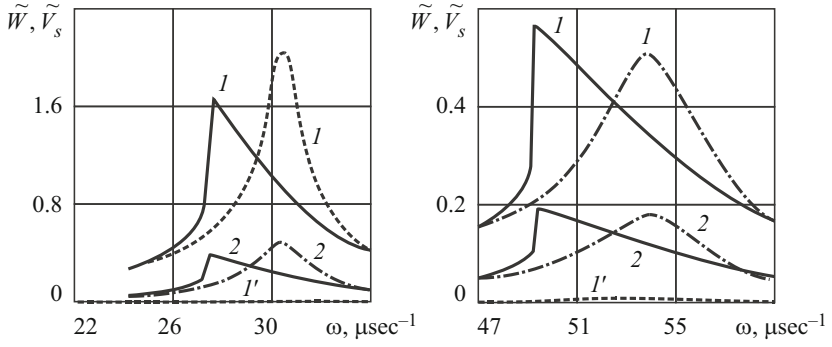

a *b*

Fig. 5.10

$$V_a^T = V_a^K [1 + c(k_m^2 + p_n^2)], \tag{5.4}$$

where V_a^T and V_a^K are the voltages calculated using the Timoshenko and Kirchhoff–Love hypotheses, respectively. If $k^2 = \pi^2 / 12$ in the Timoshenko model, then $c = \left(\frac{D}{B'}\right) = \left(\frac{2}{1-\nu}\right)\left(\frac{G}{G'}\right)\left(\frac{h}{a}\right)^2 \left[m^2 + \left(\frac{a}{b}\right)^2 n^2\right]$ in formula (5.4).

Then we have

$$V_a^{yt} = V_a^{kl} \left\{1 + \frac{2}{1-\nu}\left(\frac{G}{G'}\right)\left(\frac{h}{a}\right)^2 \left[m^2 + \left(\frac{a}{b}\right)^2 n^2\right]\right\}. \tag{5.5}$$

For the principal mode $m = n = 1$, from formula (5.5) it follows that

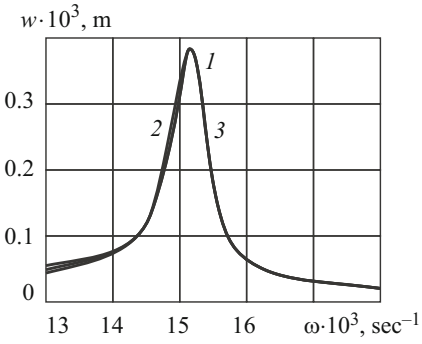

Fig. 5.11

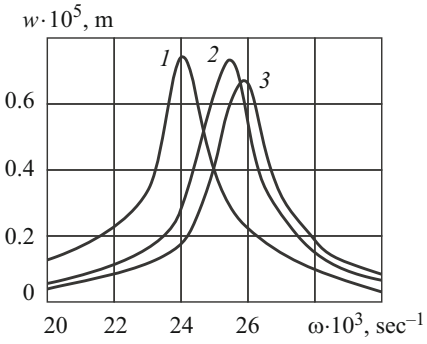

Fig. 5.12

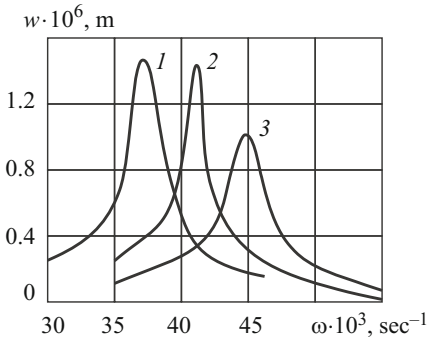

Fig. 5.13

$$V_a^{yt} = V_a^{kl}\left\{1+\frac{2}{1-\nu}\left(\frac{G}{G'}\right)\left(\frac{h}{a}\right)^2\left[1+\left(\frac{a}{b}\right)^2\right]\right\}. \tag{5.6}$$

As is seen from (5.6), the correction to the classical result depends on the ratio of shear moduli of the transversely isotropic material (G/G') and the ratio of the thickness h of the plate to the dimension a. Depending on their values, the correction may appear very large. A similar solution for the vibrations of a plate with sensors is presented in [37], where formulas for the charge on the sensor are given as well.

The influence of the shear strains on the performance of sensors and actuators and on the effectiveness of the active damping of the vibrations of a cylindrical panel and a rectangular plate hinged at the edges was studied in detail in [32, 35–37]. It was shown that the refined theories described in Sec. 2 lead to very close results.

The vibrations of a hinged cylindrical piezoelectric panel of thickness H and radius R under uniformly distributed pressure $P = P_0 \cos \omega t$ were considered in [35–37]. The electroded surfaces were kept at zero potential. This problem was also solved analytically. The panel is made of a PZT-ES-65 piezoelectric material whose complex characteristics are presented in [143].

The load on and the geometry of the panel are characterized by the following parameters: $P_0 = 10^4$ Pa, $R = 0.1$ m, $a = L =$ 0.1 m, $b = R\theta = 0.1$ m, $r_1 = 0,09$ м, $r_2 = 0,11$ м, $H = 0.001$ m. The thermal conductivity and density of the face layers: $\lambda = 1.25$ W/(m·°C), $\rho = 0.75 \cdot 10^4$ kg/m^3. Heat transfer between the environment and the panel is constant ($\alpha_T = 25$ W/(m^2·°C)). Figures 5.11–5.13 show the amplitude–frequency characteristics for $H/R = 0.01$, $P_0 = 10^2$ Pa, $H/R = 0.1$, $P_0 = 10^4$ Pa, $H/R = 0.2$, $P_0 = 10^4$ Pa, respectively.

Curves *1* correspond to the FEM, curves *2* to the refined theory, and curves *3* to the Kirchhoff–Love hypotheses. These results disregard the nonlinearity. Figures 5.14 and 5.15 show the amplitude–frequency and temperature-frequency characteristics allowing for physical nonlinearity of the first type. Curves *2* correspond to the linear problem, and curves *1* to the nonlinear problem [143].

It can be seen from Fig. 5.11, the results for a thin shell ($H/R = 0.01$) obtained with all the theories are in good agreement. It is also seen from Figs. 5.11–5.13 that the amplitudes at the resonant frequency obtained with the refined and three-dimensional theories are in very good agreement. Moreover, the results obtained using the analytic solution and the FEM are also in very good agreement.

The one-dimensional problem of the forced vibrations and self-heating of a viscoelastic circular plate of thickness h and radius R with piezoelectric actuators was solved in [132] using the discrete-orthogonalization method and Timoshenko hypotheses. The outside surfaces $z = \pm h/2$ of the plate are covered by actuators of equal thickness δ and radius r_0. The material of the passive layer is viscoelastic and isotropic, and the actuators are made of viscoelastic piezoceramics and oppositely polarized. It is assumed that the polarization in the directions $z > 0$ and $z < 0$ is characterized by the piezoelectric moduli d_{31} and $(-d_{31})$, respectively. The outside surfaces of the actuators and the interfaces between the actuators and the passive layer are covered by infinitely thin electrodes.

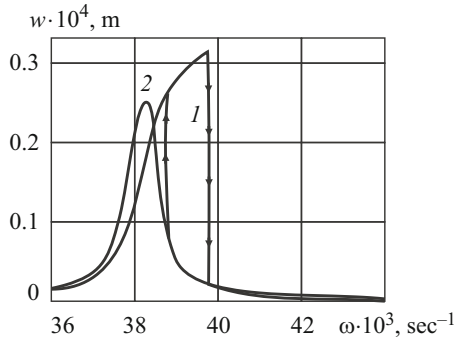

Fig. 5.14

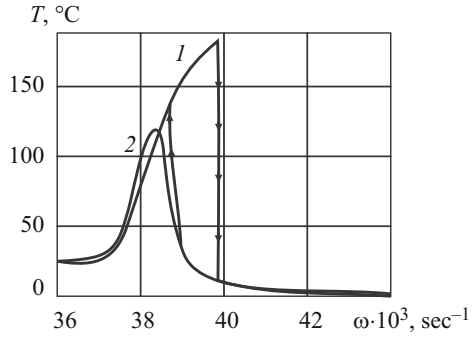

Fig. 5.15

The plate is under surface pressure $P = P_0 \cos \omega t$ harmonically varying with time t with nearly resonant circular frequency ω. A voltage $\psi(h/2+\delta) - \psi(-h/2-\delta) = 2\,\mathrm{Re}\,(Ve^{i\omega t})$ of the same frequency as that of the mechanical load is applied to the outside electrodes of the actuator. The inside electrodes are kept at zero potential. The viscoelastic behavior of the passive and piezoactive materials of the plate is described by the concept of complex moduli depending on the SHT. To model the electromechanical vibrations of the plate, the Timoshenko hypotheses for the mechanical variables are used. As for the electric field variables, it is assumed that the tangential components of electric-flux density (D_r, D_θ) in the piezolayers can be neglected compared with the normal component (D_z), which is independent of the thickness coordinate. The electrostatic equations are satisfied identically, and the tangential components of the electric-field strength (E_r, E_θ) are obtained from the three-dimensional equations of state of polarized piezoceramics. The self-heating temperature is assumed to be constant throughout the thickness of the plate.

Due to the symmetry of the plate, the polarization of the actuators, and the loading, purely flexural axisymmetric vibrations are excited in the plate. To solve the nonlinear problem, we will use the iterative method of step-by-step integration over time in combination with the discrete-orthogonalization method. After the dissipation function is found, the heat-conduction problem is solved by the explicit finite-difference method. To determine the optimal voltage V_A that should be applied to the actuator t damp the forced vibrations generated by surface pressure with amplitude P_0, we use the linear relation $V_A = -k_A P_0$, where k_A is the complex control ratio. The influence of shear strain and electromechanical coupling on the fundamental characteristics of vibrations of a polymer plate with TsTStBS-2 piezoceramic actuators under mechanical or/and electric loading was studied in [82]. The complex shear modulus of the passive polymer depends on the SHT as $G' = 968 - 8.69T$ MPa, $G'' = 87.1 - 0.7T$ MPa. The other characteristics are the following: $\nu = 0.3636$, $\rho = 929$ kg/m^3, $\lambda = 0.47$ W/(m·°C), $\alpha_0 = \alpha_R = 2$ W/(m^2·°C).

The temperature dependence of the electromechanical characteristics of piezoceramics is described in [16, 82].

Moreover, the coefficient $\nu_E = -s_{12}^0 / s_{11}^0$ is assumed constant and real; $\rho_* = 7520$ kg/m^3, $T_0 = T_c = T_R = 20$ °C. When allowing for shear strain, we set $k_s = 5/6$. For a clamped plate of radius $R = 0.2$ m and thickness $h = 0.04$ m with actuators of thickness $\delta = 0.1 \cdot 10^{-3}$ m and relative radius $x_0 = 0.8$ under harmonic pressure of intensity $P_0 = 1$ Pa, Figs. 5.16*a* and 5.16*b* show the radial distribution of the normalized deflection amplitude $(V_n, V_n^*) = |w_p| 10^{-2} / (A_n, A_n^*)$, $n = 1, 2$, and total curvatures $(\tilde{\kappa}_n, \tilde{\kappa}_n^*) = |\kappa| 10^{-2} / (A_n, A_n^*)$, respectively. The solid lines represent the calculated results obtained using the Kirchhoff–Love hypotheses, and the dashed lines represent the calculated results indicated by "asterisk" and obtained taking into account shear strains. Curves *1* ($n = 1$) correspond to the first flexural mode for $\omega_p = 0.532 \cdot 10^4$ sec^{-1}, $A_1 = 0.2045 \cdot 10^{-7}$ m (solid lines), and curves *2* ($n = 2$) to the second mode for $\omega_p = 0.219 \cdot 10^5$ sec^{-1}, $A_2 = 0.1016 \cdot 10^{-8}$ m (dashed lines). Thus, allowing for the shear strain in calculating the oscillatory characteristics of plates decreases the resonant frequencies ($\omega_p^* < \omega_p$), increases the maximum deflection ($A_{1,2}^* > A_{1,2}$), and hardly changes the vibration mode. To a greater extent, the shear strains cause redistribution of the normalized total curvature along the radius of the plate in the first and, especially, second vibration modes.

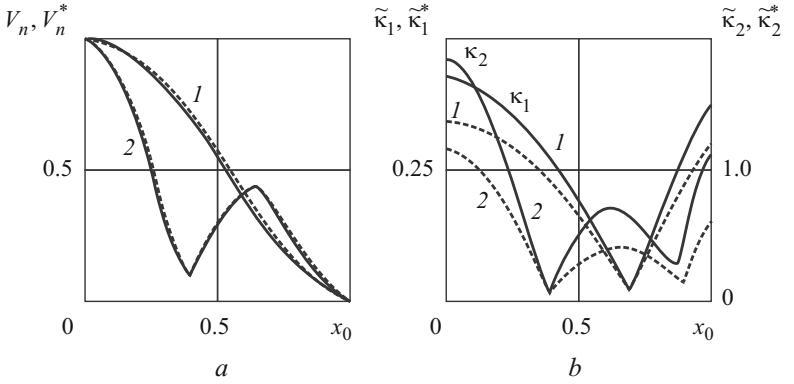

Fig. 5.16

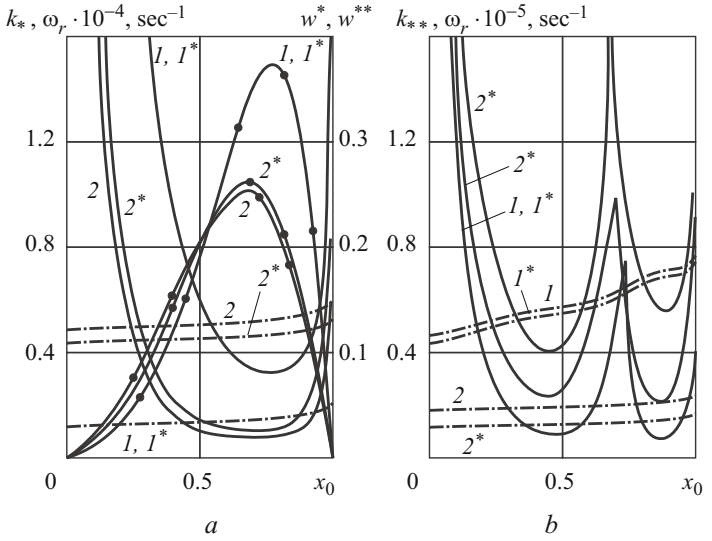

Fig. 5.17

This factor is decisive in calculating the influence of the shear strains on the control ratio. The effect of these factors weakens with decrease in the thickness of the plate ($h / R \le 1/20$).

Figure 5.17*a* and 5.17*b* show the resonant frequencies ω_p (dash-and-dot lines) and control ratios $k_* = |k_A| \cdot 10$ V/Pa, $k_{**} = |k_A| \cdot 10^2$ V/Pa (solid lines) for damping the first (Fig. 5.17*a*) and the second (Fig. 5.17*b*) modes of forced flexural vibrations calculated using the Kirchhoff–Love hypotheses (curves *1* and *2*) and taking into account the shear strains (curves 1^* and 2^*) for a clamped plate with an of radius x_0 and thickness $\delta = 0.1 \cdot 10^{-3}$ m under pressure $P_0 = 1$ Pa. Curves *1* and 1^* represent the plate of thickness $h = 0.01$ m, and curves *2* and 2^* represent the plate of thickness $h = 0.04$ m. Moreover, the solid curves with full circles in Fig. 5.17*a* show the variation in the maximum amplitude $w^* = |w_E(0)| \cdot 10^4$ m for the plate of thickness $h = 0.01$ m (curves *1* and 1^*) and the amplitude $w^{**} = |w_E(0)| \cdot 10^5$ m for the plate of thickness $h = 0.04$ m (curves *2* and 2^*) under electric loading of unit potential $V' = 1$ V, $V'' = 0$.

Thus, the actuator is the most effective (optimal) when the deflection amplitude is maximum under electric loading (solid lines with full circles). The control ratio will be minimum (solid lines). The dimensions of such an actuator depend on the thickness of the passive layer. When a clamped plate vibrates at the first resonant frequency, the maximum electrically excited amplitudes and control ratio are many-valued functions of the actuator radius x_0, and the control ratio is minimum when the outside surfaces of the plate ($0.6 \le x_0 \le 0.8$) are partially covered by piezolayers. Allowing for the shear strains somewhat increases the control ratio. This effect becomes stronger with increase in the thickness of the plate and in the frequency from the second resonant one and higher. If the plate undergoes forced vibrations at the second resonant frequency, the control ratio is a many-valued function of x_0 (Fig. 5.17*b*).

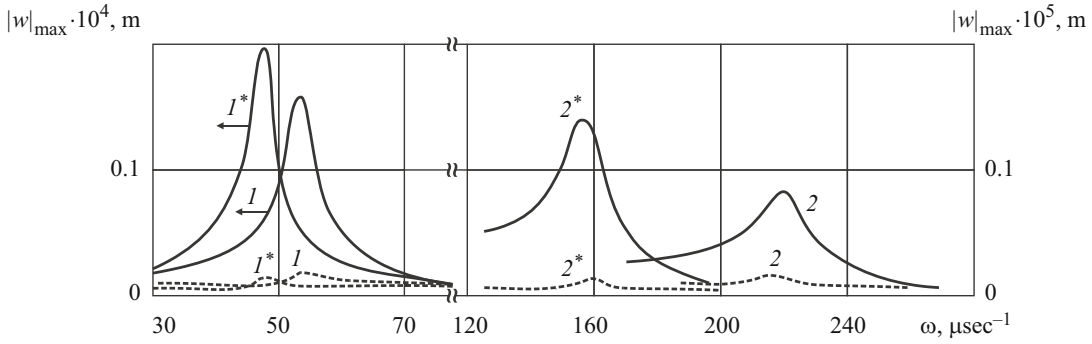

Fig. 5.18

Figure 5.18 shows the amplitude–frequency characteristics of a clamped plate of thickness $h = 0.04$ m with an actuator of relative radius $x_0 = 0.8$ and thickness $\delta = 0.1\cdot 10^{-3}$ m harmonically excited in the frequency range of the first (curves *1* and *1**) and second (curves *2* and *2**) resonances. Curves *1* and *2* correspond to the Kirchhoff–Love hypotheses, while curves *1** and *2** to allowing for the shear strains. The solid lines represent the vibrations excited by external pressure $P_0 = 0.8\cdot 10^3$ Pa. The dashed lines represent the vibrations excited by mechanical loading in combination with an electric potential V_A of the same frequency applied in antiphase to the actuators, the active (V_A') and reactive (V_A'') components having the following values: $V_A' = -6.923$ V, $V_A'' = -0.2856\cdot 10^{-1}$ V (curves *1*, *1**), $V_A' = -8.848$ V, $V_A'' = -0.5365\cdot 10^{-1}$ V (curves *2*), $V_A' = -1.990$ V, $V_A'' = -0.3166$ V (curves *1*, *1**), $V_A' = -5.541$ V, $V_A'' = -0.3418$ V (curves *2*, *2**). These results, as in the above examples, were obtained for temperature-independent ($T = T_R$) material characteristics. Comparing the solid and dashed lines in Fig. 5.18, we conclude that it is possible to damp the mechanically excited resonant vibrations of the plate by using an actuator of optimal configuration and applying to it, in antiphase, a voltage of the same frequency and appropriate amplitude. It can be seen from the calculated results that allowing for the shear strains decreases the resonant frequencies and increases the deflection amplitude at these frequencies.

From Fig. 5.18 and numerical experiments, it also follows that an actuator of the same optimal dimensions can be used to damp the forced vibrations of a plate at either the first or second resonant frequency. However, since the first vibration mode is very energy-intensive, it can be damped by applying to the actuator a voltage of higher amplitude than that for the second mode. Moreover, the reactive component V_A'' hardly contributes to the amplitude–frequency characteristics (dashed lines). Figures 5.19*a–d* show how the shear strains and the temperature dependence of the electromechanical properties of the materials affect the frequency dependence of the maximum deflection amplitude $w_{\max} = |w(0)|/h$ and self-heating temperature $T_{\max} = T(0)$ for a plate forced to vibrate by load $P_0 = 1.4\cdot 10^3$ Pa.

Figures 5.19*a*, *c* and 5.19*b*, *d* characterize the behavior of the system at the first and second resonant frequencies, respectively. The figures represent a clamped plate of radius $R = 0.2$ m with an actuator of thickness $\delta = 0.1\cdot 10^{-3}$ m and relative radius $x_0 = 0.8$ for $\alpha = 2$ W/(m$^2\cdot$°C), $\lambda = 0.47$ W/(m·°C), and $T_0 = T_R = 20$ °C. The solid curves represent temperature-independent material properties, while the dashed curves represent temperature-dependent material properties. Curves *1* and *2* correspond to the Kirchhoff–Love hypotheses, while curves *1** and *2** to allowing for the shear strains.

From Fig. 5.19 it can be seen that the effect of the temperature dependence of the material properties (dashed lines) is manifested as soft-nonlinear amplitude– and temperature–frequency characteristics and decreased resonant frequency, amplitude, and self-heating temperature. Compared to the isothermal case (solid lines), the effect of thermomechanical coupling in the refined problem statement is of the same order as in the classical statement.

5.3. Influence of Geometrical Nonlinearity. The influence of nonlinearity and self-heating on the vibrations and self-heating of thin-walled elements with sensors and actuators was studied in [25, 26, 33, 46, 51, 101, 102, 112, 131, 134, 136]. Let us consider, as an example, a flexible circular sandwich plate of radius *R*. Its core layer of thickness h_0 is made of an isotropic passive material, and two outside layers of thickness h_1 are made of transversely isotropic piezoactive materials with identical properties, but opposite polarization across the thickness [46]. The upper ($z \ge h_0/2$) and lower ($z \le -h_0/2$) piezoelectric layers are characterized by piezoelectric moduli $-d_{31}$ and d_{31}, respectively. The outside and inside surfaces of the piezoelectric actuators are electroded. The inside electrodes are kept at zero potential.

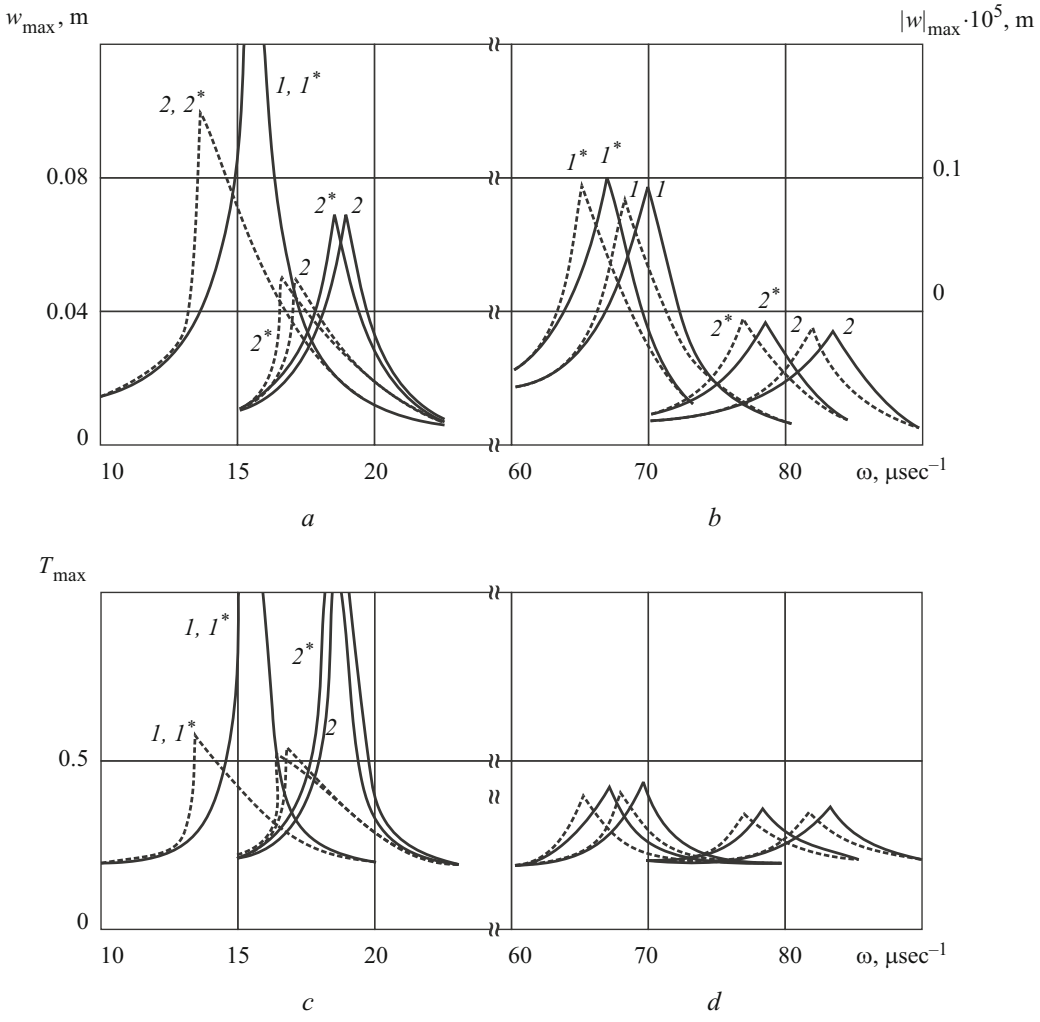

Fig. 5.19

The plate is under a surface pressure harmonically varying with time t with nearly resonant circular frequency ω. A potential difference $\varphi(h_0/2+h_1)-\varphi(-h_0/2-h_1)=\mathrm{Re}(2V_A e^{i\omega t})$ with frequency of the mechanical load is applied to the actuator of radius $r=r_0\le R$. The electrodes are short-circuited ($V_A=0$) in the region $r>r_0$. The radial edge of the plate is free and the transverse edge is hinged or clamped. Moreover, the plate transfers heat by convection to the environment of temperature T_s. For active damping of the forced vibrations of the plate caused by mechanical loading, it is necessary to solve the mechanical problem to find the amplitude and phase of the voltage to be applied to the actuator to balance the mechanical load.

The vibrations of the plate are described using the Kirchhoff–Love hypotheses supplemented with analogous hypotheses on the distribution of electric-field variables (see Sec. 3.2). The dissipative properties of the passive and piezoactive materials are described using the concept of complex characteristics. The self-heating temperature is assumed to be constant throughout the thickness of the plate. Let the strains be small, but the squared angles of rotation are kept in the kinematic equations. The equations of motion are nonlinear as well.

The problem statement and problem-solving method can be found [46]. Two types of mechanical boundary conditions are considered: hinging and clamping. In solving the problem, not only the principal frequency (frequency of loading), but also other harmonics are kept so that the oscillatory process is polyharmonic. The result is an approximate system of nonlinear differential equations that can be solved by the iterative quasilinearization method. At each iteration, the linearized system of ordinary differential equations is integrated by the discrete-orthogonalization method.

Let us consider a circular plate made of a passive viscoelastic material with characteristics presented in Sec. 5.2. The piezoelectric actuators are made of TsTStBS-2 viscoelastic ceramics [82]. The dimensions of the plate are the following: $R=0.2$ m, $\varepsilon=0.1\cdot 10^{-3}$ m, $h_0=0.01$ m, $h_1=0.5\cdot 10^{-6}$ m. Since the load causes mainly flexural vibrations of the plate, we will consider

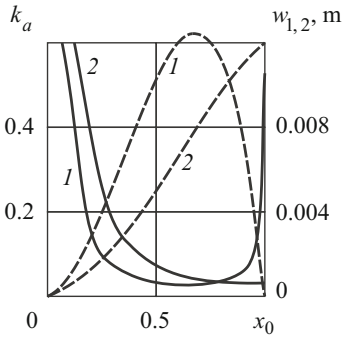

Fig. 5.20

frequencies close to the first bending resonance. Three types of loading of the plate are considered: mechanical, electric, and antiphase action of both. Let the mechanical load be uniform surface pressure of amplitude $q'_z = q_0$. To balance it, it is necessary to calculate the voltage V_A to be applied to the actuator. Similarly to the linear problem [50], we assume that the relation between V_A and q_0 is linear: $V_A = k_a(x_0)q_0$, where $x_0 = r_0 / R$ is the dimensionless radius of the circular actuator. The control ratio k_a is calculated as the ratio of the maximum deflection amplitude w_p induced by a unit mechanical load ($q_0 = 1$ Pa) at the linear resonant frequency and the deflection amplitude w_E induced by applying a unit voltage ($V'_A = 1$ V, $V''_A = 0$) to the actuator, so that $k_A = |w_{p\max}|/|w_{E\max}|$.

If the mechanical load varies harmonically with frequency ω, then the electric load must vary as $V_A \cos(\omega t + \pi) = -V_A \cos \omega t$.

Figure 5.20 shows the control ratio k_a (solid lines) and the maximum relative deflections $w_1 = 4|w_E(0)|/h_0$ and $w_2 = |w_E(0)|/h_0$ (dashed lines) caused by a unit electric load versus the dimensionless radius x_0 of the circular actuator at linear resonant frequency ω_p. Curves *1* correspond to the clamped boundary conditions, while curves *2* to the hinged boundary conditions. Figure 5.20 shows that actuators with radius $x_0 = 0.67$ on the clamped plate and $x_0 = 1$ on the hinged plate induce the maximum deflection at the minimum value of k_a. Such actuators are the most effective in active damping of forced mechanical vibrations.

Numerical results on the effects of nonlinearity are shown in Figs. 5.21–5.24, which present the solutions of linear (dashed lines) and geometrically nonlinear (solid lines) problems. Figures 5.21*a*, 5.22*a*, and 5.23*a* correspond to the hinged boundary conditions, and Figs. 5.21*b*, 5.22*b*, and 5.23*b* to the clamped boundary conditions.

Figure 5.21 shows the frequency dependence of the maximum deflection amplitude $\widetilde{w} = |w(0)|/h_0$ of a plate under a mechanical load of the following amplitudes $q_0 \cdot 10^{-4}$ [Pa]: 0.05 (curve *1*), 0.10 (curve *2*), 0.15 (curve *3*), 0.20 (curve *4*), 0.30 (curve *5*), 0.35 (curve *6*). The electric load $V_A = 0$. For these amplitudes, Fig. 5.22 shows the temperature–frequency dependence of the maximum stationary ($\tau = 0.1$) self-heating temperature for convective heat transfer coefficient $\alpha_n = \alpha_R = 15$ W/(m^2·°C) on the faces of the plate.

From Fig. 5.21 it follows that when the load induces the maximum relative deflection $\widetilde{w} \le 0.2$, it is possible to solve the linear problem. It can be seen that if the plate is clamped, the load under which such a problem statement is valid is higher. For the clamped boundary conditions, the self-heating temperature (curves *4*, Fig. 5.22*b*) is higher than for the hinged boundary conditions (curves *1*, Fig. 5.22*a*). With increase in the relative deflection amplitude ($\widetilde{w} > 0.2$), the effect of geometrical nonlinearity becomes stronger and manifests itself as an increased resonant frequency and hard-nonlinear amplitude– and temperature–frequency characteristics.

Figures 5.23*a* and 5.23*b* show the frequency-dependence of the maximum deflection amplitude $w_E = |w(0)|/h_0$ and frequency-dependence of the self-heating temperature T_m (calculated for linear (dashed lines) and nonlinear (solid lines) problem statements for a hinged plate with the optimal actuator ($x_0 = 1$) to which electric potentials $\pm V_A = 46.8$ V are applied. It can be seen that effects of nonlinearity are similar to the case of mechanical loading. With such loading, the solutions of the linear and nonlinear problems coincide with curves *3* in Fig. 5.21*a* and Fig. 5.22*a*. The dash-and-dot curves in Fig. 5.23 represent the frequency-dependence of the relative deflection $w_{pE} = |w(0)|/h_0 \cdot 10^2$ and the temperature–frequency characteristics of the

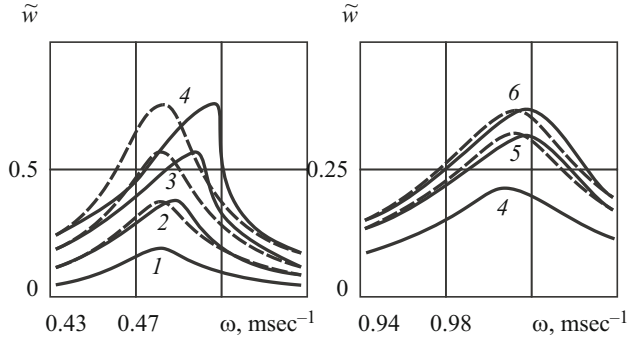

Fig. 5.21

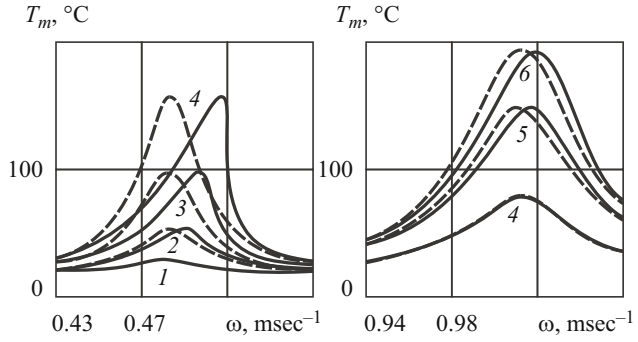

Fig. 5.22

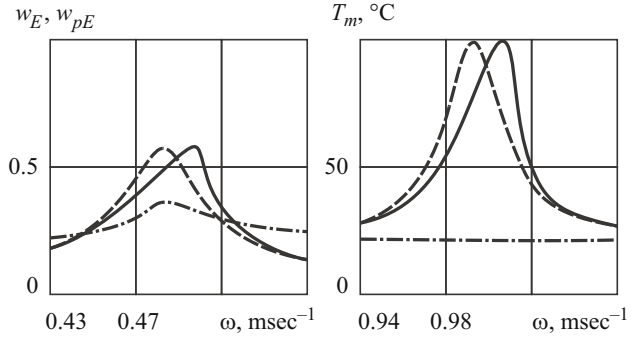

Fig. 5.23

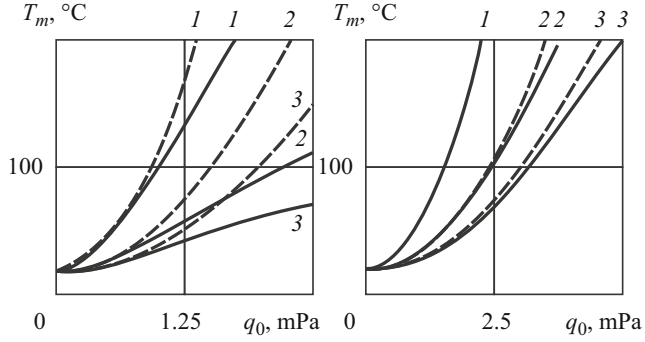

Fig. 5.24

plate under the combined action of mechanical load $q_0 = 0.15 \cdot 10^4$ Pa and voltage $\pm V_A = 46.8$ V applied in antiphase to the actuator to balance the mechanical load. They demonstrate the result of active damping of the mechanical vibrations of the plate.

Figure 5.24 shows the dependence of the maximum self-heating temperature T_m on the amplitude of mechanical load q_0 for heat-transfer coefficients $\alpha_n = \alpha_R = 5$, 15, 25 W/(m^2·°C) (curves *1–3*). The numerical results correspond to linear resonant frequencies $\omega_p = 482$ sec^{-1} for the hinged plate (Fig. 5.24*a*) and $\omega_p = 1010$ sec^{-1} for the clamped plate (Fig. 5.24*b*) in the linear (dashed lines) and geometrically nonlinear (solid lines) cases. The asterisk on the ordinate axis indicates the Curie point $T_C = 180$ °C at which TsTStBS-2 piezoceramic depolarizes. It can be seen from Fig. 5.24 that for active damping of the vibrations of viscoelastic plates, it is necessarily necessary to calculate the self-heating temperature, which depends not only on the amplitude of the load, but also on the boundary and heat-transfer conditions. Allowing for geometrical nonlinearity reduces the self-heating temperature.

Assuming that the piezoactuator loses its functionality at the Curie point, it is possible to determine the critical amplitude of the mechanical load, given heat-transfer and boundary conditions.

5.4. Influence of Nonlinearity of the First Type. The effect of nonlinearity of the first type on the amplitude- and temperature–frequency characteristics of plates and shells was studied in [54, 113–127]. Following [54], we will study the influence of the feedback factor G_2 on the effectiveness of damping by solving the problem of the active damping of a clamped cylindrical sandwich panel of thickness $H = 2h_1 + h_2$ with viscoelastic core layer under uniformly distributed pressure $P = P_0 \cos \omega t$. It transfers heat by convection to the environment of temperature T_C.

The outside layers of the panel are made of TsTStBS-2 piezoelectric whose thermal and temperature-dependent mechanical characteristics are given in [82]. The complex shear modulus $G = G' + iG''$ of the passive material depends on temperature and is calculated by the formulas

$$G' = [968 - 8.69(T - T_0)]A_0, \quad G'' = [87.1 - 0.7(T - T_0)]A_0, \quad A_0 = 10^6 \text{ Pa}, \ \nu = 0.36.$$

These data are presented in [54] and describe the behavior of the material over a wide temperature range. Let the melting point $T = 140$ °C. The geometrical parameters of the shell, loading and heat-transfer conditions are the following:

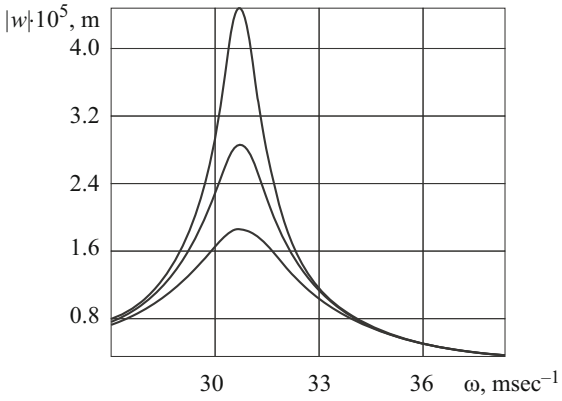

Fig. 5.25

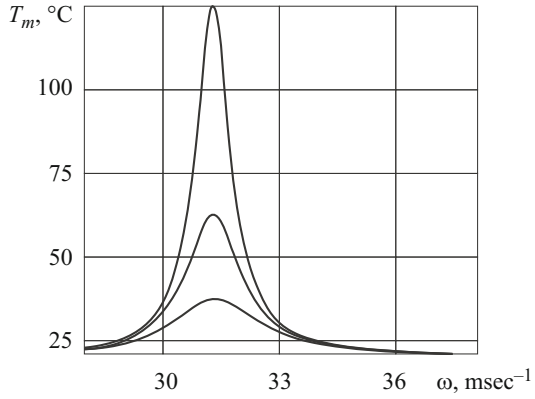

Fig. 5.26

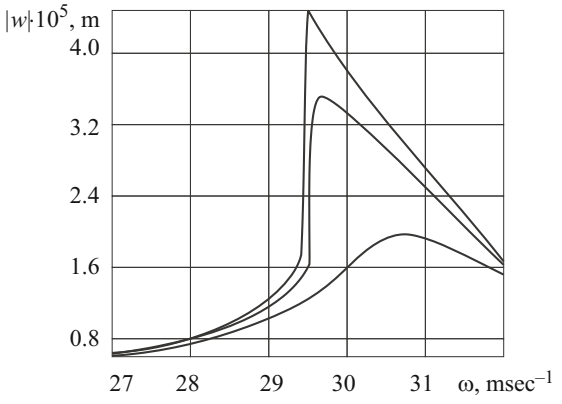

Fig. 5.27

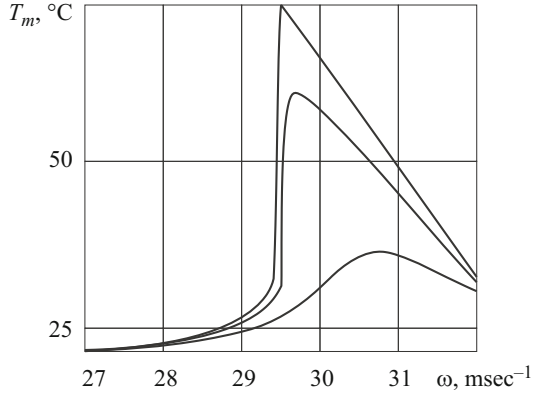

Fig. 5.28

$R = 0.1$ m, $L = 0.1$ m, $0 \le \theta \le \pi/3$, $H = 0.01$ m, $2h_1 = 0.0002$ m, $h_2 = 0.0098$ m,

$P_0 = 10^4$ Pa, $\alpha_T = 20$ W/(m^2·°C), $\lambda_T = 0.47$ W/(m·°C), $T_C = T_0 = 20$ °C,

$\rho = 0.929 \cdot 10^3$ kg/m^3.

Figures 5.25 and 5.26 show the amplitude- and temperature–frequency (in °C) characteristics at the first resonance for different values of feedback factors G_2 and $G_1 = G_3 = 0$ and the temperature-independent properties of the passive material. The upper, middle, and lower curves correspond to $G_2 = 0, G_2 = 0.2 \cdot 10^{-5}, G_2 = 0.5 \cdot 10^{-5}$. It can be seen that the feedback factor has a strong effect on the amplitude of vibrations and self-heating temperature.

Figures 5.27 and 5.28 illustrate the influence of physical nonlinearity of the first type and the feedback factor on the amplitude- and temperature–frequency characteristics. Sharp changes in these characteristics typical for physical nonlinearity can be seen.

As the feedback factor increases, these characteristics approach the dynamic characteristics for temperature-independent properties of the material.

5.5. Influence of Nonlinearity of the Second Type. The influence of this nonlinearity on the operation of piezoelectric sensors and actuators and on the effectiveness of active damping of thin-walled elements was studied in [40–42]. Let us consider, as an example, a sandwich shell of revolution. Its core layer of thickness h_2 is made of inelastic isotropic passive material and two identical outside layers, each of thickness h_1, are oppositely polarized. Uniformly distributed surface harmonic pressure $q_z = q \cos \omega t$ with nearly resonant frequency ω acts on the shell. The shell is hinged at the ends. It cools by convection. To model the electromechanical behavior of this shell, we will use the Kirchhoff–Love hypotheses for mechanical variables and assumptions for electric variables.

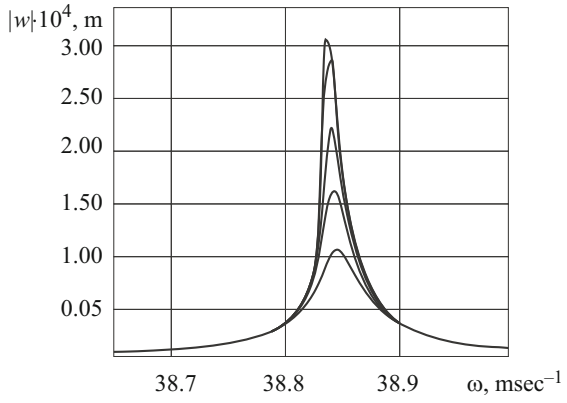

Fig. 5.29

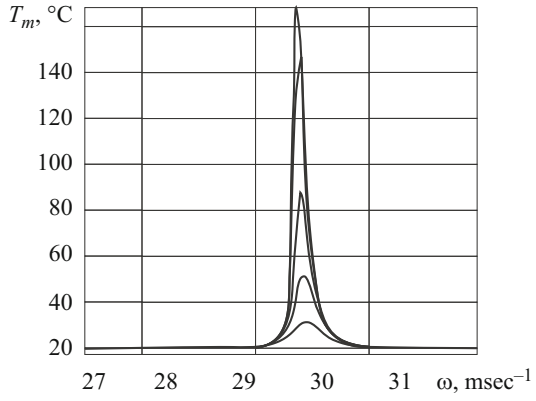

Fig. 5.30

Following [10, 142], we will model the mechanical behavior of the material assuming that the components of the complex shear modulus depend on the second invariant of the deviatoric strain tensor as follows:

$$G' = G(1 - rI_2^{\alpha}), \quad G'' = gGI_2^{\alpha}, \tag{5.7}$$

where G, r, g, α are determined experimentally. These parameters for a few materials are presented in [10, 142]. For aluminum alloy, for example, we have $G = 0.265 \cdot 10^{11}$ N/m^2, $\alpha = 0.4$, $\Delta = 0.0014$, $\tau = 12$. In (5.7):

$$g = (2G/\sqrt{2}\tau)^{\alpha}\,\frac{\Delta}{\pi}, \quad \frac{r}{g} = \frac{4}{\alpha(\alpha+2)} \cdot \frac{\Gamma(2+\alpha/2)}{\Gamma[(\alpha+1)/2]\cdot\Gamma(3/2)},$$

Γis the gamma function.

The numerical results correspond to a circular cylindrical panel with thickness of passive core layer $h_2 = 0.00999$ m. The thickness of the panel $H = h_2 + 2h_1 = 0.01$ m, and its radius $R = 0.1$ m and length $l = 0.1$ m. The length of the generatrix $s = 0.1$ m. The passive layer is made of an aluminum alloy with characteristics specified above, and the piezolayers are made of a viscoelastic piezoelectric material with characteristics presented in [143]. Poisson's ratio $\nu = 0.31$; $\rho_a = 0.75 \cdot 10^4$ kg/m^3 and $\rho_n = 0.28 \cdot 10^4$ kg/m^3 are the specific densities of the piezoelectric and passive materials. The thermal conductivity of the passive layer λ_T = 200 W/(m·°C), the heat-transfer coefficient α_T = 20 W/(m^2·°C), and initial temperature and environmental temperature $T_C = T_0 = 20$ °C. The frequency of the load is close to the resonance, and the amplitude of the mechanical load q = $0.25 \cdot 10^4$ N/m^2.

The amplitude–frequency characteristic of the panel is shown in Fig. 5.29. The approach in which the effect of the feedback factor is described by complex density was presented in [39]. The curves correspond to the following values of the complex density $\rho_n = \rho' - i\rho''$ (the curves are numbered from top to bottom): ρ'' = 0, 0.1, 0.5, 1.0, 2.0. The temperature–frequency characteristics for the same values of complex density are presented in Fig. 5.30, and the dependence of the second invariant I_2 of the strain tensor is shown in Fig. 5.31. The latter dependence is introduced for the deformation of the cylindrical panel not to exceed the elastic limits. It can be seen that the imaginary component of the complex density has a strong effect on the fundamental dynamic characteristics of vibrations of the cylindrical panel made of a physically nonlinear material of the second type. This imaginary component cane easily be determined in terms of the sensor voltage and is proportional to the feedback factor.

5.6. Combined Influence of Geometrical Nonlinearity and Physical Nonlinearity of the Second Type. To illustrate the combined effect of geometrical nonlinearity on the damping of vibrations of thin-walled elements with actuators, we will solve [156] the problem of the forced vibrations of a hinged sandwich beam with core layer made of AMg-6 aluminum alloy and outside layers made of TsTS-19 piezoceramics. The behavior of the electrically passive (without piezoelectric effect) aluminum alloy is described using the generalized flow theory [85, 86]. The piezoceramic layers are elastic and transversely isotropic. The basic relations and material characteristics can be found in [156].

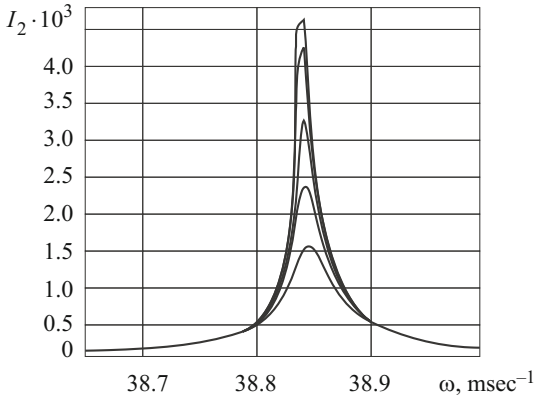

Fig. 5.31

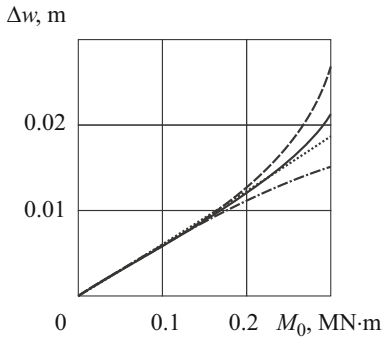

Fig. 5.32

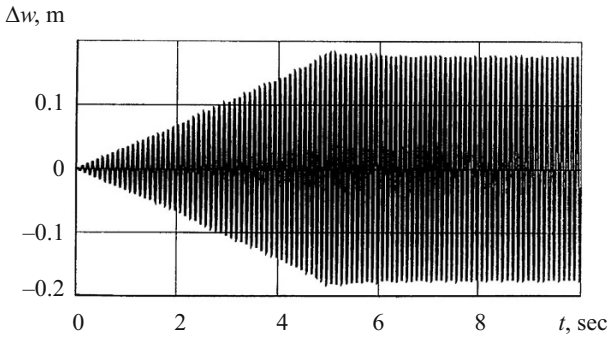

Fig. 5.33

The piezoactive layers are of equal thickness ($h_1 = h_3$), the total thickness of the beam $h = h_1 + h_2 + h_3$, where h_2 is the thickness of the aluminum layer. The length of the beam L = 0.826 m. Two cases with the following sets of thickness are considered: case A: $h = 0.3 \cdot 10^{-1}$ m, $h_1 = h_3 = 0.5 \cdot 10^{-2}$ m, $h_2 = 0.2 \cdot 10^{-1}$ m and case B: $h = 0.6 \cdot 10^{-1}$ m, $h_1 = h_3 = 0.2 \cdot 10^{-2}$ m, $h_2 = 0.56 \cdot 10^{-1}$ m. The width of the beam $b_y = 0.3 \cdot 10^{-1}$ m. The resonant frequency of the first bending vibration mode is 441 Hz in case A and 1167 Hz in case B The excitation frequency $f = 10$ Hz. The piezoactive layers are assumed preliminarily polarized across the thickness, the polarization directions of the layers being opposite (for example, the upper layer is polarized along the *Oz*-axis, while the lower layer in the opposite direction).

Two types of harmonic loading are considered: moments applied at the ends of the beam and a voltage applied to the electrodes of the piezolayers. In all cases, the harmonic load was modeled by a linear function so that the given amplitude of the load was reached in 50 cycles of vibration. This approach resulted in symmetric deflections of the beam about the axis because the direct application of the harmonic load during the first quarter of a cycle leads to the formation of a constant component of the deflection due to the inelastic deformation of the material, further vibrations occurring about this bent position.

To evaluate the combined effect of physical and geometrical nonlinearities, we will use the stiffness characteristic for the steady-state stage of the process that characterizes the dependence of the deflection amplitude on the amplitude of the bending moment (Fig. 5.32). The dotted curve corresponds to the linear case, the dash-and-dot curve to the geometrically nonlinear case, and the dashed curve to the physically nonlinear case. The solid curve represents the solution of the problem with both nonlinearities taken into account. Physical nonlinearity forms a soft-nonlinear characteristic, while geometrical nonlinearity forms a hard-nonlinear characteristic. The effect of nonlinearities depends on the load, the geometry of the beam, and the boundary conditions. It is clear that geometrical nonlinearity is dominating for thinner beams. The thicker the beam, the stronger the effect of physical nonlinearity. The inelastic deformation of thick structural members can become the major contribution to the response of the element.

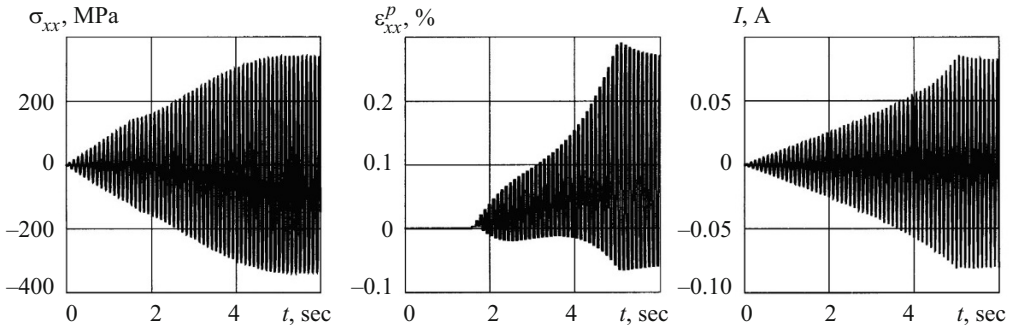

a *b* *c*

Fig. 5.34

Analyzing Fig. 5.32, we can identify the ranges of loads in which the system exhibits linear behavior ($M_0 < 0.12$ MN·m) during steady-state vibrations, geometrical nonlinearity ($0.12 < M_0 < 0.24$ MN·m) or loads under which the effect of both nonlinearities is great ($M_0 > 0.24$ MN·m) are predominant. For the beam of configuration *A*, the geometrical nonlinearity dominates over the whole range of loads.

Figure 5.33 shows, as an example, the nonstationary response of the beam to a harmonic mechanical load. It shows the history of the deflection for configuration B for $M_0 = 0.27$ MN·m with both physical and geometrical nonlinearities taken into account. It can be seen that after the first 50 cycles of vibration, when the amplitude of the load no longer changes, the deflection amplitude slightly decreases due to the hardening of the aluminum layers adjacent to the piezoceramics. After the completion of the transient, the cycle of vibration of the beam becomes symmetric about the horizontal line.

Figures 5.34*a* and 5.34*b* show the history of variation in the stress and inelastic strain, respectively, at the point $x = L/2$, $z = -h_2/2$, which is the lower extreme point of the aluminum layer in the central cross section of the beam. Figure 5.34*c* shows the evolution of the electric current in the lower piezoceramic layer operating as a sensor. A symmetric cycle of the response of the stress forms at the stage of steady-state vibration. At the load increases, the material reaches the elastic limit. This time point corresponds to the change in the slope of the envelope in Fig. 5.34*a*.

An analysis of Fig. 5.34*b* shows that if geometrical nonlinearity is present, the history of variation in the inelastic strain is not symmetric about zero because of the deformation of the beam axis. If only physical nonlinearity is present, then the history of the inelastic strain is symmetric. The beginning of inelastic deformation can easily be identified in Fig. 5.34*b*. In the sensor mode, the electric current one piezoactive layer also is characterized by weak asymmetry of the cycle about zero. This behavior is due to the fact that the occurring (due to the inverse piezoelectric effect) charge is determined by the strain of the active layer which is not symmetric about zero because of geometrical nonlinearity. Figure 5.35 details the behavior of electromechanical parameters within a stabilized cycle of vibration.

In Fig. 5.35*a*, the solid and dashed lines show the variation in the total strains at the points $(L/2, -h_2/2)$ and $(L/2, h_2/2)$, respectively, with time, the dash-and-dot line shows the time dependence of the strain of the beam axis, and the dotted line represents the time dependence of the current in the lower piezoactive layer. It can be seen that the asymmetry of the deformation cycles is due to a geometrical nonlinearity (such as the deformation of the beam axis). Since the beam axis undergoes tensile deformation, then within each half-cycle, it increases the deformation of the stretched layers and decreases the deformation of the opposite compressed layers of the beam. The situation is similar for the current. It can be seen that the curves deviate from the harmonic law. If the geometrical nonlinearity is neglected, all the curves will be symmetric, and the deformation of the beam axis will be zero.

In Fig. 5.35*b*, the solid and dashed thin lines show the variation, during a period of vibration, in the deflection of the beam and the phase of the mechanical load, respectively. The solid and dashed heavy lines correspond to the inelastic strain at the points $(L/2, -h_2/2)$ and $(L/2, h_2/2)$, and the dotted and dash-and-dot lines to the stresses at the same points. The inelastic deformation of the core layer causes a phase shift between the mechanical load and the deflection. This phase shift is small because of the smallness of the relative volume of the material that deforms inelastically. Similarly to Fig. 5.35*a*, the time dependences of the inelastic strain and stress are asymmetric about zero due to the geometrical nonlinearity. Allowing for the physical nonlinearity only makes the curves symmetric.

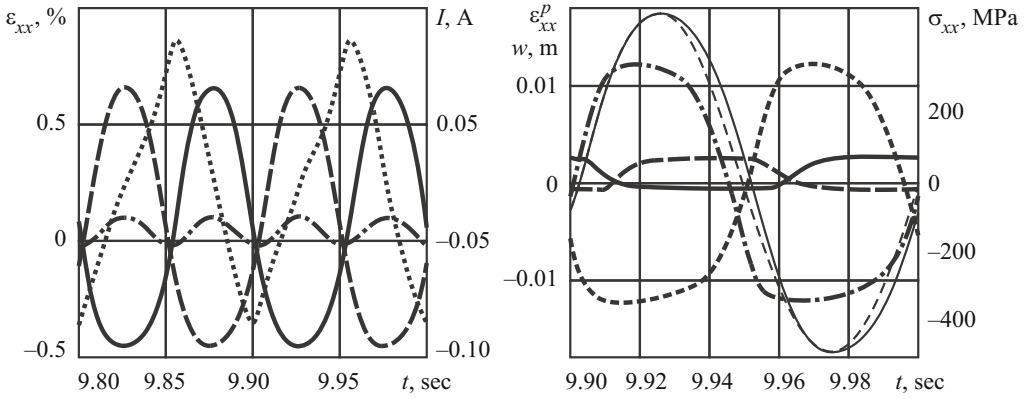

a *b*

Fig. 5.35

When vibrations are electrically excited by applying harmonic voltage to the electrodes of the piezoactive layers, the mechanical variables show similar behavior. The calculated results are presented in Figs. 5.33–5.35. Figure 5.32 has a similar form with the only difference that the abscissa axis indicates the voltage amplitude V_0.

Let us consider a hinged sandwich beam under harmonically varying mechanical moments acting at its ends. As before, the moments are assumed to vary linearly with time so that the maximum value is reached in 50 cycles of vibration. After the stabilization of the cycle of vibration, the following voltage V is applied at some time t_s to the electrodes of the piezoactive layers:

$$V = V_0 \sin(\omega t + \pi + \delta) = -V_0 \sin(\omega t + \delta), \tag{5.8}$$

where δ is some additional phase shift.

Figure 5.36 presents the calculated results for a beam of configuration *A* with allowance for physical nonlinearity only. In Fig. 5.36*a*, the dashed line corresponds to stationary vibrations without suppression by a voltage at M_0 = 100 kN·m and a frequency of 10 Hz, and the dotted line corresponds to the phase of mechanical loading. The solid curves correspond to the suppression of vibrations for $V_0 = 570$ kV and $\delta = 0$. Curve *1* is the solution of the quasistatic problem, and curves *2–6* are the solutions of the dynamic problem for $t_s = 8, 8.001, 8.004, 8.0058, 00578$ sec. Figure 5.36*b* details the solutions of the quasistatic and dynamic problems, the heavy curve corresponding to line *1* (quasistatic solution), and the thin curve to line *6* (dynamic solution) in Fig. 5.36*a*. It appears that vibrations cannot be completely suppressed at the frequency of the force. The residual vibrations are characterized by two features.

First, they occur about the bent axis of the beam. This configuration is determined by the inelastic deformation of the material and remains constant if the voltage is switched on at the stage of elastic deformation when unloading or reloading occurs in the elastic range (solid and dashed curves in Fig. 5.39*b*). If the inertial effects are neglected, the amplitude of residual vibrations will be negligible (heavy curve in Fig. 5.36*b*), and these vibrations can be suppressed by selecting the appropriate phase δ. The average component remains and can be eliminated by additionally applying a constant voltage.

Second, allowing for the dynamic effects qualitatively changes the behavior of residual vibrations. They also occur about the bent beam axis, but their amplitude is much higher increases and their frequency is equal to the natural frequency of the beam (fast components in Fig. 5.36) modulated by slowly varying residual vibrations at the frequency of the external load. In this case, the problem becomes equivalent to the problem of the elastic vibrations of a bent beam with some initial deflection and velocity. These quantities are determined by the deviation of points of the beam from the bent configuration and their velocity at the time t_s the voltage is switched on. From Fig. 5.36*a*, it can be seen that the greater this deviation, the higher the amplitude of natural vibrations. On the other hand, the amplitude also depends on the velocity of particles of the beam at the time t_s.

The change in the behavior of residual vibrations in the presence of both physical and geometrical nonlinearity is shown in Fig. 5.37 for a beam of configuration B for $M_0 = 270$ kN·m and $V_0 = 670$ kV. Curve *1* in Fig. 5.37*a* corresponds to the solution of the dynamic problem at $t_s = 10.002$ sec and $\delta = 0$. Curve *2* demonstrates the dynamic behavior of the beam at $t_s = 10.002$ sec and $\delta = \delta_{Mw}$, where δ_{Mw} is the phase shift between the mechanical load and the deflection caused by inelastic deformation.

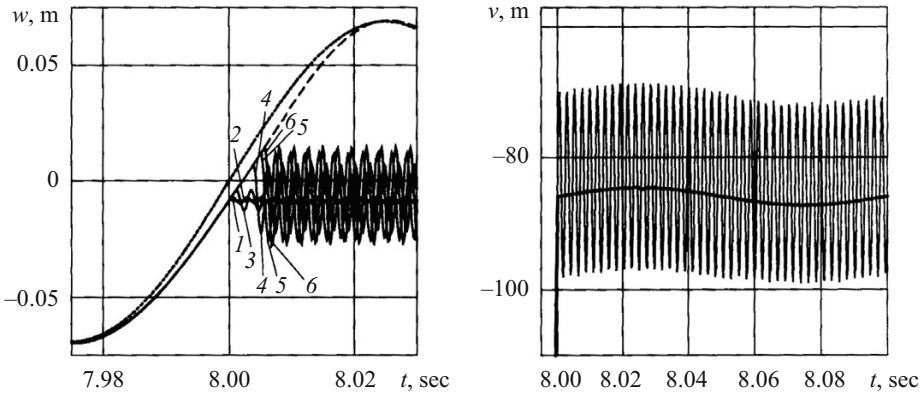

a *b*

Fig. 5.36

Curves *3* and *4* illustrate the quasistatic solution corresponding to line *1* with and without regard to geometrical nonlinearity, respectively. Curves *5a* and *6a* show the behavior of inelastic deformation at the point $(L/2, -h_2/2)$ with and without regard to geometrical nonlinearity, respectively, and curves *5b* and *6b* show the same at the point $(L/2, h_2/2)$.

Figures 5.37*b* and 5.37*c* shows stabilized cycles of vibration after switching on of the voltage. Lines *1* and *2* correspond to curves with the same numbers in Fig. 5.37*a*. Line *3* shows the history of the deflection for a law of suppression of vibrations different from (5.8):

$$V = A(t)V_0 \sin(\omega t + \pi + \delta) = -A(t)V_0 \sin(\omega t + \delta),$$

$$A(t) = \begin{cases} 0, & t \le t_s, \\ (t - t_s) f / N_C, & t_s < t < t_s + N_C f, \\ 1, & t \ge t_s + N_C f, \end{cases}$$

where f is the frequency; N_C is the number of cycles during which the amplitude of harmonic voltage increases to a preset level V_0.

Curve *3* corresponds to $t_s = 10$ sec and $N_C = 20$. Because of slow increase in the amplitude of the electric load, the mechanical load is gradually balanced and the deflection amplitude slowly decreases. As a result, beam axis does not bend and the residual vibrations occur about the line $z = 0$.

An analysis of Fig. 5.37 shows that geometrical nonlinearity manifests itself in two ways. First, the residual deflection of the bent axis of the beam decreases (lines *3* and *4* in Fig. 5.37*a*). This effect is due to the change in the behavior of inelastic deformation over the cross section, which, in turn, is due to the tension of the beam axis. Comparing curves *5* and *6* in Fig. 5.37*a* indicates that the beam becomes stiffer.

Second, geometrical nonlinearity is cubic in deflection. This gives rise to odd harmonics in the frequency spectrum of residual vibrations. Since the residual vibrations are elastic, then beating is observed in Fig. 5.37 as a result of superposition of vibrations at the frequency of the external load, multiple frequencies, and the frequency of the first bending resonance.

For symmetric piezolayers of equal thickness with opposite thickness polarization, the mechanical and electric loads appear equivalent in both deflection and stress–strain state. This fact can be used as a basis for developing a method of damping mechanically excited vibrations by applying voltage to the electrodes of the piezolayers. The physical nonlinearity of the passive layer and geometrical nonlinearity have a strong effect on the response of the sensor layer and the structure as a whole. Nonlinear behavior and interaction of nonlinearities during both transient and stationary operation hamper complete suppression of forced vibrations. Physical and geometrical nonlinearities are manifested as a phase shift between the load and the response of the system, bending of the beam axis, residual vibrations at natural frequency in the first bending mode and vibrations at frequencies multiple of the load frequency. The amplitude of residual vibrations can further be decreased through active/passive damping, such as the use of additional diffusing coatings made of highly viscous materials or the organizations of electric chains with feedback.

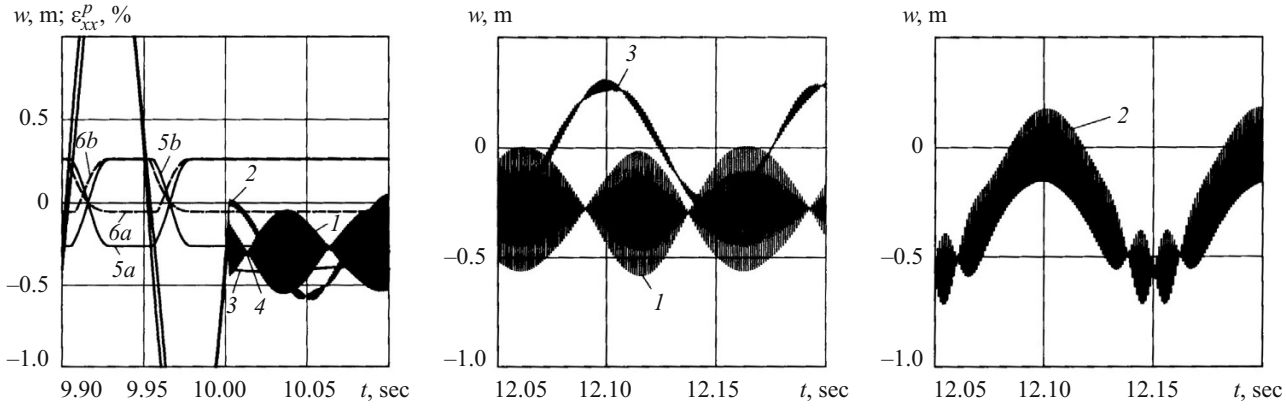

a *b* *c*

Fig. 5.37

The effect of geometrical nonlinearity on the effectiveness of active damping of the forced flexural vibrations of viscoelastic beams with piezoelectric sensors and actuators was studied in [129]. It was shown that it is sufficient to solve the linear problem to calculate the control ratio needed to find the actuator voltage balancing the mechanical load.

6. Damping of Nonstationary Vibrations. In what follows, we will address problems of the damping of nonstationary vibrations of rectangular plates with actuators. To model vibrations, the Kirchhoff–Love and Timoshenko hypotheses are used. Two methods are used to damp nonstationary vibrations. One method is to apply a voltage to the actuator to balance the most energy-intensive modes of the mechanical load. The other method is to apply a voltage determined by the optimal-control second method to the actuator. The effectiveness of both methods was compared. The influence of geometrical nonlinearity on the active damping of nonstationary vibrations of a flexible viscoelastic plate was studied as well.

It is necessary to study the active damping of nonstationary vibrations when answering the question of how quickly the vibrations become stationary under periodic mechanical and electric loads.

6.1. Active Damping of Nonstationary Vibrations of a Rectangular Plate with Piezoactuators. For effective damping of the nonstationary vibrations of plates with piezoelectric actuators, the classical approach was used above: the mechanical load is balanced by applying to the actuators a voltage that balances the most energy-intensive modes. To improve the effectiveness of the damping of nonstationary vibrations optimal-control methods [20] were used in [110].

Let us consider, as an example, a hinged rectangular elastic plate undergoing nonstationary vibrations under external normal pressure $p(x, y, t)$. The face $z = \pm h/2$ of the plate is covered with N oppositely polarized piezoelectric actuators to which voltages that cause bending vibrations are applied. Let us calculate the voltage that should be applied to the actuators to balance the mechanical load and, thus, to reduce the amplitude of vibrations. The problem is reduced to solving the standard equation of nonstationary transverse vibrations of a plate on which a load acts:

$$p(x, y) + \frac{\partial^2 M_0}{\partial x^2} + \frac{\partial^2 M_0}{\partial y^2},$$

where $M_0 = \sum_{i=1}^{N} M_0^i = \sum_{i=1}^{N} \gamma_{31}^i (h + h_i) V_a^i$, where N is the number of actuators; γ_{31}^i is the piezoelectric constant of the ith actuator; h_i is the thickness of the ith actuator; V_a^i is the voltage applied to the ith actuator. If the plate is hinged, the transverse deflection w, mechanical load $p(x, y, t)$, and electric load M_0 can be expanded into series of trigonometric functions. Doing so gives a system of ordinary differential equations with respect to time [110]:

$$\ddot{W}_{mn} + \omega_{mn}^2 W_{mn} = \frac{1}{\rho h} p_{mn} - \sqrt{\frac{1}{D\rho h}} \omega_{mn} \sum_{i=1}^{N} M_{mn}^i \qquad (m, n = \overline{1, \infty}), \tag{6.1}$$

where $\omega_{mn} = \sqrt{D/\rho h}(\pi^2 m^2 / a^2 + \pi^2 n^2 / b^2)$.

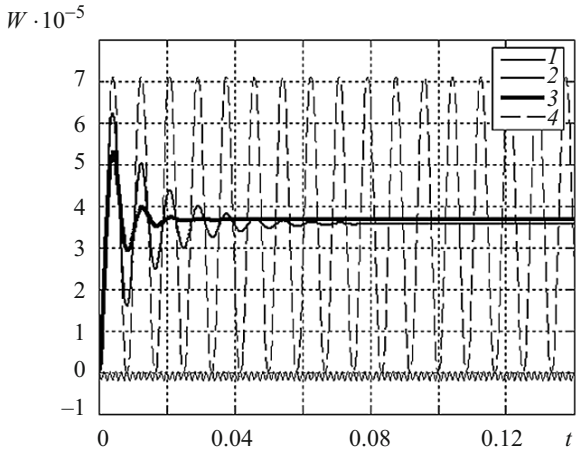

Fig. 6.1

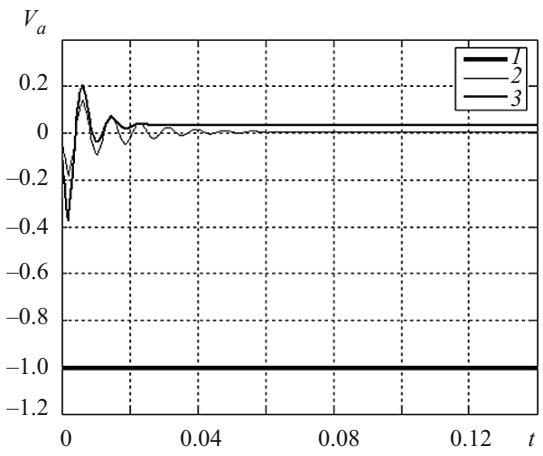

Fig. 6.2

Denoting $L^i_{mn} = \sqrt{\dfrac{1}{D\rho h}}\,\omega_{mn}\gamma^i_{31}(h+h_i)\iint_{S_i} F_{mn}\,dxdy / K_{mn}$, we represent relations (6.1) in the form

$$\ddot{W}_{mn} + \omega^2_{mn} W_{mn} = \frac{1}{\rho h K_{mn}}\, p_{mn} - \sum_{i=1}^{N} L^i_{mn} V^i_a \qquad (m, n = \overline{1,\infty}). \tag{6.2}$$

We keep Q harmonics in $m = m_1, m_2, \cdots, m_Q$ and S harmonics in $n = n_1, n_2, \ldots, n_S$. Denote: $x_{2k-1} = W_{m_q n_s}$, $x_{2k} = \dot{W}_{m_q n_s}$, $k = \overline{1,QS}$, $q = \overline{1,Q}$, $s = \overline{1,S}$. Then (6.2) yields a system of linear differential equations of order $2QS$ $\dot{x} = Ax + BV_a + F$, where A and B are $2QS \times 2QS$- and $2QS \times N$-matrices, respectively; F is a column vector of length $2QS$ [110].

Let us formulate the problem of optimizing the voltage V^i_a applied to the actuators to damp the vibrations of the plate induced by the external load and the initial conditions. The behavior of the deflection at an arbitrary point of the plate is determined by the behavior of W_{mn}. Hence, to damp the oscillatory process at minimum energy input, it is necessary to minimize the quadratic functional

$$J = \int_0^{\infty} \left(\sum_{i=1}^{2QS} q_i x_i^2 + \sum_{i=1}^{N} r_i V_a^{i^2} \right) dt,$$

where q_i and r_i are weight coefficients used to prioritize the minimization of a phase coordinate or control. Let us express the functional J in matrix form: $J = \int_0^{\infty} (\mathbf{x}^T \mathbf{Q}\mathbf{x} + \mathbf{V}_a^T \mathbf{R}\mathbf{V}_a)\,dt$; $\mathbf{Q}$ and $\mathbf{R}$ are square diagonal matrices with values of q_i and r_i on the main diagonals, respectively. These formulas allow us to design an optimal controller for a linear stationary system of differential equations based on a quadratic cost function:

$$J = \int_0^{\infty} (\mathbf{x}^T \mathbf{Q}\mathbf{x} + \mathbf{V}_a^T \mathbf{R}\mathbf{V}_a)\,dt \to \min,$$

$$\dot{\mathbf{x}} = \mathbf{A}\mathbf{x} + \mathbf{B}\mathbf{V}_a + \mathbf{F}, \qquad \mathbf{x}(0) = \mathbf{x}_0. \tag{6.3}$$

According to [20], applying the dynamic-programming method, the optimal control for problem (6.3) can be found by the formula $\mathbf{V}_a = -\mathbf{R}^{-1}\mathbf{B}^T\mathbf{K}\mathbf{x}$, where the matrix $\mathbf{K}$ follows from the algebraic matrix Riccati equation [20]:

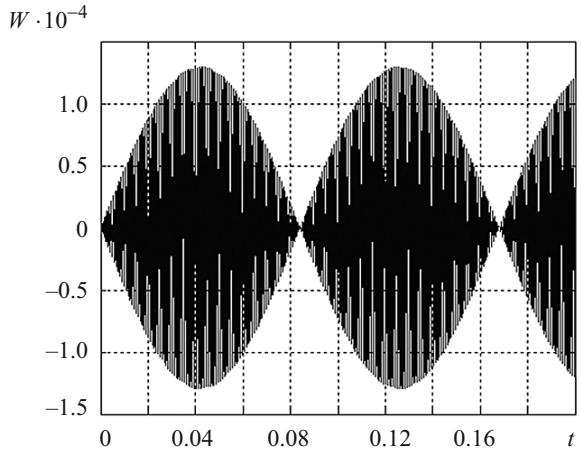

Fig. 6.3

$$\mathbf{KBR}^{-1}\mathbf{B}^T\mathbf{K}^T - \mathbf{KA} - \mathbf{A}^T\mathbf{K}^T - \mathbf{Q} = 0.$$

Let us consider, as an example, a hinged square metal plate of length $a = b = 20$ cm, thickness $h = 1$ mm, $\rho = 7850$ kg/m^3, $D = 18.315$. On the plate face, there is a square piezoelectric actuator with side length equal to that of the plate, thickness $h = 10$ mm, and coefficient $\gamma_{31} = -18.2857$ (material TsTSIBS-2). The centers of the actuator and plate coincide, and their sides are parallel. The plate is subject to a constant load $p = 100$ N/m^2 distributed over the plate surface. The plate is undeformed at time zero. To solve the problem, we will consider harmonics $m, n = 1, 3, 5$. The matrix Riccati equation is solved numerically, using the care.m Matlab routine. Figure 6.1 shows the variation in the deflection at the center of the plate without control (curve *4*), for $q_i = 50$, $i = \overline{1, 18}$, $r = 1$ (curve *2*), and for $q_i = 350$, $i = \overline{1, 18}$, $r = 1$ (curve *3*). Figure 6.2 shows the behavior of the optimal control V_a for $q_i = 50$, $i = \overline{1, 18}$, $r = 1$ (curve *2*) and for $q_i = 350$, $i = \overline{1, 18}$, $r = 1$ (curve *3*). As is seen, using only one actuator, we can quite quickly reduce the amplitude of vibrations.

Curves *1* in Figs. 6.1 and 6.2 show the variation in W and the voltage found not by optimizing the functional, but by equating to zero the right-hand side of Eq. (6.2) for the lowest harmonic $m = n = 1$ when using only one actuator with zero initial conditions. It can be seen that using the classical approach substantially decreases the deflection, but increases by an order of magnitude the voltage required to damp the vibrations. Moreover, the basic shortcoming of this approach is that it is not applicable for nonzero initial conditions because the external force is balanced and the natural vibrations of the plate are neglected.

Noteworthy is the study [135] of the active damping of a rectangular plate under impulsive loading.

6.2. Damping of the Nonstationary Vibrations of a Rectangular Plate with Piezoactuators Taking into Account Shear Strains. The optimal damping of the nonstationary vibrations of a hinged rectangular elastic plate of thickness h under external normal pressure $p(x, y, t)$ using the piezoelectric actuators on the plate surfaces $z = \pm h / 2$ was studied in [111]. Votages that cause flexural vibrations of the plate are applied to the actuators. It is necessary to define a law of variation in the actuator voltage for the maximum possible decrease in the amplitude of vibrations at the minimum energy input.

The problem statement is presented in [111]. If the plate is hinged at the edges, the solution of the problem can be expanded into series of trigonometric functions: As a result, the problem is reduced to an infinite system of ordinary linear differential equations with respect to time:

$$\ddot{W}_{mn} + \omega_{mn}^2 W_{mn} = \tilde{p}_{mn} + \sum_{i=1}^{N} L_{mn}^i V_a^i, \quad m, n = \overline{1, \infty}.$$

Its coefficients can be found in [111].

The problem is solved by the method outlined in the previous section. Let us consider, as an example, a metal plate with side lengths $a = b = 20$ cm, thickness $h = 10$ mm, and density $\rho = 7850$ kg/m^3. The plate is made of an isotropic material with the

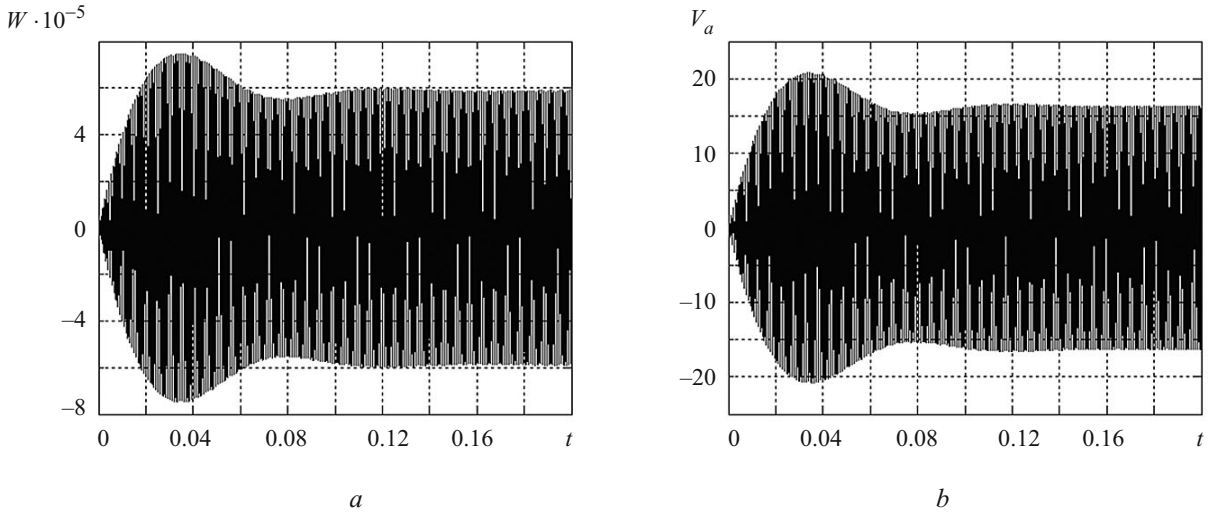

a *b*

Fig. 6.4

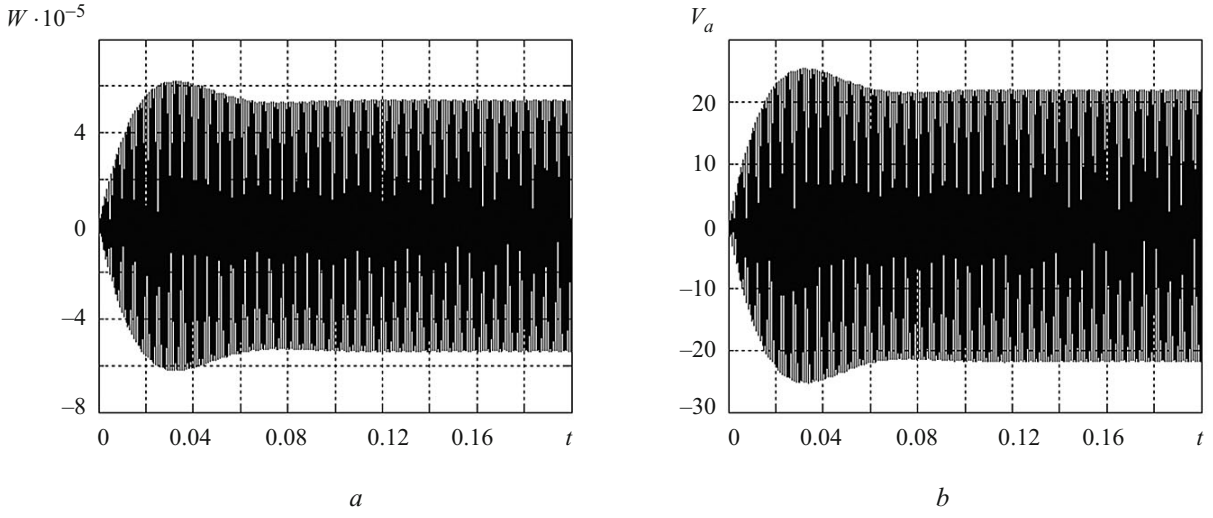

a *b*

Fig. 6.5

following mechanical characteristics: $E = 2 \cdot 10^{11}$ N/m^2, $\nu = 0.3$. The plate is covered with a square transversely isotropic piezoelectric actuator made of TsTSIBS-2 material and having side length equal to the side length of the plate of thickness $h = 10$ mm. The centers of the actuator and plate coincide, and their sides are parallel. The plate is subject to a load uniformly distributed over its surface and varying with time as $p = 7000\cos(0.99\omega_{11}t)$ N/m^2 (i.e., at a frequency close to the resonant frequency of the lowest harmonic, $m = n = 1$). The plate is undeformed at time zero. Three harmonics are considered: $m, n = 1, 3, 5$.

Figure 6.3 shows the time dependence of the deflection at the center of the plate in the absence of controls (no actuators). It can be seen that beating with amplitude $\cong 1.3 \cdot 10^{-4}$ m occurs. The variation in the deflection W of the center of the plate during active damping with the optimal actuator is shown in Fig. 6.4*a* for $q_i = 350, i = \overline{1, 18}, r = 1$ and in Fig. 6.5*a* for $q_i = 750, i = \overline{1, 18}, r = 1$. Figures 6.4*b* and Fig. 6.5*b* shows similar curves of the optimal control V_a (actuator voltage). As is seen, with an actuator, steady-state (stationary) vibrations with amplitudes much lower than those of forced vibrations can be reached quite quickly.

The curves in Figs. 6.6*a* and 6.6*b* show the variation in W and the voltage found not by optimizing the functional, but by equating to zero the right-hand side of Eq. (5.41) for the lowest harmonic $m = n = 1$when using only one actuator with zero initial conditions. It can be seen that the classical approach substantially decreases the deflection by several orders of magnitude, but increases by a factor of 1.5 to 2 the voltage required to damp the vibrations. However, the basic shortcoming of this approach is that it is not applicable for nonzero initial conditions because the external force is balanced and the natural vibrations of the plate are neglected.

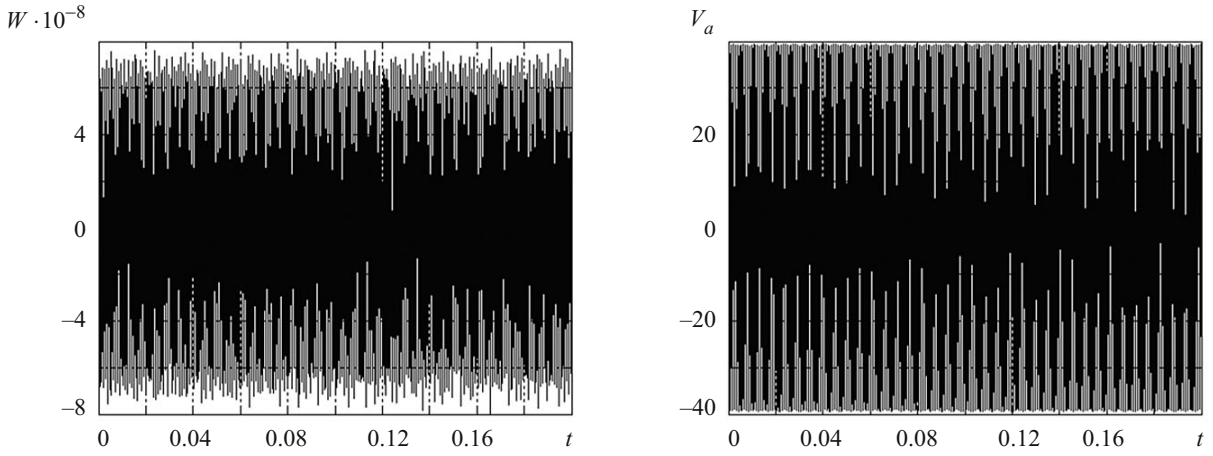

a *b*

Fig. 6.6

6.3. Active Damping of the Nonstationary Resonant Vibrations of a Flexible Rectangular Plate with Sensors and Actuators [112]. Consider a flexible rectangular thin plate made of a passive (no piezoelectric effect) viscoelastic material. Its edges are hinged. Normal pressure $q(x, y, t)$ acts on the plate. The plate is covered with piezoelectric layers with opposite thickness polarization playing the role of sensors and actuators. Let the plate have linear dimensions a and b, thickness h, and density ρ. The thickness of the piezoactive layers is denoted by h_s. To model the electromechanical behavior of such a sandwich, we will use the Kirchhoff–Love hypotheses supplemented with the assumption of smallness of the tangential components of electric-field strength and electric-flux density. To describe the geometrical nonlinearity, we will use the variation of the theory of flexible plates [112] that retains the squared angles of rotation in the kinematic equations. The tangential inertial forces in the equations of motion are neglected. The mechanical behavior of the passive material is described by integral-type linear equations of state of the theory of viscoelasticity. Introducing a force function identically satisfying the equilibrium equations for forces and using the nonlinear compatibility equation for strains, we obtain a system of nonlinear integro-differential equations for the force function Φ and the deflection W, which is known from the theory of flexible plates [112]. In this system, the transverse load q is expressed as $q - \Delta M_0$, where $M_0 = 0.5\gamma_{31}(h + h_s)V_a$ is the bending moment induced by the actuators, V_a is the voltage applied to the actuator, and γ_{31} is its piezoelectric constant.

The vibrations of the plate are damped by applying to the actuator a voltage proportional to the rate of variation in the sensor voltage: $V_a = -G\dot{V}_s$, where G is a constant feedback factor. The voltage of the sensor of area S is defined by $V_s = -\dfrac{h_s(h+h_s)}{2S}\dfrac{k_p^2}{d_{31}(1-k_p^2)}\iint_S \nabla^2 W dxdy$, and the coefficient k_p^2 is determined from the expression $k_p^2 = 2d_{31}^2/(1-\tilde{\nu})\varepsilon_{33}s_{11}$, $\tilde{\nu} = |s_{12}/s_{11}|$.

If the plate is hinged at the edges, the solution of the problem can be expanded into Fourier series of trigonometric functions satisfying the boundary conditions. An exponential kernel function is used to describe the mechanical behavior of the passive material. To study resonant vibrations in mode mn, we obtain an integro-differential equation of the second order:

$$\ddot{W}_{mn} - Gb\dot{W}_{mn} + a_1 W_{mn} - d_1 W_{mn}^3 - a_2 \int_0^t e^{-\alpha(t-\tau)} W_{mn}(\tau)d\tau + d_2 W_{mn} \int_0^t e^{-\alpha(t-\tau)} W_{mn}^2(\tau)d\tau = Q_1 q_{mn}(t), \tag{6.4}$$

where $b, a_1, a_2, d_1, d_2, Q_1$ are constant coefficients.

We will use the method outlined in [2] to solve Eq. (6.4). Let we have the integro-differential equation

$$\ddot{u}(t) = F\left(t, u(t), \dot{u}(t), \int_{t_0}^{\tau} \varphi(t, \tau, u(\tau), \dot{u}(\tau))d\tau\right) \tag{6.5}$$

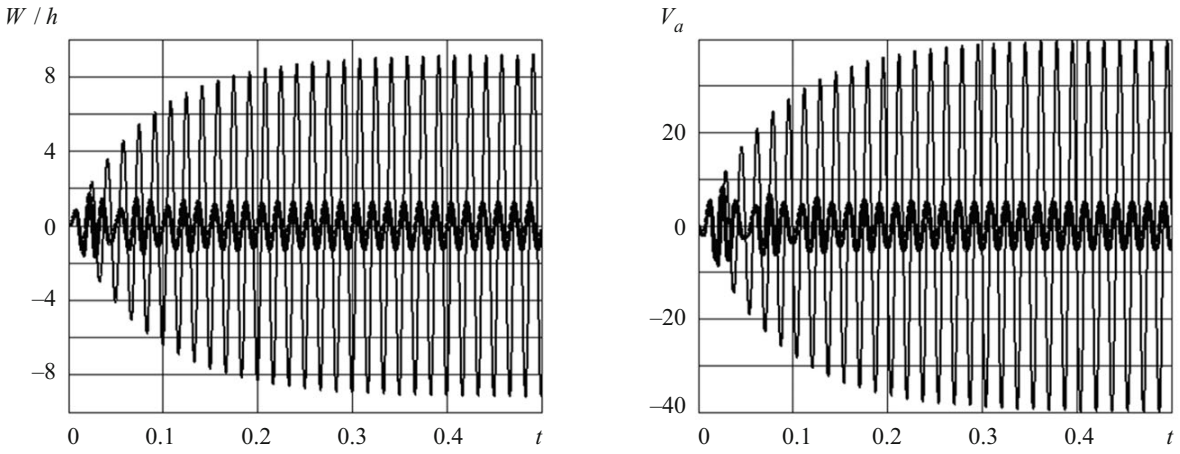

a *b*

Fig. 6.7

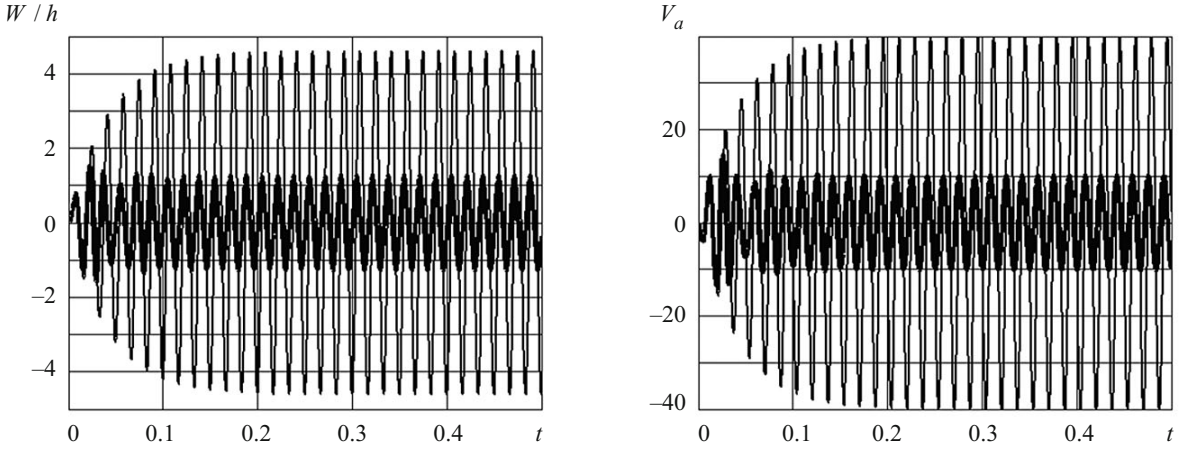

a *b*

Fig. 6.8

with the initial conditions

$$u(t_0) = u_0, \quad \dot{u}(t_0) = \dot{u}_0. \tag{6.6}$$

Twice integrating Eq. (6.5) and taking conditions (6.6) into account, we obtain

$$u(t) = \int_{t_0}^{t} (t-\tau) F\left(t, u(t), \dot{u}(t), \int_{t_0}^{s} \varphi(t, \tau, u(s), \dot{u}(s)) ds \right) d\tau. \tag{6.7}$$

The factor $(t-\tau)$ in (6.7) indicates that the subintegral function is equal to 0 at the time t. This fact makes it possible to set up an explicit algorithm for numerical solution of problem (6.5), (6.6) based on quadrature formulas [3]. Let us consider, as an example, a hinged square metal plate with side lengths $a = b = 20$ cm, thickness $h = 0.5$ mm, and density $\rho = 7850$ kg/m^3. The material of the plate is isotropic ($E = 2 \cdot 10^{11}$ N/m^2, $\nu = 0.3$).

The plate is covered with a square transversely isotropic piezoelectric actuator made of TsTSIBS-2 material and having side length equal to the side length of the plate.

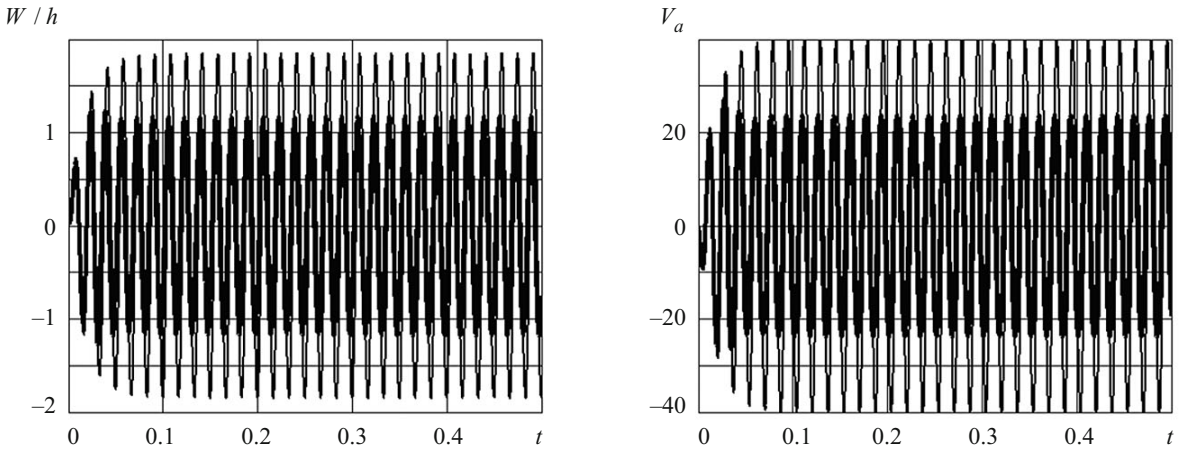

a *b*

Fig. 6.9

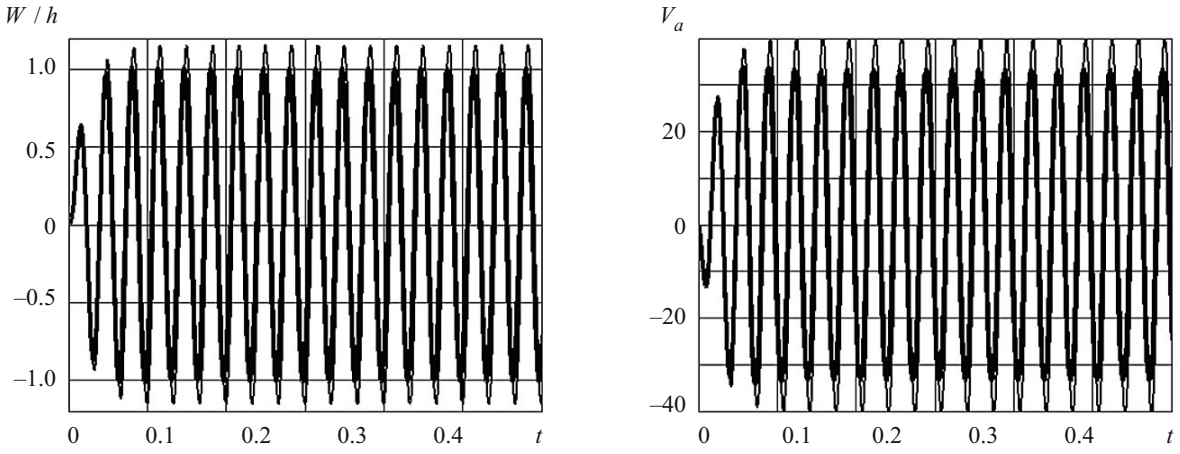

a *b*

Fig. 6.10

The centers of the actuator and plate coincide, and their sides are parallel. The plate is subject to a load uniformly distributed over its surface and varying with time as $p = 100 \sin \omega_{11} t$ N/m^2 (i.e., at a frequency close to the resonant frequency of the lowest harmonic, $m = n = 1$). The plate is undeformed at time zero.

Figures 6.7*a*–6.10*a* show the variation in the central deflection of the plate divided by its thickness for the following values of G_2 (3.11): 0.005, 0.01, 0.025, 0.04, and Figs. 6.7*b*–6.10*b* show the variation in the voltage V_a applied to the actuator. The heavy lines represent the solution of the geometrically nonlinear problem, i.e., the solution of Eq. (5.49). The thin curves correspond to the geometrically linear case.

It can be seen that with increase in G_2, the effect of geometrical nonlinearity on the amplitude of vibrations and the voltage applied to the actuator becomes weaker.

7. Thermal Failure of the System of Active Control of the Forced Vibrations of Thin-Walled Elements. As indicated in the introduction, thermal failure occurs when the SHT reaches the degradation point of the passive or active material. Two problems should be solved: (i) determine the critical load q_K under which the element loses its function and (ii) determine the critical time t_K under a load exceeding the critical ($q > q_K$). In the former case, it is sufficient to solve the stationary coupled problem of thermoelectroviscoelasticity, and in the latter case, it is necessary to solve the nonstationary coupled problem for the viscoelastic element under a postcritical load and to determine the critical time t_K in which the SHT reaches the degradation point θ_K of the material. Solving the second problem for different postcritical loads, it is possible to plot a fatigue-like curve

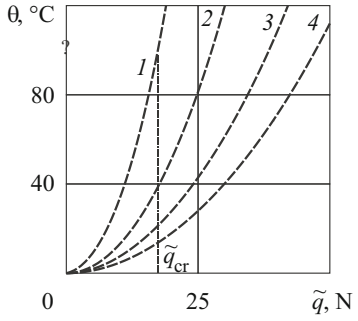

Fig. 7.1

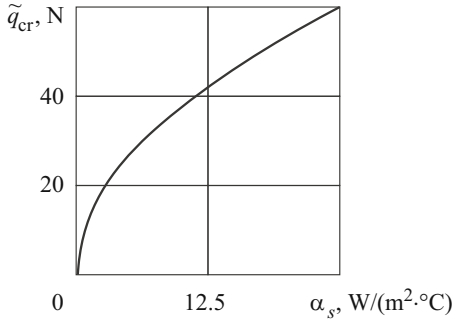

Fig. 7.2

(postcritical load versus critical time). This curve asymptotically tends to the critical load from above. The thermal failure of thin-walled structural members made of passive inelastic materials is detailed [9, 39, 66, 96, 145].

First results on thermal failure of piezoelectric thin-walled elements are reported in [103, 113] and briefly reviewed in [96, 97, 100, 101]. In [32, 34, 44, 45, 47, 49, 50, 98, 103, 107, 116, 117, 119–127, 131], the critical loads were determined from the analytic solutions to coupled problems of the vibrations of inelastic rectangular and circular plates and cylindrical and spherical shells, taking into account physical nonlinearity of the first type. The analytic formulas for the SHT were used to determine the critical load by equating the maximum temperature to the degradation point θ_K of the material. Similar solutions for circular and rectangular plates made of physically nonlinear materials of the second type are given in [34, 41, 42].

The thermal failure of a beam with physical nonlinearity of the second type undergoing transverse vibrations was studied in [92–94], where aspects of determining the critical load and critical time were also discussed. If the material properties are independent of temperature, the critical time for hinged plates and cylindrical shells under a postcritical load is determined by the Bubnov–Galerkin method, by solving a differential equation of the first order for the maximum temperature θ_0 [34]:

$$\dot{\theta}_0 = c_1 - c_2\theta_0, \tag{7.1}$$

where c_1 and c_2 are constants depending on the dimensions of the element, the mechanical and thermophysical properties of the material [34].

Integrating (7.1), we obtain the following expression for the critical time t_K:

$$t_K = \frac{c_2}{c_1} + \frac{c_2}{c_2\theta_K - c_1}. \tag{7.2}$$

If the mechanical properties of inelastic materials depend in an arbitrary manner on temperature, then we obtain more complex expressions for the amplitude- and temperature-frequency characteristics. To determine the critical load from transcendental equations, it is necessary to use numerical methods. To determine the critical time, we obtain the following expression instead of (7.2):

$$\int_0^{\theta_K} \frac{d\theta}{\Phi(\theta)} = t_K, \tag{7.3}$$

where $\Phi(\theta)$ is a function determined by fitting experimental data on the temperature dependence of mechanical characteristics.

To calculate the critical load for inelastic thin-walled elements subject to forced vibrations and self-heating, it is possible to use numerical methods for solving the stationary and nonstationary coupled problems of thermoelectroviscoelasticity. These methods reduce the original nonlinear problem to a sequence of linear problems of mechanics and linear heat-conduction problems with a known heat source. This approach allows solving problems with arbitrary dependence of mechanical characteristics on temperature and strain amplitude and nonlinear problems of vibrations of flexible thin-walled elements. In this case, however, the critical load is found by enumeration. Calculation starts with some load under which the maximum self-heating temperature is lower than the degradation point of the material. Then the mechanical load is incremented a little, and the nonlinear problem is solved for this new load. This process is continued until the maximum

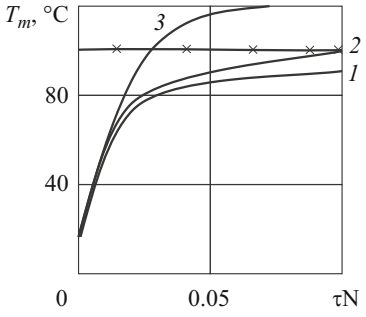

Fig. 7.3

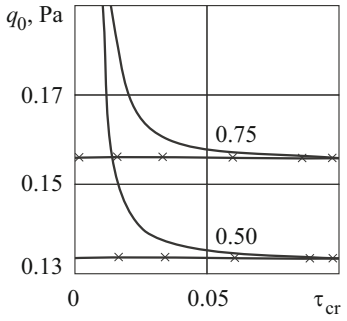

Fig. 7.4

temperature reaches the degradation point of the material. This corresponding load is critical. To determine the postcritical time, the nonstationary coupled problems of thermoelectroviscoelasticity are solved in a similar way.

Figure 7.1 shows typical curves (*1–4*) of the SHT θ of a thin-walled element on the amplitude of mechanical load $\tilde{q}$ at some frequency for temperature-independent characteristics of the passive material with different heat-transfer coefficients α_s = 2, 5, 10, 15 W/(m^2·°C), respectively [48]. The asterisk on the ordinate axis indicates the degradation point $\theta_{cr} = 100$ °C. This temperature corresponds to the critical load amplitude $\tilde{q}_{cr}$ on the abscissa axis. The typical dependence of $\tilde{q}_{cr}$ on the heat-transfer coefficient α_s is shown in Fig. 7.2 [48]. It can be seen that the critical load $\tilde{q}_{cr}$ is zero if the system is perfectly thermally insulated ($\alpha_s \to 0$) and gradually increases tending to a constant level with increase in the heat-transfer coefficient.

Figure 7.3 shows typical dependence of the maximum SHT on dimensionless time for subcritical (curves *1* and *2*) and postcritical (curve *3*) loads [44]. The degradation point is indicated by x's. Figure 7.4 shows typical fatigue-type curves for different heat-transfer coefficients [44]. The degradation point is indicated by x's. As is seen, the critical load increases with the heat-transfer coefficient, which is consistent with Fig. 7.2.

8. Active Damping of the Resonant Vibrations of Plates and Shells under an Unknown Mechanical Load. A new approach to the active damping of the resonant flexural vibrations of orthotropic viscoelastic plates with sensors and actuators under an unknown mechanical load was proposed in [43]. The essence of the method is as follows. The sensor's charge or voltage is used to determine the amplitude and phase of the external load. After that, the former method can be used: the voltage calculated from the already known load is applied to the actuator.

Let us consider, as an example, a rectangular plate under pressure harmonically varying with a frequency close to the resonant frequency of the plate. The plate is hinged at the edges. To model vibrations, the Kirchhoff–Love hypotheses are used (see Sec. 3.2). Let the vibrations be flexural. The passive layers may be made of metallic, polymeric, or composite materials. Let they be orthotropic, and the piezoactive layers transversely isotropic and polarized throughout the thickness of the plate. If there are no electrodes between layers, then they are in perfect mechanical and electric contact. The dissipative properties of the passive and piezoactive layers are described using the concept of complex characteristics. Let the plate have three layers: the core layer of thickness h_0 is passive (no piezoelectric effect), and the two face layers of thickness h_1 each are piezoelectric and oppositely polarized. For an orthotropic plate, the problem is reduced to the following equation [43]:

$$D_{11}\frac{\partial^4 w}{\partial x^4} + 2(D_{12} + 2D_{66})\frac{\partial^4 w}{\partial x^2 \partial y^2} + D_{22}\frac{\partial^4 w}{\partial y^4} - \tilde{\rho}\omega^2 w - p_0(x, y) - \left(\frac{\partial^2 M_0}{\partial x^2} + \frac{\partial^2 M_0}{\partial y^2}\right) = 0, \tag{8.1}$$

where all the stiffness characteristics are complex.

For a hinged plate, the solution of Eq. (8.1) has the form

$$w_{mn} = \frac{p_{mn} - (k_m^2 + p_n^2)M_{mn}}{[D_{11}k_m^4 + (2D_{12} + D_{66})k_m^2 p_n^2 + D_{22}p_n^4 - \tilde{\rho}\omega_{mn}^2]}. \tag{8.2}$$

Formula (8.2) indicates that the voltage to be applied to the actuator to balance the external mechanical load can be found from the expression

$$V_{mn} = p_{mn} / (k_m^2 + p_n^2)\overset{1}{\gamma}_{31}(h_0 + h_1). \tag{8.3}$$

In this case, the amplitude of vibrations in the mode being considered will be equal to zero.

If the mechanical pressure is uniform (p_0 =const), then, according to formula (8.3), the following voltage should be applied to damp the first mode:

$$V_{11} = p_{11} / (k_1^2 + p_1^2)\overset{1}{\gamma}_{31}(h_0 + h_1), \quad p_{11} = 4p_0 / k_1 p_1, \quad V_{11} = 4V_0 / k_1 p_1. \tag{8.4}$$

The approach based on formulas (8.3) and (8.4) has the following shortcomings: (i) free vibrations are not damped; (ii) the external mechanical load has to be known. The former disadvantage is compensated by the dissipative properties of the materials. To eliminate the latter shortcoming, we use the indications of the sensor covering an area S_1. When the electrodes are short-circuited, the charge is determined from the expression

$$Q = -\gamma_{31}(h_0 + h_1)\iint\limits_{(S_1)} (\kappa_1 + \kappa_2)dxdy. \tag{8.5}$$

When the electrodes are open-circuited, the voltage is determined from

$$V_S = h_1 Q / S_1 \gamma_{33}. \tag{8.6}$$

Let us discuss the damping of the principal mode, for which we derive the following expressions for the sensor voltage and charge from (8.5) and (8.6):

$$Q_{11} = 4\gamma_{31}(h_0 + h_1)(k_1 / p_1 + p_1 / k_1)w_{11}, \tag{8.7}$$

$$V_{11S} = \frac{4h_1(h_0 + h_1)\gamma_{31}}{S_1\gamma_{33}}\left(\frac{k_1}{p_1} + \frac{p_1}{k_1}\right)w_{11}. \tag{8.8}$$

The problem of the resonant mechanical vibrations of a hinged plate in the first mode has the following solution:

$$w_{11} = \frac{p_{11}}{[D_{11}k_1^4 + (2D_{12} + D_{66})k_1^2 p_1^2 + D_{22}p_1^4 - \tilde{\rho}\omega_{11}^2]}. \tag{8.9}$$

Substituting (8.9) into (8.7) or (8.8), we obtain the following relation between the sensor voltage or sensor charge and the load:

$$p_{11} = \frac{Q_{11}[D_{11}k_1^4 + (2D_{12} + D_{66})k_1^2 p_1^2 + D_{22}p_1^4 - \tilde{\rho}\omega_{11}^2]}{4\gamma_{31}(h_0 + h_1)(k_1 / p_1 + p_1 / k_1)},$$

$$p_{11} = \frac{V_{11S}S_1\gamma_{33}[D_{11}k_1^4 + (2D_{12} + D_{66})k_1^2 p_1^2 + D_{22}p_1^4 - \tilde{\rho}\omega_{11}^2]}{4\gamma_{31}(h_0 + h_1)(k_1 / p_1 + p_1 / k_1)}. \tag{8.10}$$

Substituting the load found from (8.10) into formula (8.4), we obtain expressions for the voltage that would balance this load:

$$V_{11} = \frac{Q_{11}[D_{11}k_1^4 + (2D_{12} + D_{66})k_1^2 p_1^2 + D_{22}p_1^4 - \tilde{\rho}\omega_{11}^2]}{4\gamma_{31}^2(h_0 + h_1)^2(k_1 / p_1 + p_1 / k_1)(k_1^2 + p_1^2)},$$

$$V_{11} = \frac{V_{11S}S_1\gamma_{33}[D_{11}k_1^4 + (2D_{12} + D_{66})k_1^2 p_1^2 + D_{22}p_1^4 - \tilde{\rho}\omega_{11}^2]}{4\gamma_{31}^2(h_0 + h_1)^2(k_1 / p_1 + p_1 / k_1)(k_1^2 + p_1^2)}. \tag{8.11}$$

Thus, the third method applies the voltage determined from the sensor voltage by formulas (8.11) to the actuator. With such an approach, we need to know only the electromechanical properties and dimensions of the plate. To solve the problem numerically, we proceed as follows. First, we solve a reference problem for the plate undergoing resonant vibrations under a unit load ($p_{11} = 1$ Pa). Next, we use formulas (8.5) and (8.6) to determine the sensor voltage $V_S^{(1)}$ or charge $Q_S^{(1)}$. If the load p_{11} is unknown, then

$$V_s = p_{11} V_S^{(1)}, \tag{8.12}$$

where V_S is the sensor voltage under unknown load, and $V_S^{(1)}$ is the sensor voltage under a unit load.

The unknown load is determined from (8.12):

$$p_{11} = V_s / V_S^{(1)}. \tag{8.13}$$

To calculate the voltage that should be applied to the actuator to balance the unknown load, we find the voltage $V_A^{(1)}$ that balances the unit load $p_0 = 1$ Pa. To balance the load p_{11}, it is necessary to apply the voltage

$$V_A = p_{11} V_A^{(1)}. \tag{8.14}$$

Substituting (8.13) into (8.14), we obtain the final formula

$$V_A = -|V_A^{(1)}| \,/\, |V_S^{(1)}| V_S,$$

where $V_A^{(1)}$ and $V_S^{(1)}$ are determined by solving reference problems, and V_s is the sensor voltage.

If the electrodes are short-circuited, all the above considerations remain. It is necessary to replace $V_S^{(1)}$ and V_S in the above formulas by $Q_S^{(1)}$ and Q_S, respectively.

To solve the last problem numerically, we should: (i) to determine the deflection w_P at the center of the plate for $P_0 = 1$ Pa, $V_A = 0$; (ii) to determine the deflection w_E at the center of the plate for $P_0 = 0$, $V_A = 1$ V. Then $V_A^{(1)}$ can be found by the formula $V_A^{(1)} = w_P / w_E$. Examples of using this method are given in [45, 130, 132, 137].

Conclusions. The results of the following studies have been reviewed: modeling of the resonant vibrations and self-heating of inelastic thin-walled elements with piezoelectric sensors and actuators; development of combined numerical/analytical methods for solving the corresponding nonlinear coupled boundary-value problems; analysis of the effect of various factors on the performance of sensors and actuators and the effectiveness of active damping of the vibrations of inelastic thin-walled elements by analyzing the solutions of specific problems.

The concept of complex characteristics has been used to model the thermoelectromechanical behavior of passive and piezoactive materials. Two types of physical nonlinearity have been considered: one type is due to the temperature dependence of the real and imaginary components of the complex characteristics and the dependence of the dissipation function on temperature and strains and the second type is due to the dependence of these components and the dissipation function on strains. The geometrical nonlinearity due to the nonlinear dependence of strains on displacements has been considered as well.

The vibrations and self-heating of thin-walled structural members have been described using either classical Kirchhoff–Love hypotheses or refined hypotheses supplemented with hypotheses on electric and thermal fields.

Nonlinear boundary-value problems have been solved numerically using these hypotheses and iterative methods. The original nonlinear problems have been reduced to a sequence of linear problems of mechanics and linear heat-conduction problems with a known heat source. These linear problems have been solved using the discrete-orthogonalization method (to solve one-dimensional problems) and the finite-element method (to solve two-dimensional problems). Analytical solutions have been obtained using the Bubnov–Galerkin method. Optimal-control methods have been used to study the damping of nonstationary vibrations.

The influence of the geometrical parameters and arrangement of sensors and actuators, mechanical boundary conditions, transverse-shear strains, physical nonlinearities of the first and second types, geometrical nonlinearity on the performance of sensors and actuators and the effectiveness of the active damping of resonant vibrations of thin-walled elements has been studied by analyzing numerical results. For example, when the plate is hinged, the operation of piezoinclusions during vibrations at the first resonance will be the most effective if the plate or shell is fully covered by sensors and actuators. If the plate is clamped, there are optimal dimensions of piezoinclusions that provide their most effective operation. If the plate is fully covered, then it is impossible to control vibrations. These types of physical nonlinearity have a strong effect on such fundamental dynamic characteristics as amplitude– and temperature–frequency characteristics and frequency-dependence of the damping factor.

Under certain conditions, the self-heating temperature reaches the degradation point of the material, causing the control system of the resonant vibrations of thin-walled elements to lose its functionality. For an active material, such a point is the Curie point at which a piezomaterial loses the piezoelectric effect and becomes passive. For a passive material, the degradation point is the temperature at which its mechanical characteristics, such as the melting point, change abruptly.

Methods for determining the critical electric or mechanical loads at which the temperature reaches the degradation point and methods for determining the critical time under postcritical loading have been described.

Methods for damping the vibrations of thin-walled structural members based on the sensor voltage/charge the when mechanical load is unknown have been proposed.

REFERENCES

1. S. A. Ambartsumyan, *General Theory of Anisotropic Shells* [in Russian], Nauka, Moscow (1974).
2. F. B. Badalov, *Methods for Solving Integral and Integro-Differential Equations of Hereditary Viscoelasticity* [in Russian], Mekhnat, Tashkent (1987).
3. K. J. Bathe and E. L. Wilson, *Numerical Methods in Finite Element Analysis*, Prentice-Hall, Englewood Cliffs, New Jersey (1976).
4. D. Berlinkur, D. Kerran, and G. Jaffe, "Piezoceramic electric and piezomagnetic materials and their application in transducers," in: W. P. Mason (ed.), *Physical Acoustics*, *Principles and Methods*, Vol. 1, Part A, *Methods and Devices*, Academic Press, New York–London (1964).
5. D. R. Bland, *The Theory of Linear Viscoelasticity*, Pergamon Press, Oxford (1960).
6. N. N. Bogolyubov, "Free single-frequency vibrations in nonlinear multidegree-of-freedom systems," *Sb. Trudov Inst. Stroit. Mekh. AN USSR*, No. 10, 9–21 (1949).
7. N. N. Bogolyubov and Y. A. Mitropolsky, *Asymptotic Methods in the Theory of Nonlinear Oscillations*, Gordon and Breach, New York (1962).
8. A. F. Bulat, V. I. Dyrda, V. G. Karnaukhov, E. L. Zvyagil'skii, and A. S. Kobets, *Thermomechanical Theory of Viscoelastic Bodies*, Vol. 3 of the three-volume series *Applied Mechanics of Hereditary Elastic Materials* [in Russian], Naukova Dumka, Kyiv (2013).
9. A. F. Bulat, V. I. Dyrda, V. G. Karnaukhov, E. L. Zvyagil'skii, and A. S. Kobets, *Forced Vibrations and Self-Heating of Inelastic Bodies*, Vol. 4 of the three-volume series *Applied Mechanics of Hereditary Elastic Materials* [in Russian], Naukova Dumka, Kyiv (2014).
10. K. V. Frolov (ed.), *Vibration and Impact Protection*, Vol. 6 of the six-volume handbook *Vibrations in Engineering* [in Russian], Mashinostroenie, Moscow (1981).
11. A. S. Vol'mir, *Nonlinear Dynamics of Plates and Shells* [in Russian], Nauka, Moscow (1972).
12. R. M. Wolosewick and S. Gratch, "Transient response in a viscoelastic material with temperature-dependent properties and thermomechanical coupling," *ASME*, *J. Appl. Mech.*, **32**, No. 3, 620–622 (1965).
13. B. M. Gorelik, L. P. Goncharov, V. G. Karnaukhov, et al., "Experimental and theoretical investigation of heat evolution in a short viscoelastic cylinder in cyclic compression," *Strength of Materials*, **9**, No. 1, 68–71 (1977).
14. Ya. M. Grigorenko and A. T. Vasilenko, *Theory of Shells of Variable Thickness* [in Russian], Naukova Dumka, Kyiv (1981).

15. G. A. Grinberg, M. I. Kantorovich, and M. I. Lebedev, “Evolution of thermal failure with time,” *Zh. Tekh. Fiz.*, **10**, No. 3, 199–216 (1940).
16. V. T. Grinchenko, A. F. Ulitko, and N. A. Shul’ga, *Electroelasticity*, Vol. 5 of the five-volume series *Mechanics of Coupled Fields in Structural Members* [in Russian], Naukova Dumka, Kyiv (1989).
17. A. N. Guz (ed.), J. Kabelka, S. Markus, et al., *Dynamics and Stability of Laminated Composites* [in Russian], Naukova Dumka, Kyiv (1991).
18. N. N. Davidenkov, “Energy dissipation during vibrations,” *Zh. Tekhn. Fiz.*, **8**, No. 6, 483–499 (1938).
19. V. G. Dubenets and V. V. Khil’chevskii, *Vibrations of Damped Composite Structures* [in Russian], Vol. 1, Vyshcha Shkola, Kyiv (1995).
20. V. A. Ivanov and N. V. Faldin, *Theory of Optimal Automatic Control Systems* [in Russian], Nauka, Moscow (1981).
21. A. A. Il’yushin and B. E. Pobedrya, *Fundamentals of the Mathematical Theory of Thermoviscoelasticity* [in Russian], Nauka, Moscow (1970).
22. A. Yu. Ishlinsky and D. D. Ivlev, *Mathematical Theory of Plasticity* [in Russian], Fizmatlit, Moscow (2003).
23. V. G. Karnaukhov, *Coupled Problems of Thermoviscoelasticity* [in Russian], Naukova Dumka, Kyiv (1982).
24. V. G. Karnaukhov, “Thermomechancis of coupled fields in inelastic materials and structural members under harmonic loading,” *Visn. Kyiv. Univ.*, *Ser. Fiz.-Mat. Nauky*, No. 3, 142–145 (2013).
25. V. G. Karnaukhov and T. V. Karnaukhova, “Resonant flexural vibrations of a hinged flexible viscoelastic circular plate with piezoelectric sensors,” *Teor. Prikl. Mekh.*, **45**, 124–130 (2009).
26. V. G. Karnaukhov and T. V. Karnaukhova, “Damping the resonant bending vibrations of a hinged flexible viscoelastic circular plate with sensors and actuators,” *Teor. Prikl. Mekh.*, **46**, 125–131 (2009).
27. V. G. Karnaukhov, T. V. Karnaukhova, N. V. Petrenko, and M. V. Peresunko, “Application of an analogy between problems of thermomechanics and thermoelectromechanics,” *Teor. Prikl. Mekh.*, No. 6 (52), 125–134 (2013).
28. V. G. Karnaukhov and I. F. Kirichok, *Coupled Problems for Viscoelastic Plates and Shells* [in Russian], Naukova Dumka, Kyiv (1986).
29. V. G. Karnaukhov and I. F. Kirichok, *Electrothermoviscoelasticity*, Vol. 4 of the five-volume series *Mechanics of Coupled Fields in Structural Members* [in Russian], Naukova Dumka, Kyiv (1988).
30. V. G. Karnaukhov, V. I. Kozlov, Ya. O. Zhuk, and T. V. Karnaukhova, “Coupled thermoelastic theory of layered shells with passive physically nonlinear inelastic layers and distributed piezoelectric inclusions for control of nonstationary vibrations,” *Mat. Met. Fiz.-Mat. Polya*, **44**, No. 3, 96–106 (2001).
31. V. G. Karnaukhov, V. I. Kozlov, Ya. O. Zhuk, and T. V. Karnaukhova, “Coupled thermomechanical theory of harmonic vibrations of layered shells with physically nonlinear inelastic passive layers and distributed piezoelectric inclusions for control of vibrations,” *Mat. Met. Fiz.-Mat. Polya*, **44**, No. 4, 113–122 (2001).
32. V. G. Karnaukhov, V. I. Kozlov, and T. V. Karnaukhova, “Influence of shear strains on the active damping factor of vibrations of a hinged rectangular plate,” *Teor. Prikl. Mekh.*, **42**, 112–117 (2006).
33. V. G. Karnaukhov, V. I. Kozlov, and T. V. Karnaukhova, “Modeling the forced resonant vibrations and self-heating of flexible viscoelastic plates with distributed actuators,” *Fiz.-Mat. Model. Inform. Tekhnol.*, **8**, 48–68 (2008).
34. V. G. Karnaukhov, V. I. Kozlov, and T. V. Karnaukhova, “Thermal failure of a hinged inelastic rectangular plate with piezoelectric sensors and actuators during forced resonant flexural vibrations,” *Visn. Dnipropetr. Univ.*, *Ser. Mekhanika*, **15**, No. 2, No. 5, 68–75 (2011).
35. V. G. Karnaukhov, V. I. Kozlov, and T. V. Karnaukhova, “Influence of shear strains on the vibrations and self-heating of shells of revolution with piezoelectric layers,” *Teor. Prikl. Mekh.*, No. 7 (53), 137–148 (2013).
36. V. G. Karnaukhov, V. I. Kozlov, and T. V. Karnaukhova, “Influence of shear strains on the effectiveness of piezoelectric actuators in active damping of the resonant vibrations of a cylindrical panel,” *Teor. Prikl. Mekh.*, No. 8 (54), 106–113 (2014).
37. V. G. Karnaukhov, V. I. Kozlov, and T. V. Karnaukhova, “Influence of shear strains on the effectiveness of piezoelectric sensors and actuators in active damping of the resonant vibrations of inelastic plates and shells,” *Opir. Mater. Teor. Sporud*, No. 95, 75–95 (2015).
38. V. G. Karnaukhov, A. V. Kozlov, and E. V. Pyatetskaya, “Damping the vibrations of viscoelastic plates with distributed piezoelectric inclusions,” *Akust. Visn.*, **5**, No. 4, 15–32 (2002).

39. V. G. Karnaukhov and V. V. Mikhailenko, *Nonlinear Thermomechanics of Piezoelectric Inelastic Bodies under Monoharmonic Loading* [in Russian], ZhGTU, Zhitomir (2005).
40. V. G. Karnaukhov and Ya. V. Tkachenko, "Studying the harmonic vibrations of a two-layer cylindrical shell with a physically nonlinear piezoelectric layer," *Vestn. Donetsk. Univ.*, *Ser. A: Estest. Nauki*, No. 2, 107–113 (2006).
41. V. G. Karnaukhov, Ya. V. Tkachenko, and V. F. Zrazhevs'ka, "Studying the harmonic vibrations of a spherical shell made of a physically nonlinear piezoelectric material," *Mat. Met. Fiz.-Mekh. Polya*, **50**, No. 1, 125–129 (2007).
42. V. G. Karnaukhov, A. Yu. Shevchenko, T. V. Karnaukhova, and N. V. Petrenko, "Influence of physical nonlinearity and self-heating temperature on the performance of sensors and actuators," *Teor. Prikl. Mekh.*, No. 47, 11–19 (2010).
43. T. V. Karnaukhova, "A new approach to the active damping of forced resonant flexural vibrations of isotropic viscoelastic plates," *Dop. NANU*, No. 5, 78–82 (2009).
44. I. F. Kirichok and Ya. A. Zhuk, "Influence of boundary conditions and self-heating temperature on the resonant axisymmetric vibrations of viscoelastic cylindrical shells with piezoactuators and sensors," *Teor. Prikl. Mekh.*, No. 7 (53), 133–140 (2013).
45. I. F. Kirichok and T. V. Karnaukhova, "Control of forced vibrations of circular viscoelastic plates with piezoelectric sensors and actuators," *Fiz.-Mat. Model. Inform. Tekhnol.*, No. 9, 67–78 (2009).
46. I. F. Kirichok and T. V. Karnaukhova, "Resonant vibrations and self-heating of either hinged or clamped flexible circular plates with piezoelectric actuators," *Akust. Visn.*, **14**, No. 1, 40–48 (2011).
47. I. F. Kirichok and T. V. Karnaukhova, "Axisymmetric resonant vibrations and self-heating of a viscoelastic cylindrical shell with piezoelectric sensors and temperature-dependent material properties," *Visn. Kyiv. Nats. Univ.*, *Ser. Fiz.-Mat. Nauky*, No. 3, 150–153 (2013).
48. I. F. Kirichok and T. V. Karnaukhova, "Resonant axisymmetic vibrations and self-heating of a viscoelastic closed spherical shell and their damping with piezoelectric sensors and actuators," *Visn. Zaporiz. Nats. Univ.*, No. 1, 59–66 (2013).
49. I. F. Kirichok, T. V. Karnaukhova, and N. V. Peresun'ko, "Resonant axisymmetric vibrations and self-heating of cylindrical shells controlled with piezoelectric actuators," *Teor. Prikl. Mekh.*, **46**, 132–140 (2009).
50. I. F. Kirichok, O. V. P'yatets'ka, and M. V. Karnaukhov, "Flexural vibrations and self-heating of a viscoelastic circular plate with piezoelectric actuators under electromechanical monoharmonic loading," *Visn. Kyiv. Univ.*, *Ser. Fiz.-Mat. Nauky*, No. 2, 84–92 (2006).
51. V. G. Karnaukhov and A. Yu. Shevchenko, "Resonant vibrations and self-heating of a flexible viscoelastic beam with piezoelectric sensors," *Teor. Prikl. Mekh.*, No. 4 (50), 177–185 (2012).
52. A. D. Kovalenko, *Basic Thermoelasticity* [in Russian], Naukova Dumka, Kyiv (1970).
53. V. I. Kozlov, T. V. Karnaukhova, and M. V. Peresun'ko, "Damping the forced axisymmetric vibrations of a clamped viscoelastic cylindrical shell with piezoelectric actuators," *Visn. Donetsk. Univ.*, *Ser A: Pryrodn. Nauky*, No. 1, 142–145 (2008).
54. V. I. Kozlov, T. V. Karnaukhova, and M. V. Peresun'ko, "Numerical modeling of active damping of forced thermomechanical resonant vibrations of viscoelastic shells of revolution with piezoelectric inclusions," *Mat. Met. Fiz.-Mekh. Polya*, **52**, No. 3, 116–126 (2009).
55. V. I. Korolev, *Layered Anisotropic Plates and Shells Made of Reinforced Plastics* [in Russian], Mashinostroenie, Moscow (1965).
56. A. Ya. Malkin, A. A. Askadskii, and V. V. Kovriga, *Methods for Measuring the Mechanical Characteristics of Polymers* [in Russian], Khimiya, Moscow (1978).
57. V. V. Matveev, *Damping of the Vibrations of Deformable Bodies* [in Russian], Naukova Dumka, Kyiv (1985).
58. A. N. Guz (ed.), *Mechanics of Composite Materials* [in Russian], A.S.K., Kyiv (1992–2005).
59. Yu. A. Mitropolsky, *Averaging Method in Nonlinear Mechanics* [in Russian], Naukova Dumka, Kyiv (1971).
60. Yu. A. Mitropolsky, *Nonlinear Mechanics. Single-Frequency Vibrations* [in Russian], Inst. Mat. NAN Ukrainy, Kyiv (1997).
61. Yu. A. Mitropolsky and B. I. Moseenkov, *Asymptotic Solutions of Partial Differential Equations* [in Russian], Vyshcha Shkola, Kyiv (1976).
62. A. D. Nashif, D. J. Johnes, and J. P. Henderson, *Vibration Damping*, John Wiley & Sons, New York (1985).
63. G. S. Pisarenko, *Energy Dissipation during Mechanical Vibrations* [in Russian], Izd. AN USSR, Kyiv (1962).

64. G. S. Pisarenko, *Vibrations of Mechanical Systems Made of Imperfectly Elastic Material* [in Russian], Naukova Dumka, Kyiv (1970).
65. G. S. Pisarenko, A. P. Yakovlev, and V. V. Matveev, *Vibration Damping Properties of Structural Materials* [in Russian], Naukova Dumka, Kyiv (1971).
66. V. N. Poturaev (ed.), V. I. Dyrda, V. G. Karnaukhov, et al., *Thermomechanics of Elastomeric Structural Members under Cyclic Loading* [in Russian], Naukova Dumka, Kyiv (1987).
67. Y. N. Rabotnov, *Creep Problems in Structural Members*, North-Holland, Amsterdam (1969).
68. Y. N. Rabotnov, *Elements of Hereditary Solid Mechanics*, Mir, Moscow (1980).
69. A. O. Rasskazov, I. I. Sokolovskaya, and N. A. Shul'ga, *Theory and Design of Layered Orthotropic Plates and Shells* [in Russian], Vyshcha Shkola, Kyiv (1986).
70. E. V. Savchenko, *Passive Damping of Vibrations of Composite Structures* [in Russian], Aspekt-Poligraf, Nezhin (2006).
71. W. P. Mason (ed.), *Physical Acoustics. Principles and Methods*, Vol. 2, Part B. *Properties of Polymers and Nonlinear Acoustics*, Academic Press, New York–London (1965).
72. G. N. Skanavi, *Physics of Dielectrics* [in Russian], Vol. 2, Fizmagiz, Moscow (1958).
73. E. I. Starovoitov, *Layered Viscoelastoplastic Plates and Shells* [in Russian], BelGUT, Gomel (2003).
74. A. P. Aleksandrov, A. F. Val'ter (ed.), B. M. Vul, et al., *Physics of Dielectrics* [in Russian], GTTI, Leningrad–Moscow (1932).
75. W. Von Franz, *Dielektrischer Durchschlag*, Vol. 17 of S. Flugge (ed.), Handbuch der Physik, Springer, Berlin (1956).
76. V. V. Khil'chevskii and V. G. Dubenets, *Dissipation of Energy during Vibrations of Thin-Walled Structural Members* [in Russian], Vyshcha Shkola, Kyiv (1977).
77. Ya. M. Grigorenko, E. I. Bespalova, A. T. Vasilenko, et al., *Numerical Solution of Static Boundary-Value Problems for Orthotropic Shells of Revolution on M-220 Computer* [in Russian], Naukova Dumka, Kyiv (1971).
78. V. E. Shamanskii, *Methods for Numerical Solution of Boundary-Value Problems on a Computer* [in Russian], Naukova Dumka, Kyiv (1966).
79. Yu. N. Shevchenko and V. G. Savchenko, *Thermoviscoplasticity*, Vol. 2 of the five-volume series *Mechanics of Coupled Fields in Structural Members* [in Russian], Naukova Dumka, Kyiv (1987).
80. R. A. Schapery, "Effect of cyclic loading on the temperature in viscoelastic media with variable properties," *AIAA J.*, **2**, No. 5, 827–835 (1964).
81. R. A. Schapery, "Thermomechanical behavior of viscoelastic media with variable properties subjected to cyclic loading," *Trans. ASME*, *J. Appl. Mech.*, *Ser. E*, **32**, No. 3, 611–619 (1965).
82. N. A. Shul'ga and A. M. Bolkisev, *Vibrations of Piezoelectric Bodies* [in Russian], Naukova Dumka, Kyiv (1990).
83. N. A. Shul'ga and V. L. Karlash, *Resonant Electromechanical Vibrations of Piezoelectric Plates* [in Ukrainian], Naukova Dumka, Kyiv (2008).
84. M. S. Blanter, I. S. Golovin, H. Neuauser, and H. R. Sinning, *Internal Friction in Metallic Materials*, Springer Verlag, Handbook (2007).
85. S. R. Bodner, *Unified Plasticity—An Engineering Approach*, Israel Institute of Technology, Haifa (2000).
86. S. R. Bodner and Y. Partom, "Constitutive equation for elastoviscoplastic strain hardening materials," *Trans. ASME*, *J. Appl. Mech.*, **42**, 385–389 (1975).
87. A. V. Boiko, V. M. Kulik, B. M. Seoudi, H. H. Chun, and I. Lee, "Measurement method of complex viscoelastic material properties," *Int. J. Solid Struct.*, **47**, 374–382 (2010).
88. F. Dinzart, A. Molinari, and R. Herbabach, "Thermomechanical response of a viscoelastic beam under cyclic bending; self-heating and thermal failure," *Arch. Mech.*, **60**, No. 1, 59–85 (2008).
89. Mel Schwartz (ed.), *Encyclopedia of Smart Materials*, Vol. 1–2, Wiley & Sons, New York (2002).
90. U. Gabbert and H. S. Tzou, *Smart Structures and Structronic Systems*, Kluwer, Dordrecht–Boston–London (2001).
91. F. Gandhi, "Influence of nonlinear viscoelastic material characterization on performance of constrined layer damping treatment," *AIAA J.*, **39**, No. 5, 924–931 (2001).
92. I. A. Guz, Y. A. Zhuk, and M. Kashtalyan, "Vibration analysis of thin-wall structures containing piezoactive layers," *IOP Conf. Ser.: Materials Science and Engineering*, 10 (2010) 012174 doi:10.1088/1757-899X/10/1/012174.
93. I. A. Guz, Y. A. Zhuk, and M. Kashtalyan, "Dissipative heating and thermal fatigue life prediction for structures containing piezoactive layers," *Technische Mechanik*, **32**, No. 2–5, 238–250 (2012).

94. I. A. Guz, Y. A. Zhuk, and C. M. Sands, "Analysis of the vibrationally induced dissipative heating of thin-wall structures containing piezoactive layers," *Int. J. Non-Linear Mech.*, **47**, 105–116 (2012).
95. D. I. Jones, *Handbook of Viscoelastic Vibration Damping*, Wiley&Sons, New York (2001).
96. V. G. Karnaukhov, "Thermal failure of polymer structural elements under monoharmonic deformation (review)," *Int. App. Mech.*, **40**, No. 6, 622–655 (2004).
97. V. G. Karnaukhov, "Thermomechanics of coupled fields in passive and piezoactive inelastic bodies under harmonic deformations (review)," *J. Thermal Stresses*, **28**, No. 6–7, 783–815 (2005).
98. V. G. Karnaukhov, "Thermomechanics of coupled fields in passive and piezoactive inelastic bodies under harmonic deformations," in: *Proc. 6th Int. Congr. on Thermal Stresses* (Vienna, Austria, May 2005), Vienna University of Technology, Vienna (2005), pp. 29–34.
99. V. G. Karnaukhov, "The forced harmonic vibrations and dissipative heating of nonelastic bodies," in: R. B. Hetnarski (ed.), Vol. 7 of *Encyclopedia of Thermal Stresses*, Springer, New York–Dordrecht (2014), pp. 3910–3919.
100. V. G. Karnaukhov, "Piezothermo-inelastic behaviour of structural elements: Vibrations and dissipative heating," in: R. B. Hetnarski (ed.), Vol. 4 of *Encyclopedia of Thermal Stresses*, Springer, New York–Dordrecht (2014), pp. 1711–1722.
101. V. G. Karnaukhov and T. V. Karnaukhova, "Influence of temperature of dissipative heating on an active damping of the rezonant bending vibrations of a flexible rectangular plate by the distributed sensors and actuators," *J. Math. Sci.*, **161**, No. 1, 54–61 (2009).
102. V. G. Karnaukhov, T. V. Karnaukhova, and O. Mc. Gillicaddy, "Thermal failure of flexible rectangular viscoelastic plates with distributed sensors and actuators," *J. Eng. Math.*, **78**, No. 1, 199–212 (2013).
103. V. G. Karnaukhov, T. V. Karnaukhova, V. I. Kozlov, and V. K. Luts, "Influence of dissipation and vibroheating on the vibration characteristics of three-layer piezoelectric shells of revolution," *Akust. Vestn.*, **4**, No. 3, 39–52 (2001).
104. V. G. Karnaukhov and I. F. Kyrychok, "Forced harmonic vibrations and dissipative heating-up of viscoelastic thin-walled elements (review)," *Int. App. Mech.*, **36**, No. 2, 174–195 (2000).
105. V. G. Karnaukhov, I. F. Kirichok, and M. V. Karnaukhov, "The influence of dissipative heating on active vibration damping of viscoelastic plates," *J. Eng. Math.*, **61**, No. 2–4, 399–411 (2008).
106. V. G. Karnaukhov, I. F. Kirichok, and V. I. Kozlov, "Electromechanical vibrations and dissipative heating of viscoelastic thin-walled piezoelements (review)," *Int. App. Mech.*, **37**, No. 2, 182–212 (2001).
107. V. G. Karnaukhov, V. I. Kozlov, and T. V. Karnaukhova, "Influence of dissipative heating on active damping of forced resonance vibrations of flexible viscoelastic cylindrical panel by piezoelectric actuators," *J. Math. Sci.*, **183**, No. 2, 205–221 (2012).
108. V. G. Karnaukhov and V. V. Mikhailenko, "Nonlinear single-frequency vibrations and dissipative heating of inelastic piezoelectric bodies (review)," *Int. App. Mech.*, **38**, No. 5, 521–547 (2002).
109. V. G. Karnaukhov and I. K. Senchenkov, "Generaled models of the thermomechanical behavior of viscoelastic materials with allowance for the interaction of mechanical and thermal fields (review)," *Int. App. Mech.*, **36**, No. 1, 40–63 (2000).
110. V. G. Karnaukhov and Ya. V. Tkachenko, "Damping the vibrations of a rectangular plate whith piezoelectric actuators," *Int. Appl. Mech.*, **44**, No. 3, 182–187 (2008).
111. V. G. Karnaukhov and Ya. V. Tkachenko, "Influence of shear strains on damping the vibrations of a rectangular plate with dielectric actuators," *Int. App. Mech.*, **45**, No. 12, 1365–1373 (2009).
112. V. G. Karnaukhov and Ya. V. Tkachenko, "Active damping of the resonant vibrations of a flexible rectangular plate," *Int. App. Mech.*, **47**, No. 4, 457–463 (2011).
113. T. V. Karnaukhova, "Thermal depolarization of a piezoelectric layer under harmonic quazistatic electric loading," *Prikl. Mekh.*, **34**, No. 4, 81–84 (1998).
114. T. V. Karnaukhova, "Active damping of vibrations of plates subjected to unknown pressure," *Int. App. Mech.*, **46**, No. 5, 562–566 (2010).
115. T. V. Karnaukhova, "Damping the vibrations of a clamped plate using the sensor's reading," *Int. App. Mech.*, **46**, No. 6, 683–686 (2010).
116. T. V. Karnaukhova, "Influence of the temperature of dissipative heating on the damping of forced the resonance vibrations of a simply supported viscoelastic cylindrical panel with the help of piezoelectric actuators," *J. Math. Sci.*, **167**, No. 2, 173–181 (2010).

117. T. V. Karnaukhova, “Influence of the temperature of dissipative heating on the damping of forced resonance vibrations of unelastic rectangular plates,” *J. Math. Sci.*, **165**, No. 2, 264–273 (2010).
118. T. V. Karnaukhova, “Active damping of forced resonance vibrations of an isotropic shallow viscoelastic cylindrical panel under the action of an unknown mechanical load,” *J. Math. Sci.*, **168**, No. 4, 603–612 (2010).
119. T. V. Karnaukhova and E. V. Pyatetskaya, “Basic eguations for thermoviscoelastic plates with distributed actuators under monoharmonic loading,” *Int. App. Mech.*, **45**, No. 2, 200–214 (2009).
120. T. V. Karnaukhova and E. V. Pyatetskaya, “Damping the resonant flexural vibration a hinged plate with actuators,” *Int. App. Mech.*, **45**, No. 4, 448–456 (2009).
121. T. V. Karnaukhova and E. V. Pyatetskaya, “Damping the flexural vibration a clamped viscoelastic rectangular plate with piezoelectric actuators,” *Int. App. Mech.*, **45**, No. 5, 546–557 (2009).
122. T. V. Karnaukhova and E. V. Pyatetskaya, “Basic relations of the theory of the thermoviscoelastic plates with distributed sensors,” *Int. App. Mech.*, **45**, No. 6, 660–669 (2009).
123. T. V. Karnaukhova and E. V. Pyatetskaya, “The resonant flexural vibrations of a hinged viscoelastic plate with sensors,” *Int. App. Mech.*, **45**, No. 7, 762–771 (2009).
124. T. V. Karnaukhova and E. V. Pyatetskaya, “Resonant vibrations of a clamped viscoelastic rectangular plate,” *Int. App. Mech.*, **45**, No. 8, 904–916 (2009).
125. T. V. Karnaukhova and E. V. Pyatetskaya, “Basic relations of the theory of the thermoviscoelastic plates with distributed sensors and actuators,” *Int. App. Mech.*, **46**, No. 1, 78–85 (2010).
126. T. V. Karnaukhova and E. V. Pyatetskaya, “Resonant vibrations of a hinged viscoelastic rectangular plate with sensors and actuators,” *Int. App. Mech.*, **46**, No. 2, 213–220 (2010).
127. T. V. Karnaukhova and E. V. Pyatetskaya, “Resonant vibrations of a clamped thermoviscoelastic rectangular plate with sensors and actuators,” *Int. App. Mech.*, **46**, No. 3, 296–303 (2010).
128. I. F. Kirichok, “Resonant vibration and heating of ring plates with piezoactuators under electromechanical loading and shear deformation,” *Int. App. Mech.*, **45**, No. 2, 214–222 (2009).
129. I. F. Kirichok, “Resonance vibration and dissipative hHeating of a rigidly clamped thermoviscoelastic beam with piezoactuators,” *Int. Appl. Mech.*, **50**, No. 4, 421–429 (2014).
130. I. F. Kirichok, “Control of axisymmetric resonant vibrations and self-heating of shells of revolution with piezoelectric sensors and actuators,” *Int. Appl. Mech.*, **46**, No. 8, 890–901 (2011).
131. I. F. Kirichok, “Forced monoharmonic and vibroheating of viscoelastic flexible circular plates with piezolayers,” *Int. Appl. Mech.*, **49**, No. 6, 715–725 (2013).
132. I. F. Kirichok and M. V. Karnaukhov, “Monoharmonic vibrations and vibrational heating of an electromechanically loaded circular plate with piezoelectric actuators subject to shear strain,” *Int. Appl. Mech.*, **44**, No. 9, 1041–1049 (2008).
133. I. F. Kirichok, V. V. Mikhailenko, and S. P. Davidchuk, “Nonlinear vibrations and vibroheating of a viscoelastic rod with cubic elasticity,” *Int. Appl. Mech.*, **38**, No. 9, 1125–1130 (2002).
134. V. I. Kozlov, T. V. Karnaukhova, and M. V. Peresun’ko, “Numerical modeling of the active damping of forced thermomechanical resonance vibrations of viscoelastic shells of revolution with the help of piezoelectric inclusions,” *J. Math. Sci.*, **171**, No. 5, 565–578 (2010).
135. V. D. Kubenko and I. V. Yanchevsky, “Active damping of nonstationaty vibrations of a rectangular plate under impulse loading,” *J. Vibr. Contr.*, **19**, No. 10, 1514–1523 (2013).
136. I. F. Kirichok, “Forced resonant vibrations and self-heating of a flexible circular plate with piezoactuators,” *Int. Appl. Mech.*, **48**, No. 5, 583–591 (2012).
137. I. F. Kyrychok and T. V. Karnaukhova, “Influence of boundary conditions and temperature of dissipative heating on active damping of forced axisymmetric resonant bending vibrations of circular viscoelastic plates by piezoelectric sensors and actuators,” *J. Math. Sci.*, **178**, No. 5, 480–495 (2011).
138. B. Lazan, *Damping of Materials and Members in Structural Mechanics*, Pergamon Press, Oxford (1968).
139. Z. Li and M. J. Crocker, “A review on vibration damping in sandwich composite structures,” *Int. J. Acoust. Vib.*, **10**, No. 4, 159–169 (2005).
140. Namita Nanda, “Non-linear free and forced vibrations of piezoelectric laminated shells in thermal environments,” *The IES J.*, *Part A: Civil & Structural Engineering*, **3**, No. 3, 147–160 (2010).

141. N. Ohno and M. Satra, “Detailed and simplified elastoplastic analysis of a cyclically loaded notched bar ,” *J. Eng. Mater. Technol.*, **109**, No. 3, 194–202 (1987).
142. V. A. Pal’mov, *Vibrations of Elasto-Plastic Bodies*, Springer, New York (1998).
143. R. G. Sabat, B. Mukherjee, W. Ren, and G. Yung, “Temperature dependence of the complete material coefficients matrix of soft and hard doped piezoelectric lead zirconate titanate ceramics,” *J. Appl. Phys.*, **101**, 06411-1-7 (2007).
144. R. G. Sabat, W. Ren, G. Yung, and B. Mukherjee, “Temperure dependence of the dielectric, elastic and piezoelectric material constants of lead zirconate titanate (PZT) ceramic,” *Smart Struct. Mater.*, No. 6, 1700A–61700A-8 (2006).
145. I. K. Senchenkov, Ya. A. Zhuk, and V. G. Karnaukhov, “Modelling of the thermomechanical behaviour of physically nonlinear materials under monoharmonic loading (review),” *Int. App. Mech.*, **40**, No. 9, 943–969 (2004).
146. I. K. Senchenkov and V. G. Karnaukhov, “Thermomechanical behaviour of nonlinearly viscoelastic materials under monoharmonic loading (review),” *Int. App. Mech.*, **37**, No. 11, 1400–1432 (2001).
147. I. K. Senchenkov, V. G. Karnaukhov, V. I. Kozlov, and O. P. Chervinko, “Steady oscillations and dissipative heating of viscoelastic bodies with periodical load,” *Int. App. Mech.*, **22**, No. 6, 538–544 (1986).
148. I. K. Senchenkov and G. A. Tabieva, “Determination of the parameters of the Bodner-Partom model for thermoviscoplastic deformation of materials,” *Int. App. Mech.*, **32**, No. 2, 132–139 (1996).
149. I. K. Senchenkov, G. A. Tabieva, Ya. A. Zhuk, and O. P. Chervinko, “Monoharmonic approximation in the deformation of viscoplastic bodies with a harmonic load,” *Int. App. Mech.*, **33**, No. 7, 560–566 (1997).
150. J. Tani, T. Takagi, and J. Qui, “Intelligent material systems: Application of functional materials,” *Appl. Mech. Rev.*, **51**, No. 8, 505–521 (1998).
151. E. C. Ting, “Thermomechanical coupling effects in the longitudinal oscillations of a viscoelastic cylinder,” *The J. Acoust. Soc. Amer.*, **52**, No. 3, 928–934 (1972).
152. J. F. Tormey and S. C. Britton, “Effect of cyclic loading on solid propellant grain structures,” *AIAA J.*, **1**, No. 8, 1763–1770 (1963).
153. H. S. Tzou, *Piezoelectric Shells* (*Distributed Sensing and Control of Continua*), Kluwer, Boston–Dordrecht (1993).
154. H. S. Tzou and L. A. Bergman, *Dynamics and Control of Distributed Systems*, Cambridge University Press, Cambridge (1998).
155. R. W. Young, “Thermomecbanical response of viscoelastic rod driven by a sinusoidal displacement,” *Int J. Sol. Struct.*, **13**, No. 10, 925–936 (1977).
156. Ya. A. Zhuk and I. A. Guz, “Active damping of the forced vibration of a hinged beam with piezoelectric layer, geometrical and physical nonlinearities taken into account,” *Int. App. Mech.*, **45**, No. 1, 94–108 (2009).
157. Ya. Zhuk and I. Senchenkov, “Monoharmonic approach to investigation of the vibrations and selfheating of thinwall inelastic members,” *J. Civil Eng. Manag.*, **15**, No. 1, 67–75 (2009).
158. Y. A. Zhuk, I. A. Guz, and C. M. Sands, “Monoharmonic approximation in the vibration analysis of a sandwich beam containing piezoelectric layers under mechanical or electrical loading,” *J. Sound Vibr.*, **330**, 4211–4232 (2011).